NUREG/CR-1083
LBL-6754

Sloshing of Water in Annular Pressure-Suppression Pool of Boiling Water Reactors Under Earthquake Ground Motions

Prepared by M. Aslam, W. G. Godden, T. Scalise

Lawrence Berkeley Laboratory
University of California

Prepared for
U. S. Nuclear Regulatory
Commission

Available from

GPO Sales Program
Division of Technical Information and Document Control
U.S. Nuclear Regulatory Commission
Washington, D.C. 20555

and

National Technical Information Service
Springfield, Virginia 22161

NUREG/CR-1083
LBL-6754
RO

Sloshing of Water in Annular Pressure-Suppression Pool of Boiling Water Reactors Under Earthquake Ground Motions

Manuscript Completed: August 1978
Date Published: October 1979

Prepared by
M. Aslam, W. G. Godden, D. T. Scalise

Lawrence Berkeley Laboratory
University of California
Berkeley, CA 94720

Prepared for
Division of Reactor Safety Research
Office of Nuclear Regulatory Research
U.S. Nuclear Regulatory Commission
Washington, D.C. 20555
NRC FIN No. B3025

CONTENTS

LIST OF SYMBOLS

a	Outer radius of the tank
b	Inner radius of the tank
g	Acceleration of gravity
h, H	Depth of water in the tank
J_m	Bessel functions of first kind and order m
J'_m	Derivative of J_m
p	Dynamic pressure
p_{max}	Maximum dynamic pressure
r	Radius
t	Time
U_r	Velocity in r direction
U_θ	Velocity in θ direction
U_z	Velocity in z direction
x	Ground displacement
$\dot{x}$	Ground velocity (dx/dt — dot means derivative w.r.t.t)
Y_m	Bessel functions of second kind and order m
z	z-Coordinate direction
ϕ	Velocity potential
θ	θ-Coordinate direction
ω_n	Sloshing frequency (circular)
ω_o	Ground frequency (circular)
δ	Water displacement
δ_{max}	Maximum water displacement

ABSTRACT

This report presents an analytical investigation of the sloshing response of water in annular-circular as well as simple-circular tanks under horizontal earthquake ground motions, and the results are verified with tests. This study was motivated because of the use of annular tanks for pressure-suppression pools in Boiling Water Reactors. Such a pressure-suppression pool would typically have 80 ft and 120 ft inside and outside diameters and a water depth of 20 ft.

The analysis was based upon potential flow theory and a computer program was written to obtain time-history plots of sloshing displacements of water and the dynamic pressures. Tests were carried out on 1/80th and 1/15th scale models under sinusoidal as well as simulated earthquake ground motions. Tests and analytical results regarding the natural frequencies, surface water displacements, and dynamic pressures were compared and a good agreement was found for relatively small displacements. The computer program gave satisfactory results as long as the maximum water surface displacements were less than 30 in., which is roughly the value obtained under full intensity of El Centro earthquake (N-S component 1940).

Test results from a 12-ft-diameter simple-circular tank were also compared with the computer results and again a good agreement was found between the two. The range in which the linear theory gives good results is, in general, larger in case of a simple tank compared with an annular tank of the same outside diameter.

Tests were also conducted to study the effect of vertical ground motions and these showed a negligible effect on sloshing but a very strong

effect on dynamic pressures. The effects of a damping mechanism was also studied as a means of reducing the sloshing response Tests were conducted under El Centro (1940) and Parkfield earthquakes, but analytical results are available for many other accelerograms.

KEY WORDS

Sloshing response, Pressure-suppression pool, Annular tanks, Circular tanks, Earthquake response, Dynamic pressures, Irrotational flow, Damping

1. INTRODUCTION

1.1 Objective

This investigation was undertaken to predict theoretically the sloshing response of water in annular-circular tanks (Fig. 1-1) under arbitrary horizontal ground motion and to check the results experimentally. This problem is encountered in the pressure-suppression pool of Boiling Water Reactors (BWR) where the outer and inner diameters are typically 120 ft and 80 ft respectively, and the depth of water is typically 20 ft. These structures are considered to be rigid for this analysis. A cross section through the annulus of a typical pressure-suppression pool of BWR is shown in Fig. 1-2.

A considerable amount of both experimental and theoretical work has been reported in the literature on the sloshing of water in cylindrical tanks and a list of these is provided in the references section [1 through 11]. Most of this work deals only with steady-state response and very little with the response of water under earthquake-type loading.

On the other hand, very little work has been done on annular tanks. There has been no experimental or theoretical study reported on the sloshing response of water in annular tanks under arbitrary ground motions. Bauer's [12] theoretical analysis for such tanks deals only with steady-state harmonic ground motion and cannot be applied to earthquake accelerograms.

The main object of this study was to estimate the water surface displacements during an earthquake. This is necessary to ensure that the water surface displacements are not excessive to the point of causing an escape of superheated steam. This would occur if the water surface dropped to level C-C in Fig. 1-2.

1.2 Scope of the Investigation

The scope of this report, in order of presentation, consists of the analytical study, computed steady state and seismic response, small-scale and large-scale model tests, and finally a general discussion of the data.

Chapter 2 discusses the sloshing theory. Assuming that flow remains irrotational, a velocity potential function ϕ was derived by solving the Laplace equation with time-dependent boundary conditions and free-surface-pressure conditions. Water displacements, velocities and pressures can be derived from ϕ at any point in the fluid. However, for this analysis, only the water surface displacements and pressures along the inner and outer boundaries were calculated, as these quantities were measured in the seismic tests.

The corresponding eigenvalue problem was solved to determine the frequencies and mode shapes. Based upon the above theory a computer program called "SLOSH" was written to solve the problem numerically and plot the important results. This computer program determines frequencies and modes shapes of water in an annular-cylindrical shape for arbitrary inner and outer diameters and any depth of water. The program also calculates time-history response of water surfaces at a section along the axis of ground excitation and gives a time-history plot of surface water displacements at the inner and outer boundaries.

Dynamic pressures were calculated along inner and outer boundaries at a vertical section along the axis of excitation. Thus a variation of dynamic pressure with depth could be plotted at any moment during the earthquake. Time-history Calcomp plots were also obtained for maximum pressures at the bottom of the tank at inner and outer boundaries. The computed response is discussed in Chapter 3.

The computer program SLOSH works equally well for simple circular tanks by letting the inner radius approach a small value. The computer solution was verified by comparison with the test data on a 12-ft-diameter simple-circular tank. The agreement between the measured and analytical results for water surface displacement due to seismic-type ground motion was within ±9%. Chapters 4 and 5 describe the tests carried out on small-scale plexiglass models of annular circular tanks, and also on a large-scale steel model, to determine the accuracy and range of the linear analytical model.

Chapter 4 describes small-scale tests conducted on plexiglass models of 18-in. outside diameter (Fig. 1-3) mounted on a small shaking table capable of providing harmonic motions. The two models had 12-in. and 6-in. internal diameters. The table used was constructed for these tests because the large table at the Earthquake Engineering Research Center is not readily available for prolonged testing to study basic phenomena. Only water surface displacements were measured under steady-state harmonic motions; the pressures being too low to measure. Natural sloshing frequencies of water were measured and results, when compared with the analytical solution, indicated a very good agreement. Steady-state response of water surface waves under harmonic motion was also compared with the analytical results and again a satisfactory agreement was found.

Chapter 5 gives details of large-scale tests conducted on a steel tank having inside and outside diameters equal to 5 ft 5 in. and 8 ft respectively (Fig. 1-4). These tests were done basically to obtain experimental data under simulated earthquake motions. Both water surface displacements and dynamic pressures were measured. There were a total of

6 water displacement gages and 3 pressure gages. Tests were carried out on the 20 ft × 20 ft shaking table at the Earthquake Engineering Research Center, University of California, Berkeley. Tests were done both for harmonic and earthquake ground motions. The test data was digitized at the rate of 100 samples per second. Again, a comparison between the test data and analytical results, both for water surface displacements and dynamic pressures, showed a satisfactory agreement.

In subsequent testing, screens were also used in the annulus as a means of creating turbulence to reduce the sloshing response of water. The effective damping introduced into the dynamic system by this device was determined by observing the decay of freely sloshing water.

The report ends with a general discussion and conclusions.

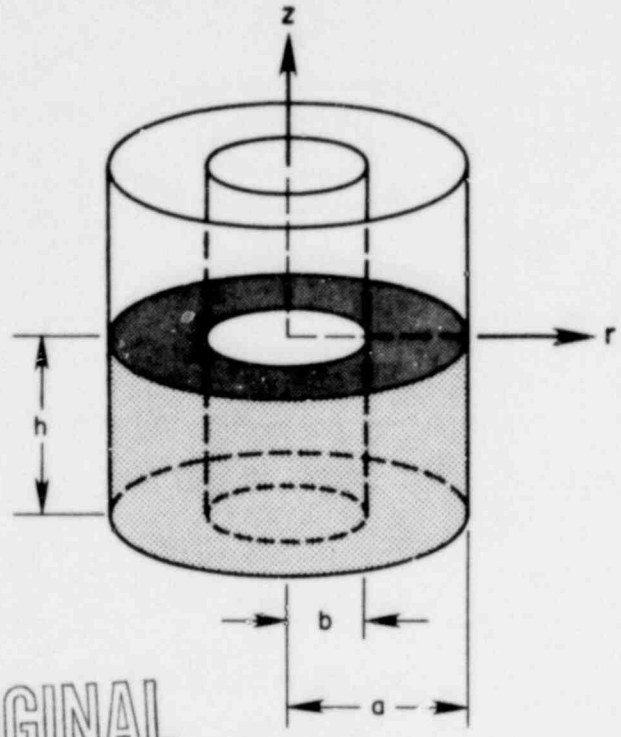

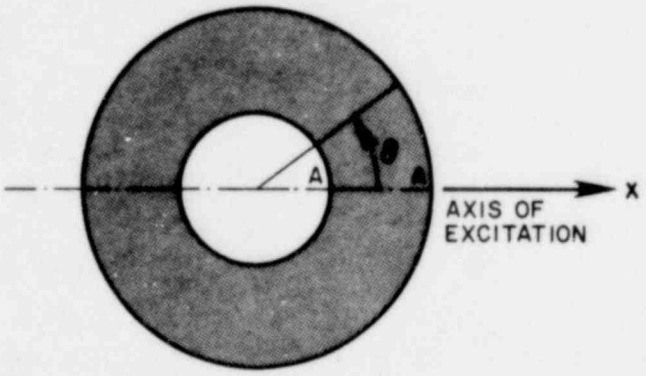

PLAN VIEW

FIG. I-1 ANNULAR TANK SHOWING COORDINATE SYSTEM

XBL 782-7210

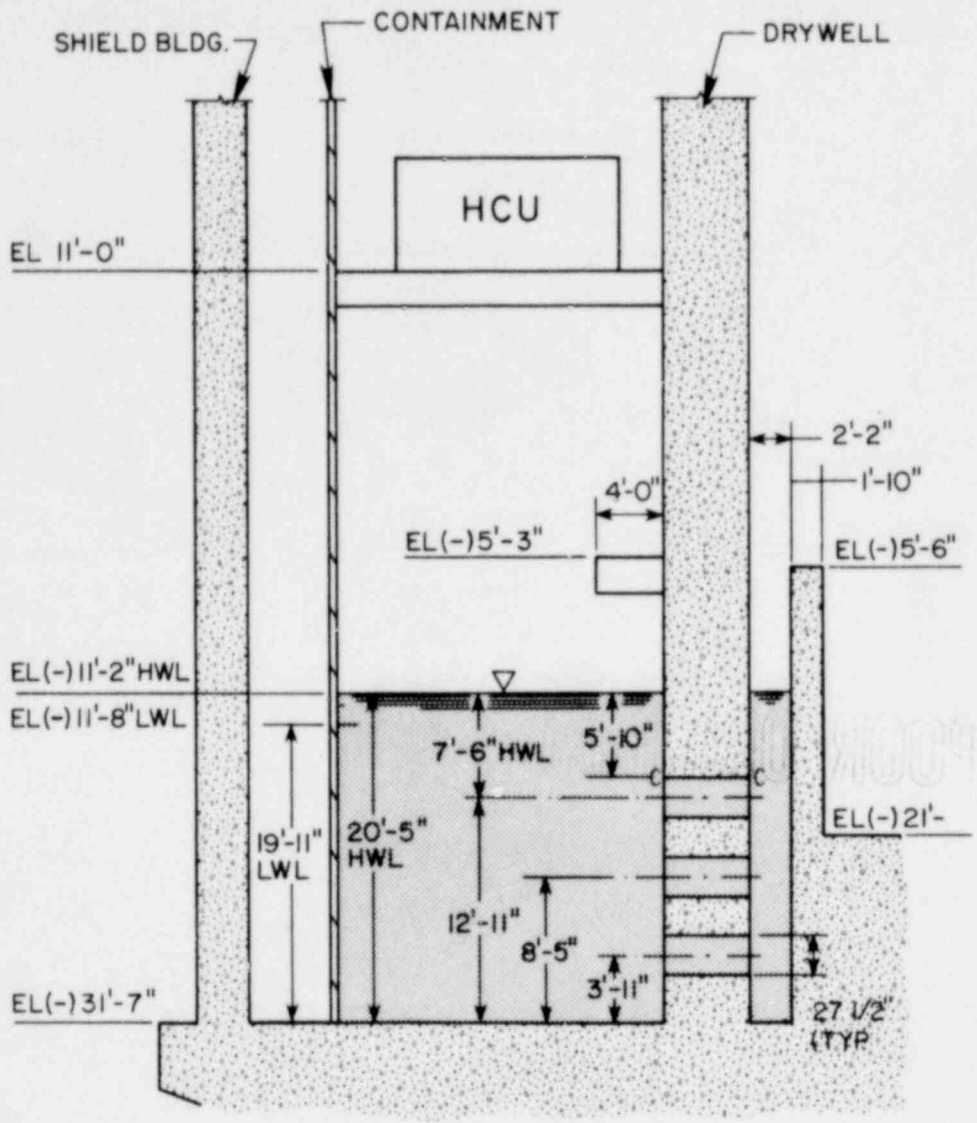

FIG. 1-2 CROSS-SECTION THROUGH THE ANNULUS OF A TYPICAL PRESSURE SUPPRESSION POOL OF A BOILING WATER REACTOR (MARK III)

XBL 7812-13917

CBB 762-1197A

FIG. I-3 SMALL SCALE PLASTIC MODELS

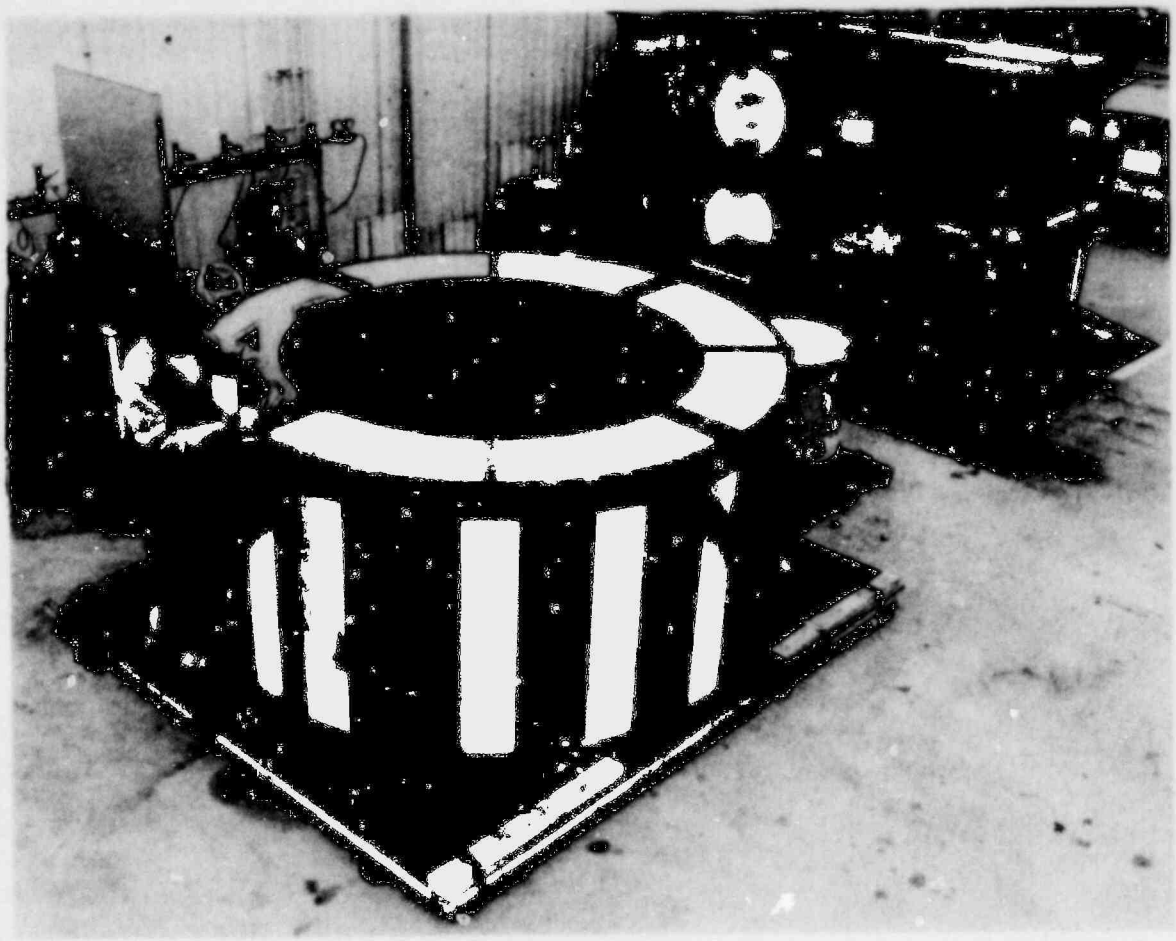

CBB 768-7272A

FIG. 1-4 LARGE SCALE STEEL MODEL, OUTER AND INNER DIA. 8FT. AND 5 1/2 FT. RESPECTIVELY

2. ANALYTICAL STUDY

2.1 Introduction

The assumption for mathematical formulation and the solution to the basic equations are described in this chapter. The Laplace equation is solved to derive a velocity potential. Ground motion is introduced into the solution through boundary conditions which are time dependent. The associated eigenvalue problem is solved to determine the natural frequencies and mode shapes of the sloshing mass of water. Water displacements and dynamic pressures are derived from the velocity potential. A computer program named SLOSH was developed to solve the problem numerically and plot a time-history response of displacements and dynamic pressures. At the end of this Chapter an approximate method is given to determine the natural frequencies of annular-circular tanks. This is based on the natural frequencies in simple rectangular tanks.

2.2 Assumptions for Mathematical Model

The mathematical analysis is based on the following assumptions:

- *Rigid tank walls.* The assumption is made that the tank walls are rigid and hence the tank moves as a rigid body. This is realistic because of the massive structures used for suppression pools. Also the sloshing response is a low-frequency phenomenon and it will be seen later that even if the structure were more flexible, there would be little effect on the overall sloshing response of the water (i.e., water surface displacements) which is the main concern of this study. It should, however, be noted that dynamic pressures are dependent to a greater

degree on the flexibility of the tank walls as these may be high-frequency phenomena.

- *Small displacements.* It is assumed that the displacements and velocities are small so that linear theory can be used.

- *Incompressible fluid.* The water is treated as an incompressible fluid and with the low dynamic pressures expected in the prototype structures, this assumption is considered reasonable.

- *Non-viscous fluid.* The viscosity of the water is neglected. The model tests gave a value of the overall damping of freely sloshing water as less than 0.4% of the critical value. This would even be lower in the prototype structures and therefore damping (viscosity) can be neglected for practical purposes for relatively short durations of earthquakes. Neglecting the viscosity can cause problems if the ground motion is harmonic and the frequency of motion is the same as one of the natural sloshing frequencies of the mass of water in the tank. This event, however, is unlikely during an earthquake and therefore of no practical significance in this investigation.

- *Irrotational flow.* It is assumed that there are no sources and sinks present in the tank and thus as a result of the assumption of small displacements and non-viscous fluid, flow remains irrotational throughout the duration of the earthquake.

2.3 Basic Equations and Boundary Conditions

Since the flow has been assumed to be irrotational, there exists a velocity potential ϕ which will satisfy the Laplace equation which in a

3-D cylindrical coordinate system is

$$\frac{\partial^2\phi}{\partial r^2} + \frac{1}{r}\frac{\partial\phi}{\partial r} + \frac{1}{r^2}\frac{\partial^2\phi}{\partial\theta^2} + \frac{\partial^2\phi}{\partial z^2} = 0 \qquad (2\text{-}1)$$

The coordinate system is shown in Fig. 1-1. The z axis is taken in the middle of the tank, positive upwards, and zero in the horizontal plane passing through the undisturbed water surface. r and θ are the radial and angular coordinates; θ is the angle of any radial line with the axis of horizontal ground excitation x which is a function of time. b and a are the inner and outer radii of the annular tank, and h is the depth of water in the tank.

It should be noted that the velocity of water at the boundaries should always be equal to the wall velocity which can be stated mathematically as follows:

1. $\left.\frac{\partial\phi}{\partial r}\right|_{r=a} = \dot{x}\cos\theta$

2. $\left.\frac{\partial\phi}{\partial r}\right|_{r=b} = \dot{x}\cos\theta$

3. $\left.\frac{\partial\phi}{\partial z}\right|_{z=-h} = 0$

where $\dot{x} = \frac{dx}{dt}$ = tank wall velocity, and t = time. Also, the linearized free-surface boundary condition is given by the following equation [13]

4. $\frac{\partial^2\phi}{\partial t^2} + g\frac{\partial\phi}{\partial z} = 0 \qquad$ at $\qquad z = 0$

where g is the acceleration of gravity.

2.4 Solution of the Associated Eigenvalue Problem

To determine the sloshing frequencies and mode shapes, it is necessary to solve the free vibration problem, in which case the mass of water in the tank may be given an initial displacement or velocity (or both) but the boundary conditions will be zero. Thus we have to solve equation (2-1) with the same boundary conditions as above (Section 2.3) except that boundary conditions 1 and 2 will become

$$\left.\frac{\partial\phi}{\partial r}\right|_{r=a} = \left.\frac{\partial\phi}{\partial r}\right|_{r=b} = 0$$

Assume

$$\phi = R(r)\ \Theta(\theta)\ \ Z(z)\ T(t)$$

where T(t) will be harmonic. Substituting for ϕ in Eq. (2-1), we have

$$R''\Theta Z + \frac{1}{r} R'\Theta Z + \frac{1}{r^2} R\Theta''Z + R\Theta Z'' = 0$$

or

$$\frac{r^2R''}{R} + \frac{rR'}{R} + \frac{r^2Z''}{Z} = -\frac{\Theta''}{\Theta} = v^2 \qquad (2\text{-}2)$$

where v^2 is a constant and primes indicate the partial derivatives. From the above equation we have

$$\Theta'' + v^2\Theta = 0$$

$$\therefore\quad \Theta(\theta) = C \sin v\theta + D \cos v\theta$$

where C and D are constants. In order for ϕ to be a single-valued function, v has to be an integer. Call v = m, where m = 0,1,2,... ∞.

$$\therefore\quad \Theta(\theta) = C \sin(m\theta) + D \cos(m\theta)$$

Also from Eq. (2-2),

$$\frac{r^2R''}{R} + \frac{rR'}{R} + \frac{r^2Z''}{Z} = m^2$$

or

$$\frac{Z''}{Z} = \frac{m^2}{r^2} - \frac{R'}{rR} - \frac{R''}{R} = +\lambda^2 \qquad [\lambda^2 \leqslant 0 \text{ is not possible}] \tag{2-2a}$$

or

$$r^2R'' + rR' + (\lambda^2r^2 - m^2)R = 0 \qquad \text{[Bessel's equation]}$$

Note that λ, C, D, E, and F have a subscript $m = 0,1,2,\ldots\infty$ and this is dropped for convenience.

$$\therefore \quad R(r) = EJ_m(\lambda r) + FY_m(\lambda r) \tag{2-3}$$

where E and F are constants and J_m and Y_m are Bessel functions of first and second kind and of order m. Primes indicate their derivatives with respect to r. Consider the following boundary condition

$$\left.\frac{\partial\phi}{\partial r}\right|_{r=a} = \left.\frac{\partial R}{\partial r}\right|_{r=a} \Theta Z = 0$$

Θ and Z in general are not equal to zero. Therefore

$$\left.\frac{\partial R}{\partial r}\right|_{r=a} = 0$$

Similarly,

$$\left.\frac{\partial R}{\partial r}\right|_{r=b} = 0$$

Applying these two boundary conditions to Eq. (2-3), we have

$$EJ_m'(\lambda a) + FY_m'(\lambda a) = 0 \qquad (2\text{-}3a)$$

$$EJ_m'(\lambda b) + FY_m'(\lambda b) = 0 \qquad (2\text{-}3b)$$

The solution of the above set of equation exists if the determinant of the coefficient matrix is equal to zero, i.e.,

$$J_m'(\lambda a)\, Y_m'(\lambda b) - J_m'(\lambda b)\, Y_m'(\lambda a) = 0 \qquad (2\text{-}4)$$

The solution to this equation gives infinite values of λ_n for each value of m. Therefore C, D, E, F, and λ will have double subscripts m and n varying between zero and infinity but dropped here for convenience.

From Eq. (2-2a) we have

$$Z'' - Z\lambda^2 = 0$$

the solution of which is

$$Z(z) = A\cosh(\lambda z) + B\sinh(\lambda z) \qquad (2\text{-}5)$$

Applying the boundary condition at the bottom of the tank

$$\left.\frac{\partial Z}{\partial z}\right|_{z=-h} = A\lambda \sinh(-\lambda h) + B\lambda \cosh(-\lambda h) = 0$$

$$B = \frac{A \sinh(\lambda h)}{\cosh(\lambda h)}$$

1364 172

Substituting for B in Eq. (2-5) and simplifying gives

$$Z(z) = \frac{A\left[\cosh(\lambda z + \lambda h)\right]}{\cosh(\lambda h)} \qquad (2\text{-}6)$$

Calculating F from Eq. (2-3a) and substituting in Eq. (2-3) we get

$$R(r) = \frac{E[J_m(\lambda r)\ Y_m'(\lambda a) - J_m'(\lambda a)\ Y_m(\lambda r)]}{Y_m'(\lambda a)} \tag{2-7}$$

Let $\lambda a = \xi$. Substituting in terms of ξ into Eqs. (2-6) and (2-7), we get

$$Z(z) = \frac{A\left[\cosh \xi\left(\frac{z}{a} + \frac{h}{a}\right)\right]}{\cosh\left(\frac{\xi h}{a}\right)} \tag{2-8}$$

$$R(r) = \frac{E\left[J_m\left(\frac{\xi r}{a}\right)\ Y_m'(\xi) - J_m'(\xi)\ Y_m\left(\frac{\xi r}{a}\right)\right]}{Y_m'(\xi)} \tag{2-9}$$

Substituting for R, Θ, Z and T; combining A and E with C and D, and bringing back the subscripts m and n which we omitted for convenience, we have

$$\phi = \sum_{m=0}^{\infty} \sum_{n=0}^{\infty} e^{i\omega_{mn} t}\left[C_{mn}\sin(m\theta) + D_{mn}\cos(m\theta)\right] \frac{\cosh \xi\left(\frac{z}{a} + \frac{h}{a}\right) C_m\left(\xi_{mn}\ \frac{r}{a}\right)}{\cosh\left(\xi_{mn}\ \frac{h}{a}\right) Y_m'(\xi_{mn})} \tag{2-10}$$

where

$$C_m\left(\xi_{mn}\ \frac{r}{a}\right) = J_m\left(\xi_{mn}\ \frac{r}{a}\right) Y_m'(\xi_{mn}) - J_m'(\xi_{mn})\ Y_m\left(\xi_{mn}\ \frac{r}{a}\right) \tag{2-11}$$

and $T(t) = e^{i\omega_{mn} t}$.

To determine the natural frequencies, we now apply the free-surface boundary condition

$$\frac{\partial^2 \phi}{\partial t^2} + g\frac{\partial \phi}{\partial Z} = 0 \qquad \text{at} \qquad Z = 0$$

substituting for $\partial^2\phi/\partial t^2$ and $\partial\phi/\partial z$, we get

$$\sum_{m=0}^{\infty}\sum_{n=0}^{\infty} -\omega_{mn}^2 e^{i\omega_{mn}t}[C_{mn}\sin m\theta + D_{mn}\cos m\theta]\frac{C_m\left(\xi_{mn}\frac{r}{a}\right)}{Y_m'(\xi_{mn})}$$

$$+\frac{g}{a}\sum_{m=0}^{\infty}\sum_{n=0}^{\infty} e^{i\omega_{mn}t}\xi_{mn}[C_{mn}\sin m\theta + D_{mn}\cos m\theta]\frac{C_m\left(\xi_{mn}\frac{r}{a}\right)\tanh\left(\xi_{mn}\frac{h}{a}\right)}{Y_m'(\xi_{mn})} = 0$$

comparing the coefficients, we have

$$\omega_{mn}^2 = \left(\frac{g}{a}\right)\xi_{mn}\tanh\left(\xi_{mn}\frac{h}{a}\right) \qquad (2\text{-}12)$$

Equations (2-12) and (2-11) give sloshing frequencies and mode shapes of water in a circular annular tank. Equation (2-10) gives the velocity potential for free vibration and the values of the constants C_{mn} and D_{mn} will be determined by initial conditions.

2.5 Sloshing Response for Arbitrary Ground Motions

Equation (2-1), with the boundary conditions given in Section 2-3, will be solved for the velocity potential ϕ which can then be used to derive displacements velocities and pressures anywhere in the fluid.

Since the boundary conditions are non-homogeneous, assume a solution of the form

$$\phi(r,\theta,z,t) = \phi_1(r,\theta,z,t) + \phi_c(r,\theta,t) \qquad (2\text{-}13)$$

ϕ_c is taken independent of z because of the rigid tank walls.

$$\frac{\partial\phi}{\partial r} = \frac{\partial\phi_1}{\partial r} + \frac{\partial\phi_c}{\partial r} = \dot{x}\cos\theta \qquad \text{at} \quad r = a \quad \text{and} \quad r = b$$

Let

$$\frac{\partial \phi_c}{\partial r} = \dot{x} \cos \theta$$

then

$$\frac{\partial \phi_1}{\partial r} = 0 \qquad \text{at} \quad r = a \quad \text{and} \quad r = b$$

Substituting Eq. (2-13) into Eq. (2-1), we have

$$\left[\frac{\partial^2 \phi_1}{\partial r^2} + \frac{\partial^2 \phi_c}{\partial r^2}\right] + \frac{1}{r}\left[\frac{\partial \phi_1}{\partial r} + \frac{\partial \phi_c}{\partial r}\right] + \frac{1}{r^2}\left[\frac{\partial^2 \phi_1}{\partial \theta^2} + \frac{\partial^2 \phi_c}{\partial \theta^2}\right] + \frac{\partial^2 \phi_1}{\partial z^2} = 0$$

or

$$\frac{\partial^2 \phi_1}{\partial r^2} + \frac{1}{r}\frac{\partial \phi_1}{\partial r} + \frac{1}{r^2}\frac{\partial^2 \phi_1}{\partial \theta^2} + \frac{\partial^2 \phi_1}{\partial z^2} = 0 \qquad (2\text{-}14)$$

with the boundary conditions

$$\left.\frac{\partial \phi_1}{\partial r}\right|_{r=a} = 0$$

$$\left.\frac{\partial \phi_1}{\partial r}\right|_{r=b} = 0$$

$$\left.\frac{\partial \phi_1}{\partial z}\right|_{z=-h} = 0$$

and

$$\frac{\partial^2 \phi_c}{\partial r^2} + \frac{1}{r}\frac{\partial \phi_c}{\partial r} + \frac{1}{r^2}\frac{\partial^2 \phi_c}{\partial \theta^2} = 0 \qquad (2\text{-}15)$$

with the boundary conditions

$$\left.\frac{\partial \phi_c}{\partial r}\right|_{r=a} = \dot{x} \cos \theta$$

$$\left.\frac{\partial \phi_c}{\partial r}\right|_{r=b} = \dot{x} \cos \theta$$

Assume

$$\phi_c = R(r)\ \Theta(\theta)\ T(t)$$

Substitute in Eq. (2-15)

$$\frac{\partial^2 R}{\partial r^2}\Theta T + \frac{1}{r}\frac{\partial R}{\partial r}\Theta T + \frac{1}{r^2}\frac{\partial^2 \Theta}{\partial \theta} RT = 0$$

or

$$\frac{r^2}{R}\frac{\partial^2 R}{\partial r^2} + \frac{r}{R}\frac{\partial R}{\partial r} = -\frac{\partial^2 \Theta}{\Theta \partial \theta^2} = +\nu^2$$

Therefore we have

$$\frac{r^2}{R}\frac{d^2 R}{dr^2} + \frac{r}{R}\frac{dR}{dr} - \nu^2 = 0 \qquad (2\text{-}16)$$

and

$$\frac{d^2 \Theta}{d\theta^2} + \nu^2 \Theta = 0 \qquad (2\text{-}17)$$

The solution of Eq. (2-17) will be

$$\Theta = A \cos \nu\theta + B \sin \nu\theta \qquad (2\text{-}18)$$

with boundary conditions at r = a and r = b

$$\frac{\partial \phi}{\partial r} = \frac{\partial R}{\partial r} \cdot \Theta \cdot T = \dot{x} \cos \theta \quad \rightarrow$$

Therefore

$$\Theta(\theta) = \cos\theta = A \cos \nu\theta + B \sin \nu\theta \qquad (2\text{-}19)$$

and $$T(t) = \dot{x}$$

From Eq. (2-19), $A = \nu = 1$, and $B = 0$. Now consider Eq. (2-16),

$$\frac{r^2}{R} \frac{d^2R}{dr^2} + \frac{r}{R} \frac{dR}{dr} - 1 = 0$$

$$r^2 \frac{d^2R}{dr^2} + r \frac{dR}{dr} - R = 0 \qquad (2\text{-}20)$$

This is the Cauchy equation, and the solution will be of the form $R = r^K$. Substituting in Eq. (2-20),

$$K(K-1)r^K + Kr^K - r^K = 0$$

$$K^2 - 1 = 0 \qquad \text{giving} \qquad K = \pm 1$$

$$R(r) = C_1 r + C_2 r^{-1}$$

$$\frac{\partial R}{\partial r} = C_1 - C_2 r^{-2}$$

$$\frac{\partial \phi}{\partial r} = \frac{\partial R}{\partial r} \cdot \Theta \cdot T$$

$$\left.\frac{\partial \phi}{\partial r}\right|_{r=a} = \dot{x} \cos \theta = \dot{x} \cos \theta (C_1 - C_2 r^{-2})$$

Comparing the coefficients

$$C_1 = 1$$

$$C_2 = 0$$

Therefore

$$\phi_c = R\Theta T = \dot{x}\, r \cos\theta \tag{2-21}$$

Now consider the free-surface boundary condition

$$\frac{\partial^2\phi}{\partial t^2} + g\,\frac{\partial\phi}{\partial z} = 0 \qquad \text{at} \qquad Z = 0$$

$$\frac{\partial^2\phi_1}{\partial t^2} + \frac{\partial^2\phi_c}{\partial t^2} + g\,\frac{\partial\phi_1}{\partial z} = 0$$

$$\frac{\partial^2\phi_1}{\partial t^2} + g\,\frac{\partial\phi_1}{\partial z}\bigg|_{z=0} = -\frac{\partial^2\phi_c}{\partial t^2} = -\ddot{x}\, r\cos\theta \tag{2-22}$$

Therefore we have to solve Eq. (2-14) with the additional boundary condition at the free surface given by Eq. (2-22).

Equation (2-14) is similar to Eq. (2-1) and the boundary conditions at the walls and bottom of the tank are the same in both cases. Therefore the general form of the solution in these two cases will be similar except that the time function T(t) will be different for the solution of Eq. (2-14) which was simply harmonic for the free vibration case. Thus the solution of Eq. (2-14) will be of the form

$$\phi_1 = \sum_{m=0}^{\infty}\sum_{n=0}^{\infty}\left[C_{mn}\sin m\theta + D_{mn}\cos m\theta\right]\frac{\cosh\xi_{mn}\left(\frac{z}{a}+\frac{h}{a}\right)C_m\left(\xi_{mn}\frac{r}{a}\right)T_{mn}(t)}{Y'_m(\xi_{mn})\cosh\left(\xi_{mn}\frac{h}{a}\right)} \tag{2-23}$$

The above is the general solution and covers all types of modes. It should be noted, however, that the horizontal ground motion which we are considering at present does not excite all types of modes. It will excite only antisymmetric modes which correspond to an m value equal to 1. Therefore we can drop the sum on m and it is understood that in all subsequent equations we are referring only to the class of modes which correspond to m = 1 and which are antisymmetric about an axis perpendicular to the axis of excitation. Thus ϕ_1 becomes

$$\phi_1 = \sum_{n=0}^{\infty} \frac{[C_n \sin\theta + D_n \cos\theta] \cosh \xi_n\left(\frac{z}{a} + \frac{h}{a}\right) C_1\left(\xi_n \frac{r}{a}\right) T_n(t)}{Y_1'(\xi_n) \cosh\left(\xi_n \frac{h}{a}\right)} \qquad (2\text{-}24)$$

where

$$C_1\left(\xi_n \frac{r}{a}\right) = J_1\left(\xi_n \frac{r}{a}\right) Y_1'(\xi_n) - J_1'(\xi_n) Y_1\left(\xi_n \frac{r}{a}\right) \qquad (2\text{-}25)$$

and ξ_n are the roots of the equation.

$$J_1'(\xi)\ Y_1'(K\xi) - J_1'(K\xi)\ Y_1'(\xi) = 0 \qquad (2\text{-}26)$$

wnere K = b/a.

$T_n(t)$ are the time functions yet to be determined. C_n and D_n are the constants to be determined from the initial conditions. Now we apply the free-surface (z = 0) boundary condition given by Eq. (2-22) and we have

$$\sum_{n=0}^{\infty} \frac{[C_n \sin\theta + D_n \cos\theta] \cosh\left(\xi_n \frac{h}{a}\right) C_1\left(\xi_n \frac{r}{a}\right) \ddot{T}_n}{Y_1'(\xi_n) \cosh\left(\xi_n \frac{h}{a}\right)}$$

1251 179

$$+ \frac{g}{a} \sum_{n=0}^{\infty} \xi_n [C_n \sin\theta + D_n \cos\theta] \frac{\sinh\left(\xi_n \frac{h}{a}\right) C_1\left(\xi_n \frac{r}{a}\right) T_n}{Y_1'(\xi_n) \cosh\left(\xi_n \frac{h}{a}\right)} = -r \cos\theta\, \ddot{x}$$

gathering sin and cos terms and dividing both sides by a

$$\frac{1}{a}\sum_{n=0}^{\infty} C_n \sin\theta\, C_1\left(\xi_n \frac{r}{a}\right)\frac{\left[\ddot{T}_n + \frac{g}{a}\xi_n \tanh\left(\xi_n \frac{h}{a}\right) T_n\right]}{Y_1'(\xi_n)}$$

$$+\frac{1}{a}\sum_{n=0}^{\infty} D_n \cos\theta\, C_1\left(\xi_n \frac{r}{a}\right)\frac{\left[\ddot{T}_n + \frac{g}{a}\xi_n \tanh\left(\xi_n \frac{h}{a}\right) T_n\right]}{Y_1'(\xi_n)} = -\frac{r}{a}\cos\theta\, \dddot{x} \qquad (2\text{-}27)$$

Now we want to express r/a as Bessel's Fourier series in terms of $C_1(\xi_n\, r/a)$ using the orthogonality property of the eigenfunctions

$$\frac{r}{a} = \sum_{n=0}^{\infty} A_n C_1\left(\xi_n \frac{r}{a}\right) = A_0 C_1\left(\xi_0 \frac{r}{a}\right) + A_1 C_1\left(\xi_1 \frac{r}{a}\right) + \ldots + A_n C_1\left(\xi_n \frac{r}{a}\right) + \ldots$$

Multiplying both sides by $rC_1(\xi_n\, r/a)$ and integrating within the limit b to a, we have

$$\int_b^a \frac{r^2}{a} C_1\left(\xi_n \frac{r}{a}\right) dr = 0 + 0 + \ldots. + A_n \int_b^a rC_1^2\left(\xi_n \frac{r}{a}\right) dr + 0 + \ldots$$

Substituting for $C_1(\xi_n\, r/a)$ from Eq. (2-25) into the above equation, integrating within the limits b to a and simplifying gives the values of the constants A_n determined by the equation

$$A_n = \frac{2\left[\frac{2}{\pi\xi_n} - KC_1(K\xi_n)\right]}{\frac{4}{\pi^2}\xi_n^2(\xi_n^2 - 1) + C_1^2(K\xi_n)\left[1 - K^2\xi_n^2\right]} \qquad (2\text{-}28)$$

thus

1364 180

$$\frac{r}{a} = \sum_{n=0}^{\infty} A_n C_1\left(\xi_n \frac{r}{a}\right) \qquad (2\text{-}29)$$

where A_n are given by Eq. (2-28). Substituting for r/a into Eq. (2-27) we have

$$\frac{1}{a}\sum_{n=0}^{\infty}\left[C_n \sin\theta\right] C_1\left(\xi_n \frac{r}{a}\right) \frac{\left[\ddot{T}_n + \frac{g}{a}\xi_n \tanh\left(\xi_n \frac{h}{a}\right) T_n\right]}{Y_1'(\xi_n)}$$

$$+ \frac{1}{a}\sum_{n=0}^{\infty} \frac{D_n \cos\theta\, C_1\left(\xi_n \frac{r}{a}\right)\left[\ddot{T}_n + \frac{g}{a}\xi_n \tanh\left(\xi_n \frac{h}{a}\right) T_n\right]}{Y_1'(\xi_n)}$$

$$= -\sum_{n=0}^{\infty} A_n \cos\theta\, C_1\left(\xi_n \frac{r}{a}\right) \dddot{x} \qquad (2\text{-}30)$$

comparing coefficients, it is clear that

$$\frac{D_n}{a} \frac{\left[\ddot{T}_n + \frac{g}{a}\xi_n \tanh\left(\xi_n \frac{h}{a}\right) T_n\right]}{Y_1'(\xi_n)} = -A_n \dddot{x}$$

or

$$\ddot{T}_n + \omega_n^2 T_n = -\frac{a}{D_n} Y_1'(\xi_n) A_n \dddot{x} = E_n \dddot{x} \qquad (2\text{-}31)$$

where

$$\omega_n^2 = \frac{g}{a}\xi_n \tanh\left(\xi_n \frac{h}{a}\right) \qquad (2\text{-}32)$$

and

$$E_n = -\frac{a}{D_n} Y_1'(\xi_n) A_n$$

since

$$\ddot{T}_n + \frac{g}{a} \xi_n \tanh\left(\xi_n \frac{h}{a}\right) T_n \neq 0$$

therefore $C_n = 0$.

Equation (2-31) is a second order ordinary non-homogenous equation, whose homogenous solution will be

$$T_n = F_n \sin \omega_n t + G_n \cos \omega_n t$$

Let

$$Y_p = \text{particular solution}$$

then

$$Y_p = U_1(t) \sin \omega_n t + U_2(t) \cos \omega_n t$$

using variation of parameters, we have

$$U_1 = \int_0^t \frac{E_n}{\omega_n} \cos \omega_n \tau \, \ddot{x} \, d\tau$$

$$U_2 = -\int_0^t \frac{E_n}{\omega_n} \sin \omega_n \tau \, \ddot{x} \, d\tau$$

Therefore the general solution for T_n will be

$$T_n = F_n \sin \omega_n t + G_n \cos \omega_n t + \frac{E_n}{\omega_n} \sin \omega_n t \int_0^t \ddot{x}(\tau) \cos \omega_n \tau \, d\tau$$

$$- \frac{E_n}{\omega_n} \cos \omega_n t \int_0^t x(\tau) \sin \omega_n \tau \, d\tau \qquad (2\text{-}33)$$

Thus the solution for ϕ_1 becomes

$$\phi_1 = \sum_{n=0}^{\infty} \frac{\cos\theta \cosh \xi_n \left(\frac{z}{a} + \frac{h}{a}\right) C_1\left(\xi_n \frac{r}{a}\right) T_n(t)}{Y_1'(\xi_n) \cosh\left(\xi_n \frac{h}{a}\right)} \tag{2-34}$$

where T_n is given by Eq. (2-33) and $C_1(\xi_n\, r/a)$ is given by Eq. (2-25). Now, using Eq. (2-13) we have the solution of the Laplace equation with time-dependent horizontal boundary conditions. The solution for ϕ will be obtained by Eqs. (2-21) and (2-34). Thus

$$\phi = r\cos\theta\, \dot{x} + \sum_{n=0}^{\infty} \frac{\cos\theta \cosh \xi_n \left(\frac{z}{a} + \frac{h}{a}\right) C_1\left(\xi_n \frac{r}{a}\right)}{Y_1'(\xi_n) \cosh\left(\xi_n \frac{h}{a}\right)}$$

$$\cdot \left[F_n \sin\omega_n t + G_n \cos\omega_n t + \frac{E_n}{\omega_n} \sin\omega_n t \int_0^t \dddot{x}(\tau) \cos\omega_n \tau\, d\tau \right.$$

$$\left. - \frac{E_n}{\omega_n} \cos\omega_n t \int_0^t \dddot{x}(\tau) \sin\omega_n \tau\, d\tau \right]$$

Now apply the initial ("at rest") conditions

(1) $\phi(r,\theta,z,0) = 0$

(2) $\frac{\partial\phi}{\partial t}(r,\theta,z,0) = 0$

using conditions (1) and (2), $F_n = G_n = 0$

$$\phi = r\cos\theta\, \dot{x} + \sum_{n=0}^{\infty} \frac{\cos\theta \cosh \xi_n \left(\frac{z}{a} + \frac{h}{a}\right) C_1\left(\xi_n \frac{r}{a}\right)}{Y_1'(\xi_n) \cosh\left(\xi_n \frac{h}{a}\right)}$$

$$\cdot \left[\frac{E_n}{\omega_n} \sin\omega_n t \int_0^t \dddot{x} \cos\omega_n \tau\, d\tau - \frac{E_n}{\omega_n} \cos\omega_n t \int_0^t \dddot{x} \sin\omega_n \tau\, d\tau \right]$$

substituting for E_n and rearranging the above equation,

$$\phi = \cos\theta \left\{ r\dot{x} - a \sum_{n=0}^{\infty} A_n \frac{\cosh \xi_n \left(\frac{z}{a} + \frac{h}{a}\right) C_1\left(\xi_n \frac{r}{a}\right)}{\omega_n \cosh\left(\xi_n \frac{h}{a}\right)} \right.$$

$$\left. \cdot \left[\sin \omega_n t \int_0^t \ddot{x} \cos \omega_n \tau \, d\tau - \cos \omega_n t \int_0^t \ddot{x} \sin \omega_n \tau \, d\tau \right] \right\} \qquad (2\text{-}35)$$

where A_n and $C_1(\xi_n \, r/a)$ are given by Eqs. (2-28) and (2-25), respectively. Equation (2-35) is the expression for the velocity potential in an annular-circular tank and will be used to derive the displacements, velocities, and pressures at any point in the liquid.

2.6 Derivation of Displacements, Velocities and Dynamic Pressures

Once the expression for the velocity potential is known, we can easily derive the fluid displacements, velocities, and dynamic pressures anywhere in the fluid. Let

δ = fluid displacement

U_r = fluid velocity in the direction of r

U_θ = fluid velocity in the direction of θ

U_z = fluid velocity in the direction of z

p = dynamic pressure

then

$$\delta(r,\theta,z,t) = -\frac{1}{g} \frac{\partial \phi}{\partial t} (r,\theta,z,t)$$

$$U_r(r,\theta,z,t) = \frac{\partial \phi}{\partial r} (r,\theta,z,t)$$

$$U_\theta(r,\theta,z,t) = \frac{1}{r}\frac{\partial\phi(r,\theta,z,t)}{\partial\theta}$$

$$U_z(r,\theta,z,t) = \frac{\partial\phi(r,\theta,z,t)}{\partial z}$$

$$p(r,\theta,z,t) = -\rho\frac{\partial\phi(r,\theta,z,t)}{\partial t}$$

where ρ = density of the fluid. From Eq. (2-35) we have

$$\frac{\partial\phi}{\partial t} = \cos\theta\left\{r\ddot{x} - a\sum_{n=0}^{\infty} A_n \frac{\cosh\xi_n\left(\frac{z}{a}+\frac{h}{a}\right) C_1\left(\xi_n\frac{r}{a}\right)}{\cosh\left(\xi_n\frac{h}{a}\right)}\right.$$

$$\left.\cdot\left[\cos\omega_n t\int_0^t \dddot{x}(\tau)\cos\omega_n\tau\,d\tau + \sin\omega_n\tau\int_0^t \dddot{x}(\tau)\sin\omega_n\tau\,d\tau\right]\right\} \quad (2\text{-}36)$$

Thus general expressions for δ and p become

$$\delta(r,\theta,z,t) = -\frac{\cos\theta}{g}\left\{r\ddot{x} - a\sum_{n=0}^{\infty} A_n \frac{\cosh\xi_n\left(\frac{z}{a}+\frac{h}{a}\right) C_1\left(\xi_n\frac{r}{a}\right)}{\cosh\left(\xi_n\frac{h}{a}\right)}\right.$$

$$\left.\cdot\left[\cos\omega_n t\int_0^t \dddot{x}\cos\omega_n\tau\,d\tau + \sin\omega_n t\int_0^t \ddot{x}\sin\omega_n\tau\,d\tau\right]\right\} \quad (2\text{-}37)$$

$$p(r,\theta,z,t) = -\rho\cos\theta\left\{r\ddot{x} - a\sum_{n=0}^{\infty} A_n \frac{\cosh\xi_n\left(\frac{z}{a}+\frac{h}{a}\right) C_1\,\xi_n\frac{r}{a}}{\cosh\left(\xi_n\frac{h}{a}\right)}\right.$$

$$\left.\cdot\left[\cos\omega_n t\int_0^t \dddot{x}\cos\omega_n\tau\,d\tau + \sin\omega_n t\int_0^t \dddot{x}\sin\omega_n\tau\,d\tau\right]\right\} \quad (2\text{-}38)$$

where A_n, C_1, ξ_n, and ω_n are given by Eqs. (2-28), (2-25), (2-26), and (2-32), respectively.

Similar expressions can be derived for velocity components U_r, U_θ, and U_z from Eq. (2-35).

2.7 Steady-State Response

Let the ground acceleration $\ddot{x} = x_o \sin \omega_o t$, where x_o = amplitude of the ground acceleration, and ω_o = circular frequency of the ground motion. Substituting for $\ddot{x}$ in Eq. (2-37) and simplifying, we get

$$\delta(r,\theta,z,t) = -\frac{\cos\theta}{g}\left\{ r\ddot{x} - a\sum_{n=0}^{\infty} A_n \frac{\cosh \xi_n \left(\frac{z}{a}+\frac{h}{a}\right) C_1\left(\xi_n \frac{r}{a}\right)}{\cosh\left(\xi \frac{h}{a}\right)} \cdot \left[-\frac{x_o \sin \omega_o t}{\left(\frac{\omega_n}{\omega_o}\right)^2 - 1} + \frac{x_o \sin \omega_n t}{\frac{\omega_n}{\omega_o} - \frac{\omega_o}{\omega_n}} \right] \right\} \qquad (2\text{-}39)$$

The term $x_o \sin \omega_n t/[\omega_n/\omega_o - \omega_o/\omega_n]$ in Eq. (2-39) is the transient term. If the sinusoidal ground motion is applied for a sufficiently long period of time the transient motion will disappear due to the small damping present in the system and the sloshing response of the fluid will become steady state. Thus the steady-state response of the fluid displacements will be given by the following equation:

$$\delta(r,\theta,z,t) = -\frac{\cos\theta}{g}\left\{ r x_o \sin \omega_o - a\sum_{n=0}^{\infty} A_n \frac{\cosh \xi_n \left(\frac{z}{a}+\frac{h}{a}\right) C_1\left(\xi_n \frac{r}{a}\right)}{\cosh\left(\xi_n \frac{h}{a}\right)} \cdot \left[-\frac{x_o \sin \omega_o t}{\left(\frac{\omega_n}{\omega_o}\right)^2 - 1} \right] \right\} \qquad (2\text{-}39a)$$

This equation will give good results for steady-state response under sinusoidal ground acceleration as long as one of the sloshing frequencies ω_n is not too close to the frequency of the ground motion ω_o and if $\omega_n = \omega_o$, then resonance occurs and the solution given by Eq. (2-39) becomes infinite. This was understood as the damping was assumed to be zero to begin with.

Similarly, steady-state pressure response will be given by

$$p(r,\theta,z,t) = -\rho \cos\theta \left\{ r\, x_o \sin \omega_o - a \sum_{n=0}^{\infty} A_n \frac{\cosh \xi_n\left(\frac{z}{a} + \frac{h}{a}\right) C_1\left(\xi_n \frac{r}{a}\right)}{\cosh\left(\xi_n \frac{h}{a}\right)} \cdot \left[- \frac{x_o \sin \omega_o t}{\left(\frac{\omega_n}{\omega_o}\right)^2 - 1} \right] \right\} \qquad (2\text{-}40)$$

2.8 Approximate Analysis for Natural Frequencies

A simple approximation for determining the sloshing frequencies in an annular tank can be determined from the classical solution for sloshing in a rectangular tank of length 2ℓ and water depth h. This solution has a further advantage in that it stays close to the physical aspects of the problem and enables simple physical arguments to be made for the correct design of a damping system and also enables the more precise solutions to be understood physically.

The first sloshing frequency in a rectangular tank (see Fig. 2-1) is given by

$$\omega_1^2 = \sqrt{\frac{5}{2}}\, \frac{g}{\ell} \tanh \sqrt{\frac{5}{2}}\, \frac{h}{\ell}$$

and this one relationship can be used to estimate all of the sloshing frequencies in the annular tank as follows.

It is assumed that the radial and tangential water particle motions are uncoupled, that is, for any natural mode the particle motion is either (a) tangential, or (b) radial. This assumption leads to all three types of sloshing modes.

2.8.1 Tangential motion

In this case the wavelength is measured on the mid-circumference of the water surface, at a radius of $C = (a+b)/2$. Using symmetry conditions the node and anti-node points of the mode can be determined by inspection. The first four such modes are indicated in Fig. 2-2, with H and L indicating the high and low lines of the water surface, and 0 representing a zero line (see Fig. 2-2). The following can be deduced from this simple approximation:

a) For any mode n the half wavelength is given by $2\ell = \pi c/n$.

b) The even-numbered modes cannot be excited by horizontal ground motion.

c) In the odd-numbered modes, mode 1 will be strongly excited by horizontal ground motion, mode 3 very little, and as the mode number increases, the participation reduces.

Observations a) and b) agree with test observations. It was found extremely difficult to excite any of the tangential modes by horizontal table motion with the obvious exception of mode 1.

d) In any tangential mode the water surface gradient on any radius is almost zero. This was observed in mode 1.

2.8.2 Radial motion

In the simplest form of radial motion, the lines of equal water-surface elevation are circumferential. Taking an element of the water between two closely spaced radii, the length of the equivalent rectangular tank is a-b. Hence there is a family of mode shapes given by the half wavelength $2\ell = (a-b)/n$, where n is the node number. The first three such modes are indicated below as radial symmetric modes (Fig. 2-3). Clearly there is a closely related set of modes (when considering horizontal ground motion) of the same frequencies and mode shapes on any radius, but whose distribution of displacement is antisymmetric across a diameter. These are indicated as radial antisymmetric modes (Fig. 2-3). The accuracy of these simple approximations can be seen in Table 2-1 which shows the approximate and exact values for the sloshing frequencies in two different tanks at two different water levels. The following can be deduced from this simple approximation:

a) For any mode n, the half wavelength is given by $2\ell = (a-b)/n$.

b) In comparing this with sloshing in a rectangular tank, it should be noted that the boundaries of the water element in this case are not parallel as they are radii. Hence it can be expected that the vertical water displacement on the inner boundary will be greater than on the outer boundary. This was verified by both observation and the exact analysis (see Fig. 4-5).

c) Horizontal ground motion will not excite any of the radial symmetric modes.

d) Horizontal ground motion will excite the odd-numbered

radial antisymmetric modes, there being a decreasing chance of this as the mode number increases.

e) In the radial antisymmetric modes there are circumferential water surface gradients as well as radial gradients, and clearly provided the radial gradients predominate, the approximation will be valid. As the inner radius b is reduced the ratio of radial/circumferential gradient reduces and hence the approximation is likely to get less precise. However, even when $a/b = 3$ as in the case of Model 2, the results are still remarkably accurate.

f) An understanding of the direction of water particle motion associated with each mode which comes from this approximate analysis is essential when designing damping devices. Radial dampers are required to reduce circumferential motion and circumferential dampers are required to reduce radial motion. To reduce seismic response, both are required.

TABLE 2-1. Comparison of approximate and exact sloshing frequencies for Models 1 and 2.

	Natural Sloshing Frequencies (Hz)			
	Model 1		Model 2	
	Approx	Exact	Approx	Exact
water depth = 3 in.				
First antisymmetric circumferential	0.70	0.70	0.87	0.88
First antisymmetric radial	3.16	3.17	2.16	2.31
Second antisymmetric radial	4.47	4.47	3.18	3.22
Third antisymmetric radial	5.48	5.47	3.90	3.92
water depth = 5 in.				
First antisymmetric circumferential	0.87	0.87	1.05	1.07
First antisymmetric radial	3.16	3.18	2.24	2.37
Second antisymmetric radial	4.47	4.50	3.19	3.22
Third antisymmetric radial	5.48	5.51	3.90	3.91

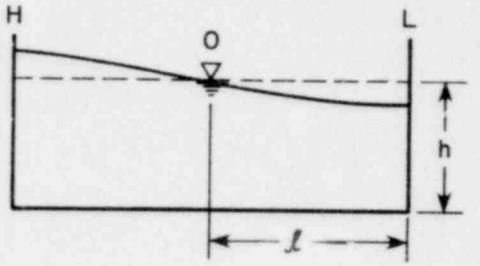

FIG. 2-1 RECTANGULAR TANK

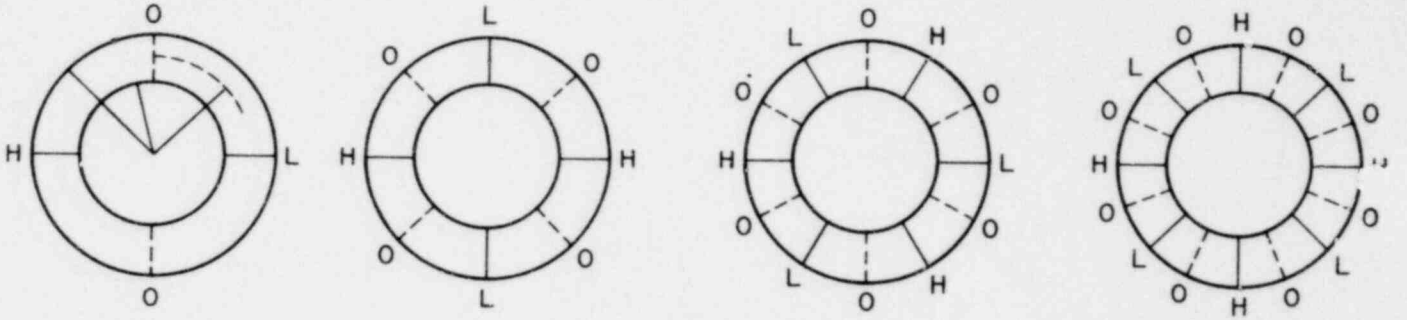

FIG. 2-2 TANGENTIAL MODES

XBL 7812-13916

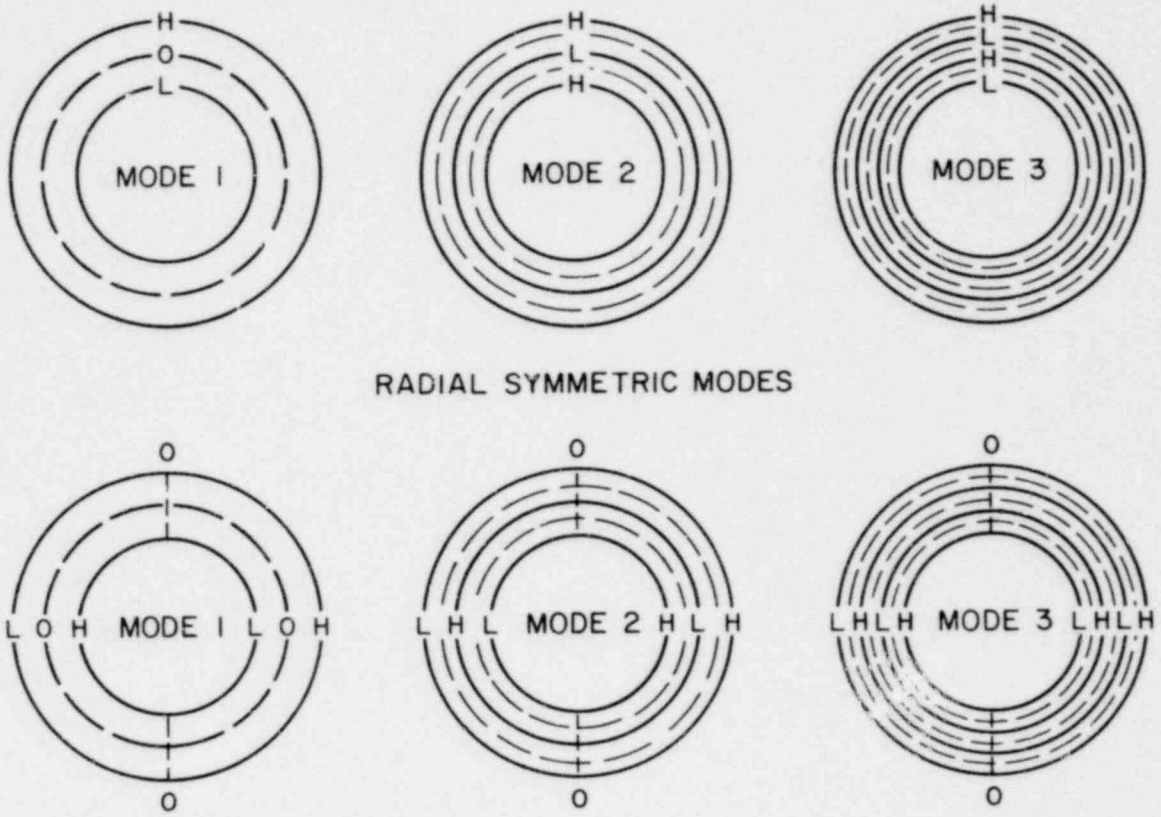

FIG. 2-3 RADIAL MODES

XBL 7812-13915

3. SLOSHING RESPONSE ANALYSIS WITH THE COMPUTER PROGRAM "SLOSH"

3.1 Computer Program SLOSH

A computer program named SLOSH was developed to solve for the sloshing response of water in annular or simple-circular tanks under actual earthquake ground accelerations. The program determines a pre-specified number of sloshing frequencies and mode shapes and gives the displacements of water at the free surface. It also determines the pressure variations with depth along the walls of the tanks.

The frequencies are determined by solving Eq. (2-32) and the values of ξ_n in that equation are substituted by solving Eq. (2-26) which involves the derivatives of Bessel functions of the first and second kind. This equation which would be satisfied for an infinite values of ξ_n was solved by trial and error for the required number of modes. Corresponding mode shapes were determined by using Eq. (2-25). It should be noted that Eqs. (2-25) and (2-26) give mode shapes and frequencies which are anti-symmetric about an axis perpendicular to the axis of ground excitation. These are the only modes which are excited by horizontal ground motion and they correspond to Bessel functions of order 1 as can be seen in Eqs. (2-25) and (2-26). The modes of this type will be termed as modes of class 1, as they correspond to Bessel functions of order 1.

Another class of modes which corresponds to Bessel functions of order zero in Eqs. (2-25) and (2-26) will be presented here. This class of modes will be termed as modes of class 0. Modes of class 0 are symmetrical about z-axis (see Fig. 1-1) and they have a close relationship with the modes of class 1. Frequencies and mode shapes of class 0 were

determined by equations similar to Eqs. (2-25, (2-26), and (2-32) except that 1 was replaced by 0 in those equations.

The computer program calculates displacements of water at Section A-A shown in Fig. 1-1. At this section $z = 0$ and $\theta = 0$ and r varies between b and a. Displacements were determined at thirteen points along Section A-A, giving a complete profile at that section. Profile of water surface at any other section can be determined by simply multiplying with $\cos\theta$. Thus in this way a complete profile of the surface becomes known.

Since the earthquake input is usually given in the form of acceleration, Eq. (2-37) was reduced to the following form to determine the displacements of water at the free surface.

$$\delta(r,0,0,t) = -\frac{1}{g}\left\{ r\ddot{x} - a\sum_{n=0}^{\infty} A_n C_1\left(\xi_n \frac{r}{a}\right)\left[\ddot{x}(t) + \omega_n \cos\omega_n t\int_0^t \ddot{x}(\tau)\sin\omega_n\tau\, d\tau - \omega_n \sin\omega_n t\int_0^t \ddot{x}(\tau)\cos\omega_n\tau\, d\tau\right]\right\} \quad (3\text{-}1)$$

From the digitized earthquake accelerograms, numerical integration is carried out to evaluate the integrals in Eq. (3-1) for each mode of vibration and the values of $C_1(\xi_n\, r/a)$ are calculated at thirteen different locations between the radii a and b for each mode and the summation is carried out over the significant number of modes. It was found that the convergence is fast and only the first few modes contribute more than 99% of the sloshing response. Usually the first ten modes were included for this analysis.

The computer program SLOSH determines the pressures at thirteen points along the depth at inner and outer walls at Section A-A (Fig. 1-1), i.e., at $\theta = 0$. To calculate the pressures at the walls the general equation for pressure [Eq. (2-38)] was used. Substituting for $r = a$ and $r = b$, respectively, and integrating by parts we get the pressures at the outer and inner walls given by the following two equations:

$$p(a,0,z,t) = -\rho \left[a\ddot{x} - a \sum_{n=0}^{\infty} \frac{A_n \cosh \xi_n \left(\frac{z}{a} + \frac{h}{a}\right)}{\cosh \left(\xi_n \frac{h}{a}\right)} C_1(\xi_n) \left\{ \ddot{x}(t) + \omega_n \cos \omega_n t \int_0^t \ddot{x}(\tau) \sin \omega_n \tau \, d\tau - \omega_n \sin \omega_n t \int_0^t \ddot{x}(\tau) \cos \omega_n \tau \, d\tau \right\} \right] \tag{3-2}$$

and

$$p(b,0,z,t) = -\rho \left[b\ddot{x} - a \sum_{n=0}^{\infty} A_n \frac{\cosh \xi_n \left(\frac{z}{a} + \frac{h}{a}\right) C_1(K\xi_n)}{\cosh \left(\xi_n \frac{h}{a}\right)} \left\{ \ddot{x}(t) + \omega_n \cos \omega_n t \int_0^t \ddot{x}(\tau) \sin \omega_n \tau \, d\tau - \omega_n \sin \omega_n t \int_0^t \ddot{x}(\tau) \cos \omega_n \tau \, d\tau \right\} \right] \tag{3-3}$$

These equation were solved numerically as before for thirteen different values of z between 0 and h, to get a complete distribution of the pressure variation along the depth at the inner and outer walls. Once a complete distribution of the pressure variation is known for Section A-A in Fig. 1-1 (i.e., for $\theta = 0$), the pressure variation along any other section at the inner and outer walls can be determined by multiplying the pressures

at Section A-A (i.e., the section along the ground excitation) by $\cos\theta$. Thus the pressure distributions become known everywhere along the walls of the tank. Note that the pressures given by Eqs. (3-2) and (3-3) are the dynamic pressure only, and to get the total pressure at a point the static pressure must be added to the dynamic pressure.

The computer program SLOSH reads in the dimensionsof the tank and the digitized accelerogram and prints out the natural frequencies and mode shapes. Water surface displacements at various radii along the axis of excitation and the pressures along the inner and outer walls at various depths at Section A-A (Fig. 1-1) are also printed at each interval of time. Time of maximum displacement and the water surface profile at that moment are also printed. Maximum pressures are also printed.

A time-history Calcomp plot of the displacements of water surfaces at the inner and outer walls is also plotted on the computer for a visual inspection. Similarly, time-history Calcomp plots of maximum pressures are also plotted on the computer. These maximum pressures occur at the bottom of the inner and outer walls along the axis of excitation.

3.2 Mode Shapes and Frequencies Computed by SLOSH

Figures 3-1 and 3-2 show the mode shapes of antisymmetric (modes of class 1) and symmetric modes (modes of class 0) in an annular tank having a b/a ratio of 0.667. The antisymmetric-mode shapes in Fig. 3-1 which represent the first four modes are at Section A-A of Fig. 1-1, and the water surface profile at any other section will be given as a function of $\cos\theta$ where θ is the angle between that section and Section A-A. This

is not true however for the symmetric-mode shapes shown in Fig. 3-2 where the profile of water surface for any section in the annulus of the tank will be the same. This can also be seen in Fig. 3-3. Figure 3-3(a) shows water at rest in an annular tank, whereas Fig. 3-3(b) and 3-3(d) show the first and second modes of vibration of antisymmetric modes, respectively. It should be noted that in all of these modes the water surface profiles at a section perpendicular to Section A-A remain at initial water surface levels and the water surface displacements in the z direction are zero. Figure 3-3(c) shows the first symmetric mode of vibration indicating same water surface profiles at each section, making the mode symmetrical about the z-axis. It can also be noted that the modes of class 1 are antisymmetric about the section which is perpendicular to A-A and that is why they are called here antisymmetric modes.

Although the symmetric modes cannot be produced by horizontal ground motions and thus they do not contribute to the sloshing response in circular tanks, they do have a close relationship with the antisymmetric modes, and that is why they have been presented here. This close relationship between the mode shapes and frequencies of class 0 and class 1 can be seen in Figs. 3-1 and 3-2 and Table 3-1. Table 3-1 shows the natural sloshing frequencies in a typical prototype structure where the inner and outer radii are 60 ft and 40 ft and the depth of water is 20 ft. It can be seen that the second, third, fourth .... frequencies in the antisymmetric modes agree (to the second figure accuracy) with the first, second, third ... frequencies of the symmetric modes respectively. The same holds true for the mode shapes when we compare Figs. 3-1 and 3-2.

From the above fact, it is clear that under certain circumstances

TABLE 3-1. Sloshing frequencies of prototype (a = 60', b = 40', h = 20') modes of class 1 and 0.

Frequency number	Frequency in (Hz)	
	Antisymmetric modes (class 1)	Symmetric modes (class 0)
1	0.079	0.36
2	0.36	0.51
3	0.51	0.62
4	0.62	0.72
5	0.72	0.80
6	0.80	0.88

there may be an energy transfer and some symmetrical mode may also be excited as a result of imperfections in the tank. This phenomenon was observed by Jacobsen [14] in his tests on simple cylindrical tanks under horizontal ground motions where he saw a concentration of water in the center of the tank and could not explain it because the center spot should have suffered no vertical water displacements.

It can be observed in Fig. 3-1 that for b/a = 0.667, the water surface in the annulus along a radial line remains almost horizontal in the first antisymmetric mode with the maximum displacement occurring at the outside wall, but the displacement being within 1% at the inner wall. In all other sloshing modes the maximum water surface displacement always occurs at the inner wall and the displacement at the outer wall is always about 82% of that of the inside wall displacement, and may be in phase or out of phase by 180° depending upon the frequency number. For the symmetric modes (Fig. 3-2), maximum displacement for each mode shape occurs at the inner wall while the displacement at the outer wall is again about 82% of that of the inner wall.

From the mode shapes presented in Fig. 3-1, it can be expected that if the first mode were not dominant during the sloshing of water in geometrically similar tanks, the maximum displacement of water-surface displacement would occur at the inner wall and not at the outer wall. This was indeed observed for the prototype structure (a = 60 ft, b = 40 ft, h = 20 ft) that under all the earthquake accelerograms used for this analytical study, the maximum sloshing response of water always occurred at the inner wall because the dominant mode of vibration was not the first mode but always the second mode.

3.2.1 Effect of water depth on the sloshing frequencies

The effect of the water depth on the sloshing frequencies in anti-symmetric mode was analyzed for the typical prototype structure (a = 60 ft, b = 40 ft) and the results are presented in Table 3-2. Analysis was made for water depths (h) of 20, 60, 80 and 120 ft respectively. It is interesting to note in Table 3-2 that for various depths above 20 ft all the frequencies except the first one agree to the second significant figure although they will not be exactly the same. Since the sloshing response of water in the prototype structure under actual earthquakes is predominantly in the second mode, we should not expect any significant difference in the water surface displacements under a given ground motion when the depth of water is varied beyond 20 ft as will be seen in the next article. If the depth of water is increased beyond 120 ft, even the change in the first sloshing frequency will become insignificant.

TABLE 3-2. Sloshing frequencies of prototype for various water depths for modes of class 1.

Frequency number	Frequency in (Hz) for depth h			
	h = 20'	h = 60'	h = 80'	h = 120'
1	0.0791	0.117	0.123	0.127
2	0.36	0.36	0.36	0.36
3	0.51	0.51	0.51	0.51
4	0.62	0.62	0.62	0.62
5	0.72	0.72	0.72	0.72
6	0.80	0.80	0.80	0.80

3.3 Sloshing Response of Water in the Prototype Tank Under Various Earthquake Accelerograms

An analytical study of the sloshing response of water for a typical pressure-suppression pool used in Boiling Water Reactors was made under the effect of various earthquake accelerograms. The analysis was carried out on the computer using the program SLOSH. Output included the printing of water surface profile at Section A-A (Fig. 1-1) and the pressure variation across depth along the inner and outer walls at $\theta = 0$, i.e., along the axis of excitation. Maximum water displacements and pressures were plotted on the Calcomp plots and they are shown in Figs. 3-4 through 3-14. Normal depth of water in such a typical pressure-suppression pool is about 20 ft; however, the depth of water was varied to see the effect on sloshing response. Inner and outer radii of the prototype tank were 40 ft and 60 ft respectively. The following earthquake accelerograms were used for this analytical study:

1) Pacoima Dam Accelerogram (S16°E) recorded at Pacoima Dam in the San Fernando earthquake of 1971. The maximum acceleration was 1.24 g.
2) El Centro (N-S) Accelerogram (1940) — the actual accelerogram was scaled up to a maximum acceleration of 0.53 g compared with 0.32 g actually recorded.
3) Parkfield Earthquake Accelerogram (1966) — the maximum acceleration value was 0.5 g.
4) Artificial Earthquake Accelerograms.— These eight accelerograms named A1, A2, B1, B2, C1, C2, D1 and D2, were produced artificially by Jennings [15]. Accelerograms of type A and B represent earthquakes of magnitudes 8 and 7 respectively.

The shaking expected in the epicentral area of a magnitude 5-6 earthquake is represented by Type C and has the same average intensity as the record obtained at Golden Gate Park during the 1957 San Francisco earthquake. For earthquakes of Type D, which model the shaking close to the fault in a shallow magnitude of 4.5 - 5.5 earthquake. the motions have been scaled to have a maximum acceleration of about 0.5 g. Earthquakes of Type B have the same spectral intensity as the El Centro 1940 record.

A brief discussion of the sloshing behavior regarding the water surface waves and the pressure distributions is given in the following pages.

3.3.1 Water surface displacements

Table 3-3 gives the maximum values (δ_{max}) of the water displacements at the surface in the typical protype structure under the various earthquake accelerograms mentioned above. The depth of water in all cases was 20 ft and the outer and inner radii of the tank were 60 ft and 40 ft respectively. Table 3-3 also gives the maximum values of the ground acceleration for each earthquake accelerogram.

Figures 3-4 through 3-14 show time-history plots of the displacements of water surface at the inner and outer walls along the axis of ground excitation for various earthquake accelerograms. Thus the displacement plots in these figures represent the displacements $\delta(b,0,0,t)$ and $\delta(a,0,0,t)$ at the inner and outer boundaries of the annular tank respectively. The ground accelerations in Fig. 3-4 through 3-14 have units of g, the water displacements scale is in inches, and the horizontal scale

TABLE 3-3. Maximum water surface displacements (δ_{max}) and pressures (p_{max}) in prototype (a = 60', b = 40', h = 20') under various earthquake accelerograms.

Name of the accelerogram	Max. ground acceleration (g)	δ_{max} (inches)	p_{max} (psi)
Pacoima (S16°E)	1.24	59.8	6.37
El Centro (1940)	0.53	48.8	2.85
Parkfield	0.50	26.0	2.70
A1	0.41	91.6	2.14
A2	0.45	68.6	2.36
B1	0.38	32.2	1.92
B2	0.32	37.8	1.69
C1	0.07	2.9	0.36
C2	0.06	2.0	0.31
D1	0.485	9.7	2.56
D2	0.492	9.8	2.63

represents time in seconds.

Figure 3-15 shows the profile of water surface at Section A-A (Fig. 1-1) at the time when maximum displacement (δ_{max}) of water occurs in the tank. The plots show profiles for earthquake accelerograms A2, B1, Pacoima and El Centro, and the displacements are given in inches.

Figures 3-16 through 3-19 show the time-history plots of surface water displacements at inner and outer walls of the prototype tank as the depth of the water (h) is changed from normal depth of 20 ft to a depth of 120 ft.

The following observations can be made regarding water displacements and sloshing modes:

1) The maximum displacement of water (δ_{max}) shown in Table 3-3 always occurs at the inner wall of the tank as can be seen in time-history plots of Figs. 3-4 through 3-14. This happens because the dominant mode of vibration in the prototype under all the earthquake accelerograms used here is the second mode. Maximum displacements occur under the accelerograms A1 and A2 and are 92" and 69" respectively. This should be expected as they represent very strong earthquake (magnitude 8) and thus the ground motions will have longer periods of vibrations. It can be noticed that although A1 has maximum acceleration which is only one-third of that of Pacoima record, the displacement is 50% higher under the artificial earthquake accelerogram A1. Comparing the sloshing response of water under the accelerogram B1, C1, D1 with that of under B2, C2 and D2, respectively, it can be seen that the δ_{max} values are quite

comparable in the two cases as they represent the same type of ground motion characteristics.

In general, it can be said that earthquake accelerograms with long period components of ground motion will give higher sloshing response of water in the prototype because of rather long fundamental periods of sloshing mass of water (first and second sloshing periods of water in the prototype are 12.6 and 2.8 seconds respectively). It should also be pointed out that at present there is more uncertainty about long period ground motion than short period.

2) It can be noticed from Figs. 3-4 through 3-15 that second mode is the dominant mode of vibration of the water sloshing in the prototype structure under all the earthquake accelerograms. Figures 3-4 through 3-14 show that the sloshing period of water is very close to the second natural period of 2.8 seconds in almost every case. The water surfaces at the inner and outer walls are always opposite in phase as they should be in the second mode of vibration.

Figure 3-15, which shows the profile of water surface across the annulus is another indication of the dominance of second mode. The water surface profile in this figure when the water is sloshing under various earthquakes closely resembles the second antisymmetric mode of vibration (compare with Fig. 3-1).

3) Comparison of Figs. 3-16 through 3-19 shows that the sloshing response of water in the prototype annular tank remains almost

unchanged as the water depth is varied from 20 ft to 120 ft. This can be explained on the basis of the effect of depth on natural frequencies of sloshing. It was pointed out in the previous article that as the depth of water is increased beyond 20 ft, there is very little change in the second or higher natural sloshing frequencies (see Table 3-2) of the prototype. Since the dominant mode of vibration is not the first mode, but the second mode, therefore, little change in the sloshing response should be expected as the depth of water is increased beyond 20 ft. The reverse may not, however, be true depending upon how the natural frequencies are affected as the depth is decreased. When the depth of water is rather small, then even the higher frequencies will be sensitive to variations in depth.

4) For a given earthquake accelerogram, if the intensity of accelerations is increased or decreased by a certain factor, then the sloshing response will also increase or decrease by the same factor. This follows from the linearity assumption on which the theory is based and can be seen by comparing Figs. 3-16 and 3-20. Both figures show the surface water displacements under the El Centro earthquake accelerograms with the difference that the accelerations in Fig. 3-20 are only 50% of those of Fig. 3-16. It will be observed that the water displacements in Fig. 3-20 are also reduced by 50% compared with the corresponding values of Fig. 3-16. The maximum displacements in Figs. 3-16 and 3-20 are 48.8 and 24.4 inches respectively.

5) It should be noted that the displacements given in Table 3-3 and Figs. 3-4 through 3-20 are all given at a section along the axis of ground excitation for which the angle θ is zero. To determine the corresponding values at any other section, simply multiply by $\cos\theta$ the corresponding values of Section A-A where θ is the angle from Section A-A.

3.3.2 Dynamic pressures

Table 3-3 gives the maximum values of the dynamic pressures in the prototype structure under various earthquake accelerograms. Figure 3-21 shows the distribution of dynamic pressures along the depth of the tank walls and Figs. 3-22 through 3-26 are the time-history plots of the maximum pressures at the inner and outer boundaries at Section A-A of Fig. 1-1. From Table 3-3 and Figs. 3-21 through 3-26, we can make the following observations:

1) The values shown in Table 3-3 for maximum pressures (p_{max}) occur at the bottom of the outside wall of the tank and they are approximately proportional to the maximum ground acceleration to which the tank is subjected. (Compare the values of dynamic pressure to the maximum ground accelerations for various earthquakes in Table 3-3.)

2) The pressure distribution along the depth at the inner and outer walls is shown in Fig. 3-21 for the prototype structure at a maximum ground acceleration of 0.34 g. It is seen that the dynamic pressure is more uniform along the inner wall compared with the distribution along the outer wall of the

tank. This distribution of dynamic pressures was taken from the time-history analysis under El Centro earthquake at the time of the peak ground acceleration and is valid only for a depth of water equal to 240 inches.

3) Time-history plots of Figs. 3-22 and 3-23 show that the dynamic pressures at the bottom of the tank along inner and outer walls are out of phase when the depth of water is 240 inches. However, this is not true for dynamic pressures at the bottom of the tank at larger depths as in Figs. 3-24, 3-25, and 3-26. Here the pressures at inner and outer walls (at the bottom of the tank) are in phase and this fact was verified by tests.

4) The maximum pressures do not vary linearly as the depth of water is increased (compare Figs. 3-24, 3-25 and 3-26).

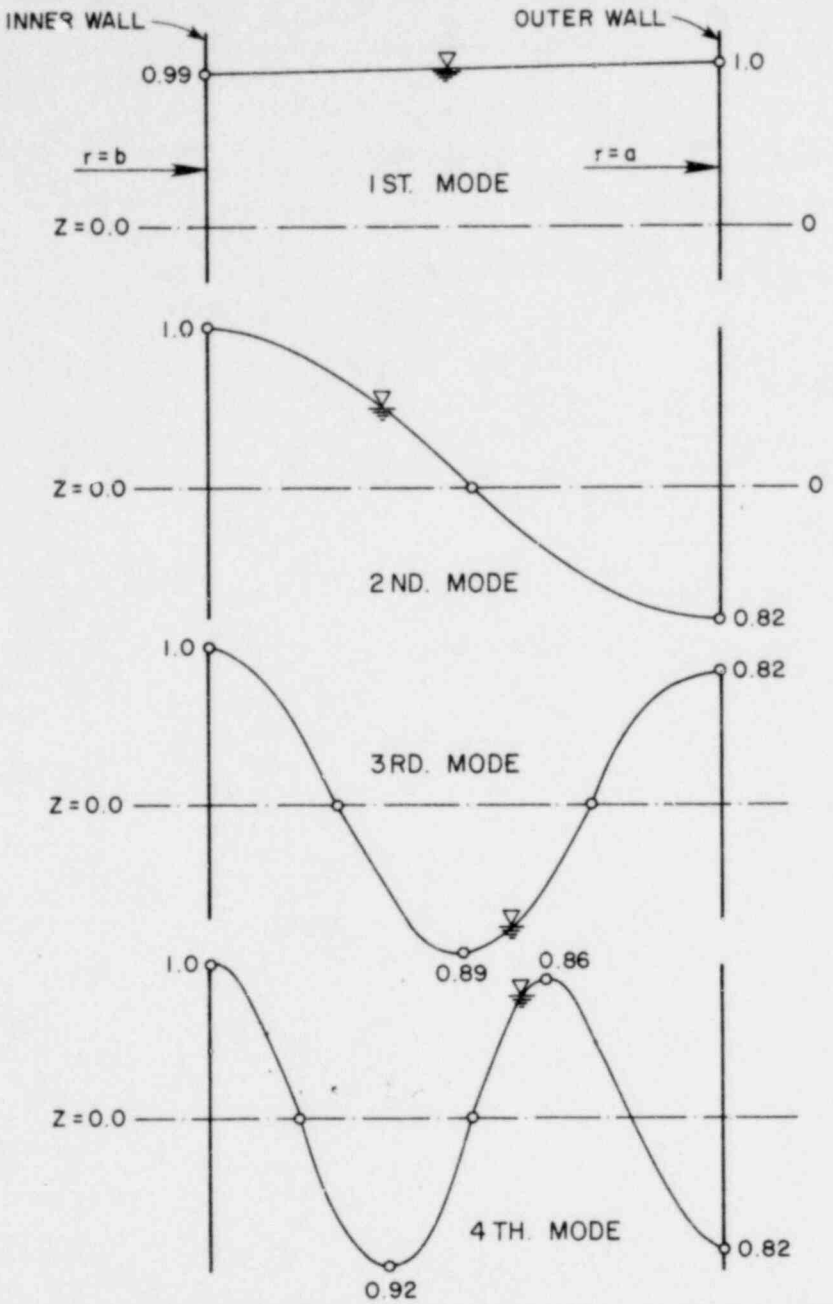

FIG. 3-1 ANTISYMMETRIC MODE SHAPES (CLASS I) FOR ANNULAR TANK (b/a = 0.667) ALONG THE SECTION A-A OF FIG. 1-1

XBL 782-7212

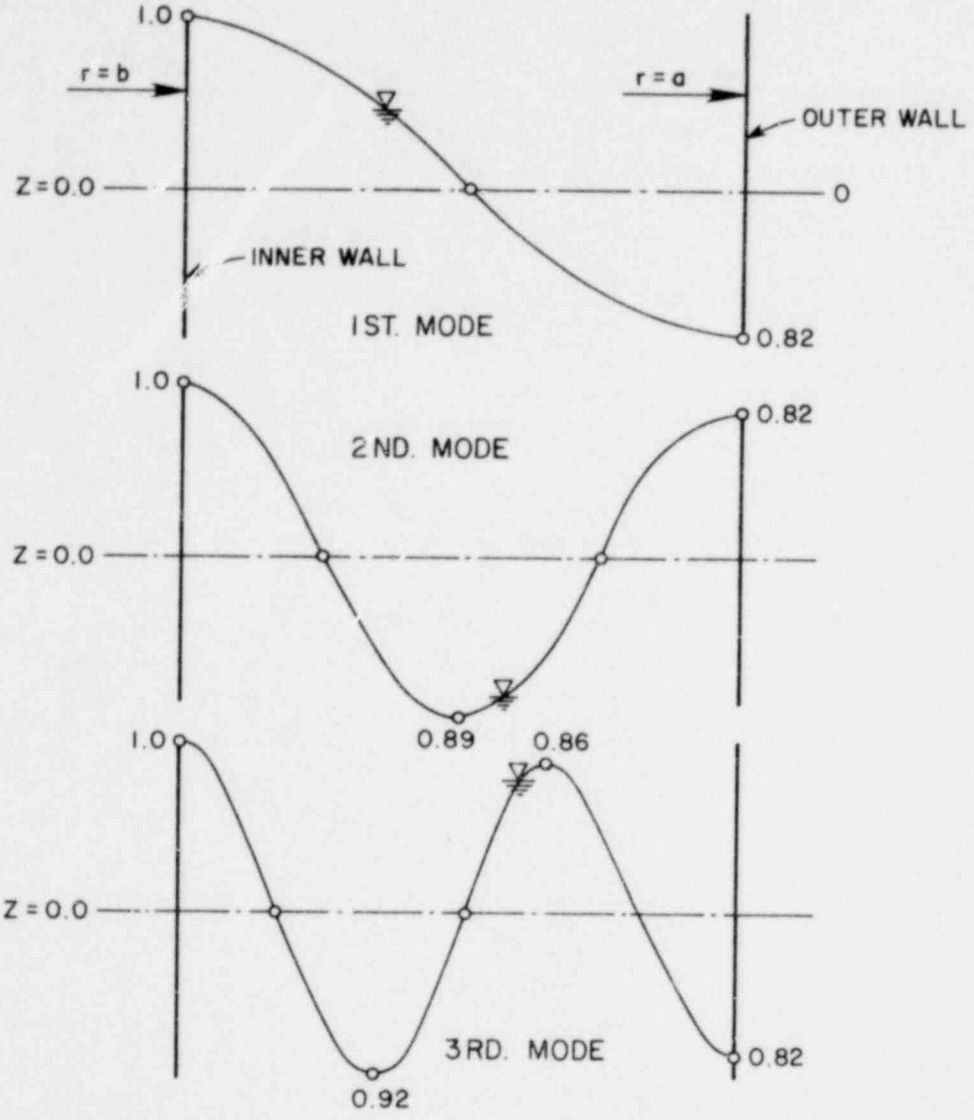

FIG. 3-2 SYMMETRIC MODE SHAPES (CLASS 0) FOR ANNULAR TANK (b/a = 0.667)

XBL 782-7211

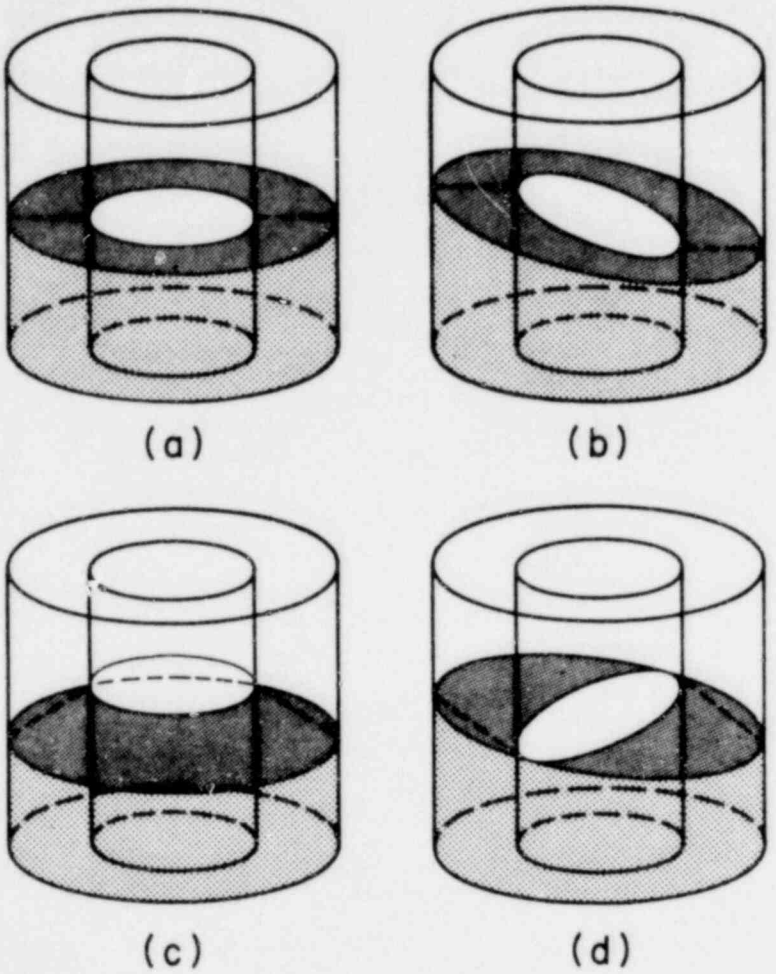

FIG. 3-3 MODE SHAPES IN AN ANNULAR TANK (b) AND (d) ARE THE ANTISYMMETRIC MODES, (c) IS THE FIRST SYMMETRIC MODE

XBL 782-7214

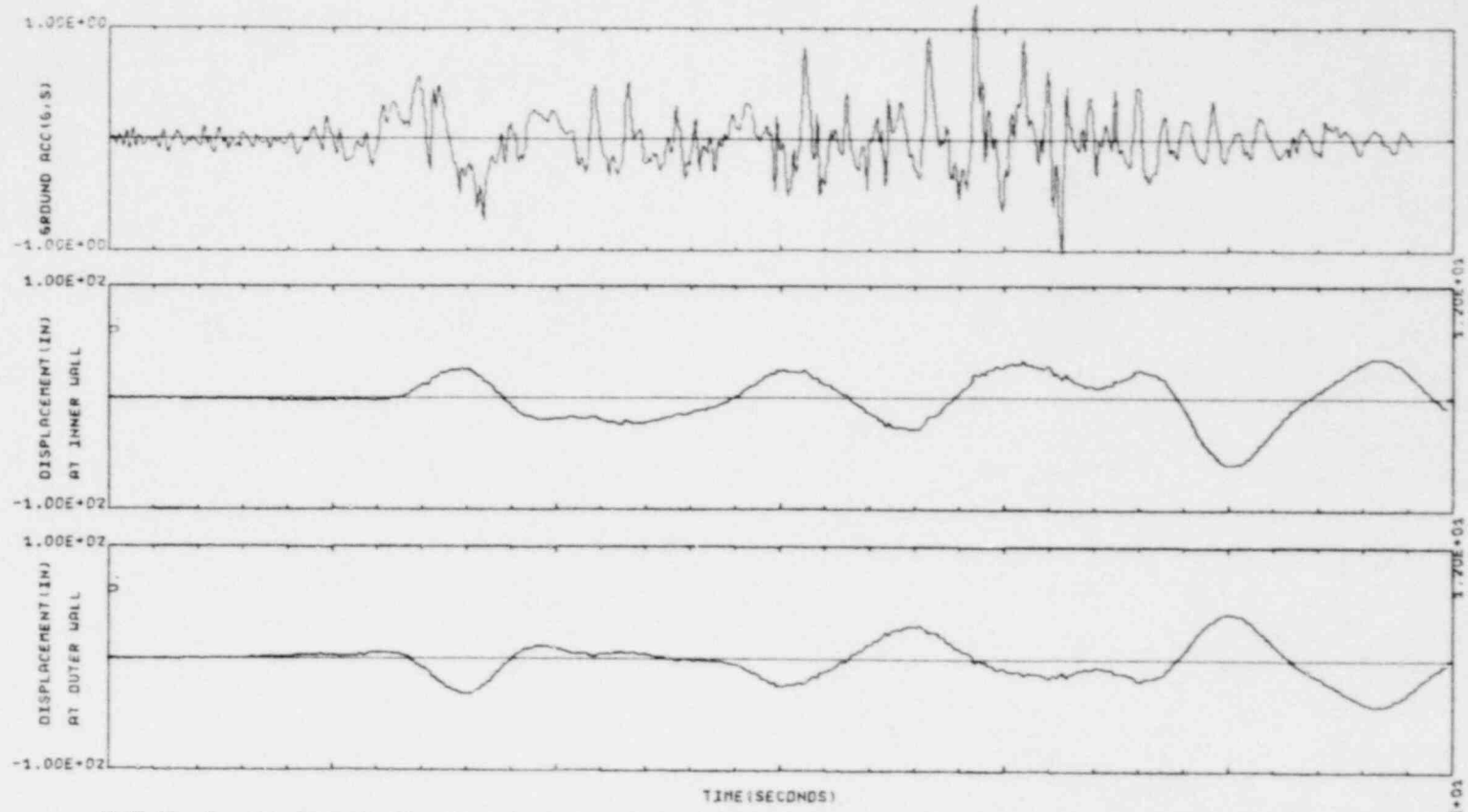

FIG. 3-4 SLOSHING RESPONSE OF WATER IN ANNULAR TANK(INNER RADIUS =480 IN, OUTER RAD=720 IN, DEPTH OF WATER=240 IN) UNDER PACOIMA DAM ACCELEROGRAM(S16E) 1971

XBL 7812-13926

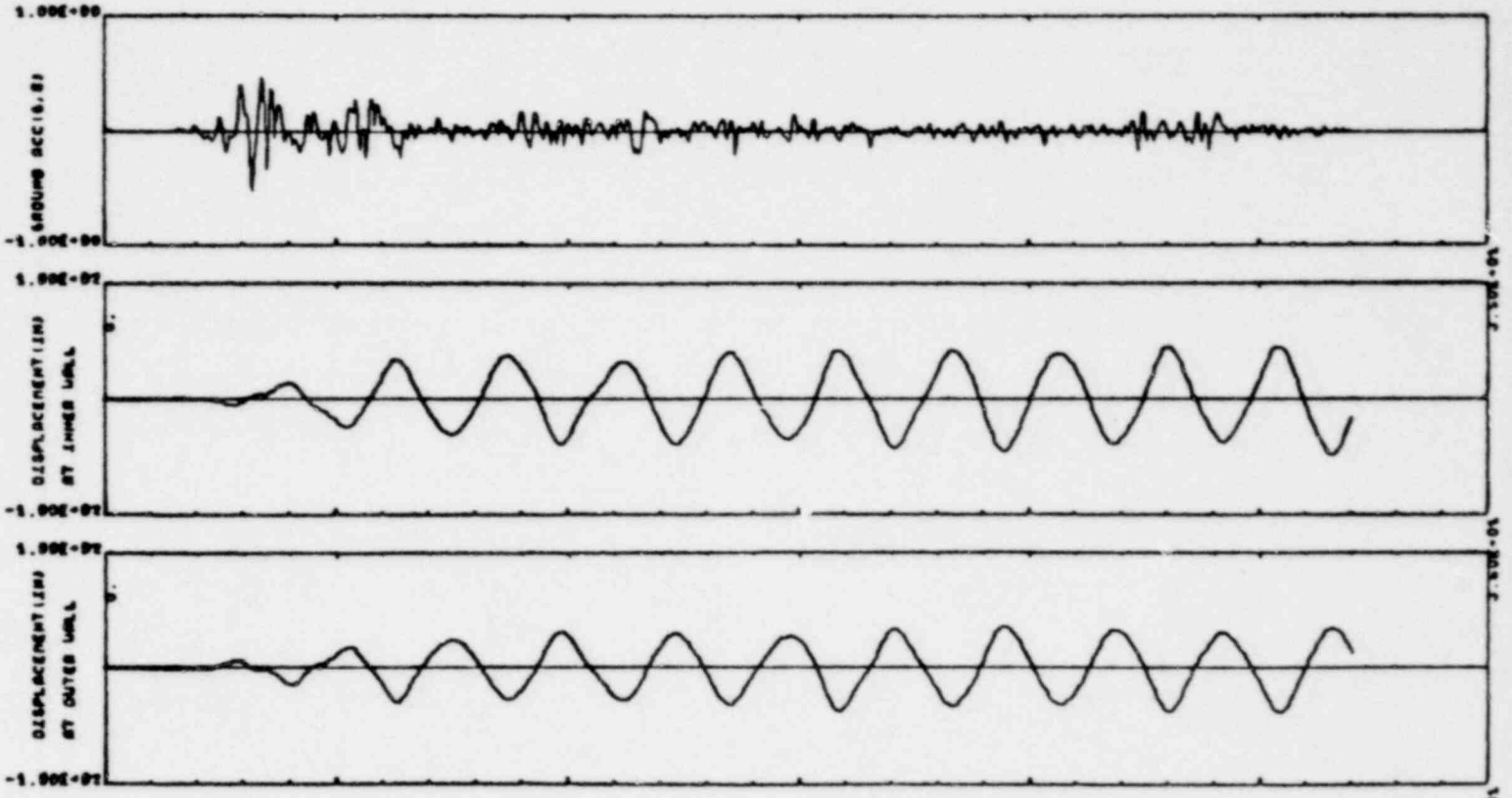

FIG.3-5 SLOSHING RESPONSE OF WATER IN ANNULAR TANK(INNER RADIUS =480 IN, OUTER RAD=720 IN, DEPTH OF WATER=240 IN) UNDER ELCENTRO EARTHQUAKE ACCELEROGRAM(1940)

XBL 7812-13962

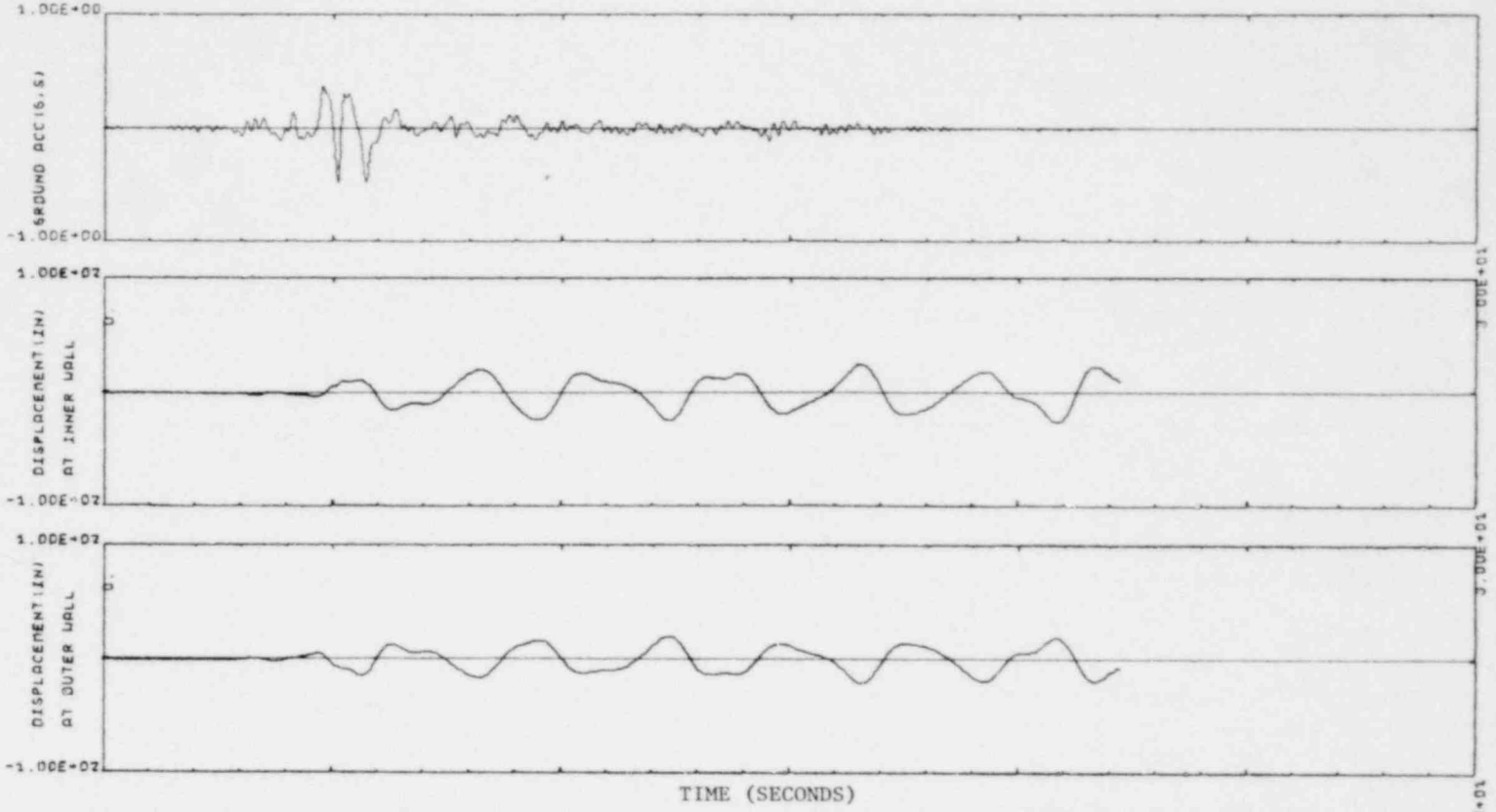

FIG. 3-6 SLOSHING RESPONSE OF WATER IN ANNULAR TANK (INNER RADIUS =480 IN, OUTER RAD=720 IN, DEPTH OF WATER=240 IN) UNDER PARKFIELD EARTHQUAKE TIME SCALE=1.

XBL 7812-13925

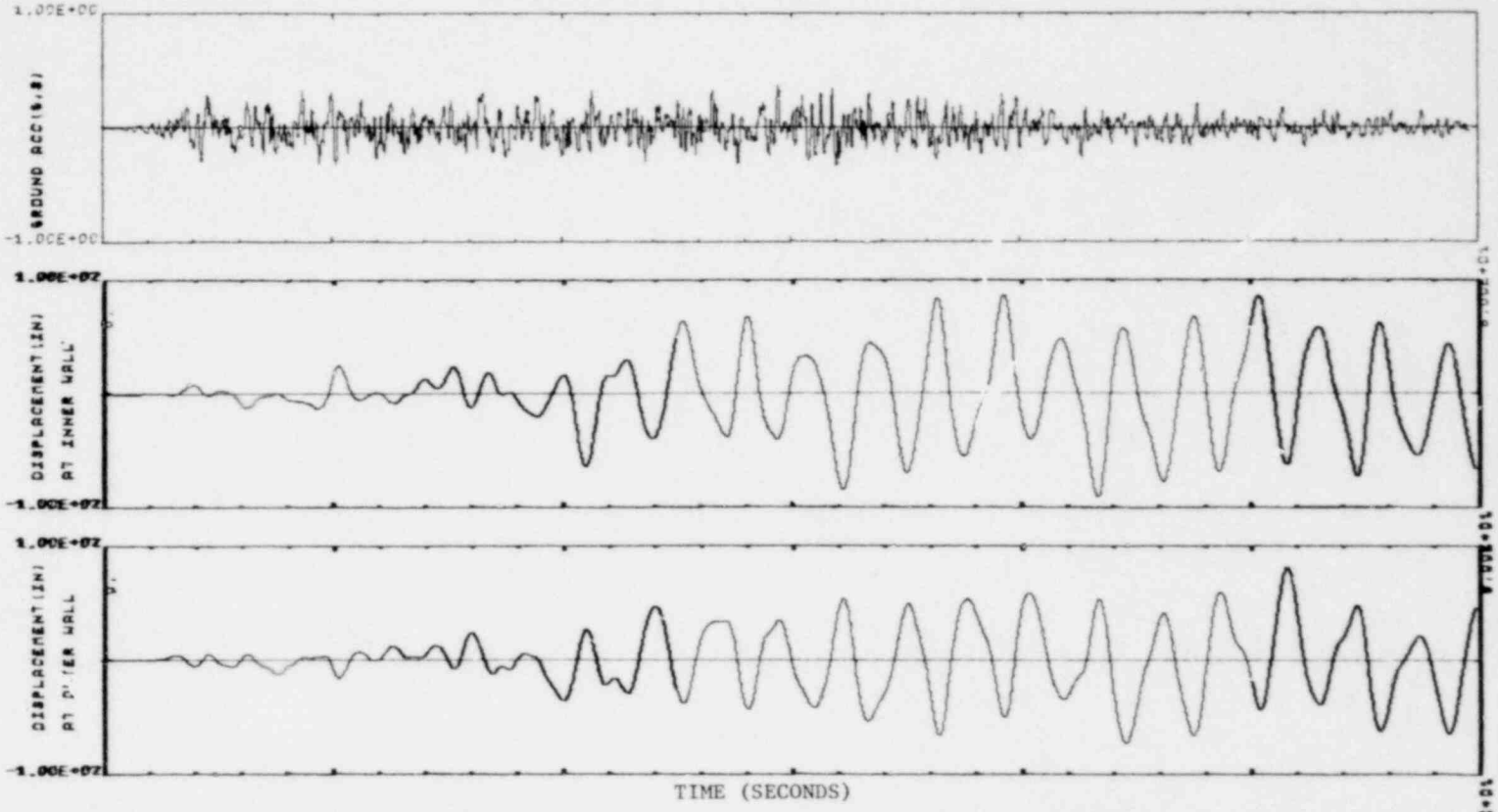

FIG. 3-7 SLOSHING RESPONSE OF WATER IN ANNULAR TANK(INNER RADIUS =480 IN, OUTER RAD=720 IN, DEPTH OF WATER=240 IN) UNDER ARTIFICIAL EARTHQUAKE ACCELEROGRAM A1

XBL 7812-13901

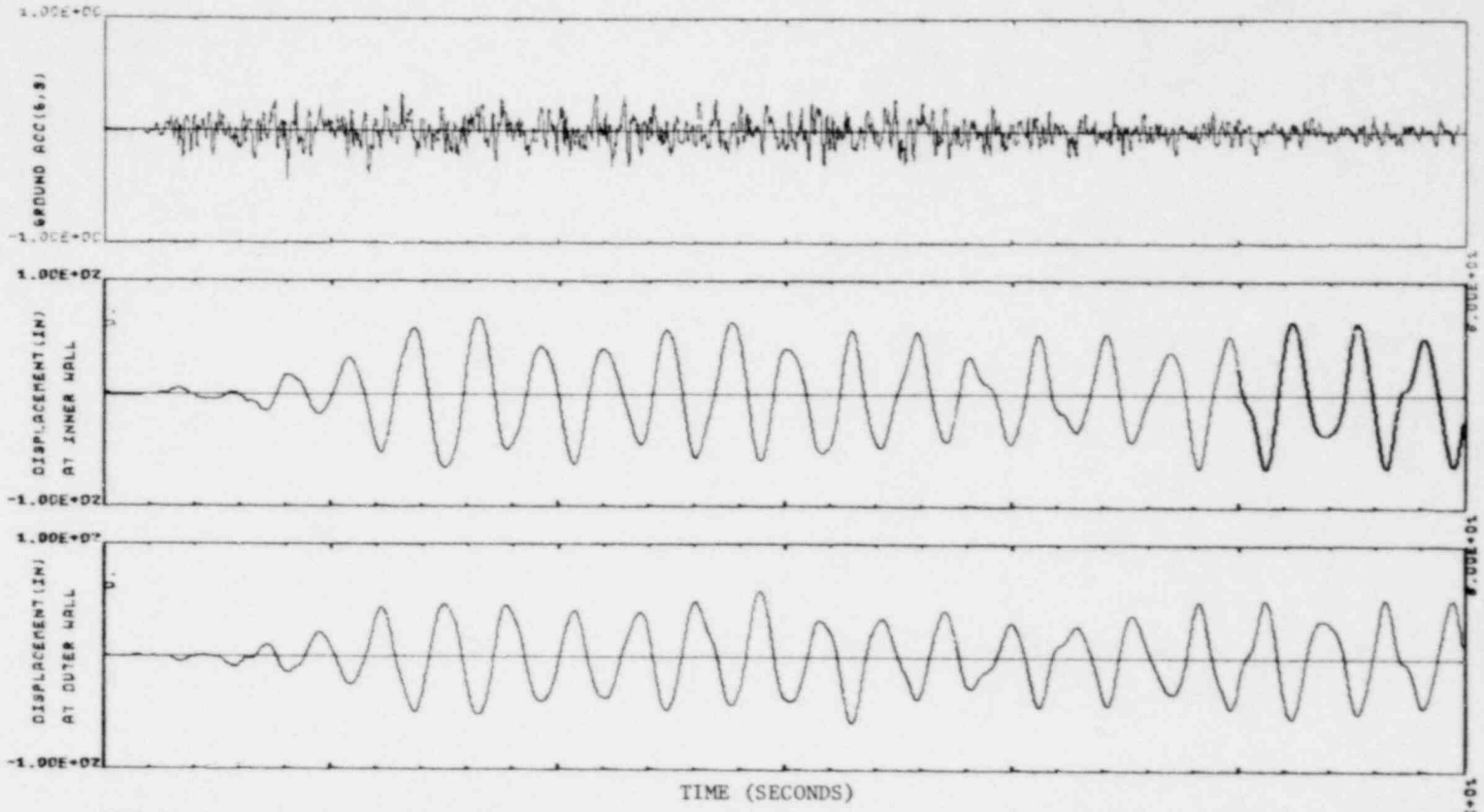

FIG. 3-8 SLOSHING RESPONSE OF WATER IN ANNULAR TANK(INNER RADIUS =480 IN, OUTER RAD=720 IN, DEPTH OF WATER=240 IN) UNDER ARTIFICIAL EARTHQUAKE ACCELEROGRAM A2

XBL 7812-13902

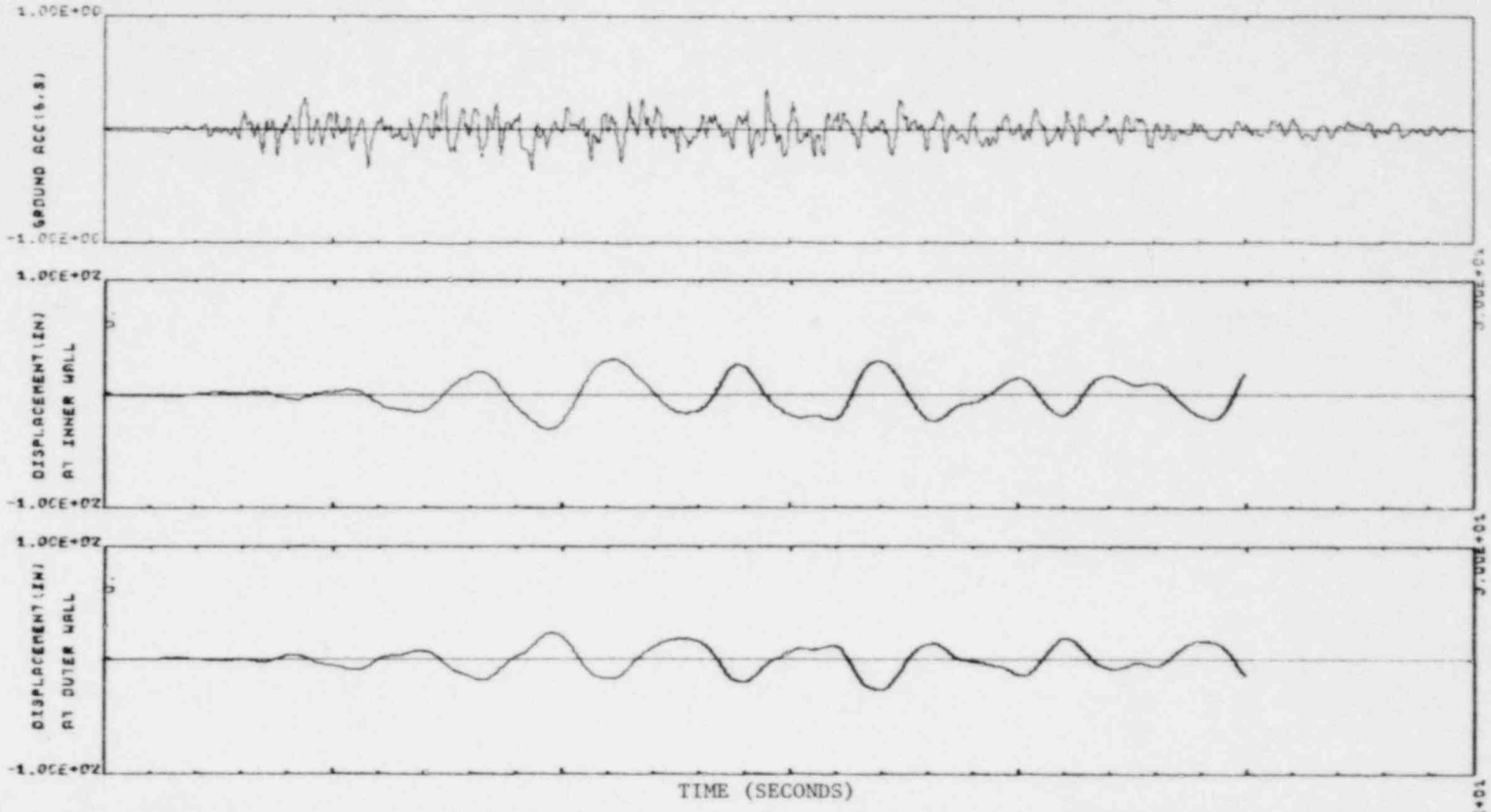

FIG. 3-9 SLOSHING RESPONSE OF WATER IN ANNULAR TANK(INNER RADIUS =480 IN, OUTER RAD=720 IN, DEPTH OF WATER=240 IN) UNDER ARTIFICIAL EARTHQUAKE ACCELEROGRAM S1

XBL 7812-13903

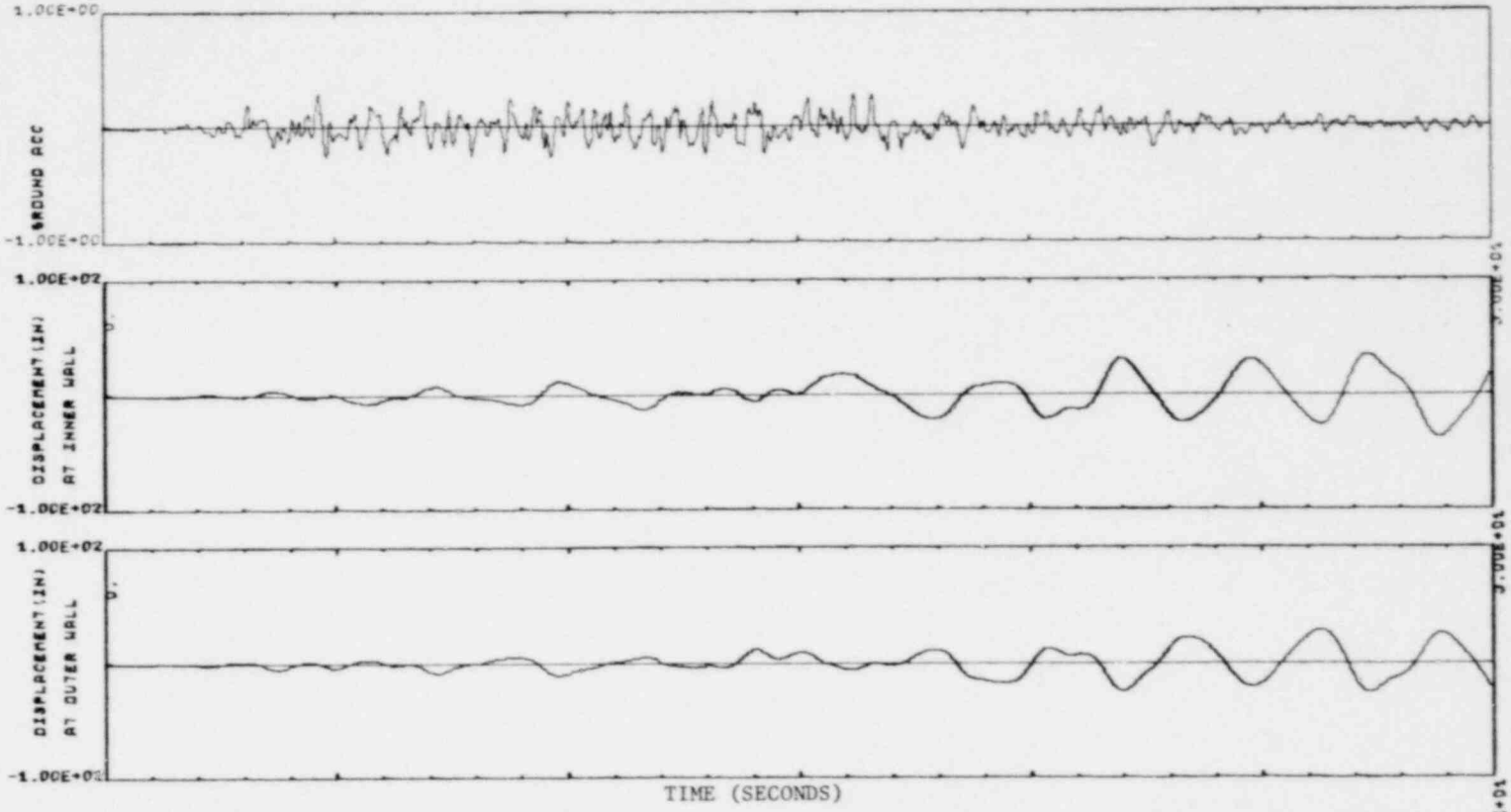

FIG. 3-10 SLOSHING RESPONSE OF WATER IN ANNULAR TANK(INNER RADIUS =480 IN, OUTER RAD=720 IN, DEPTH OF WATER=240 IN) UNDER ARTIFICIAL EARTHQUAKE ACCELEROGRAM B2

XBL 7812-13904

FIG. 3-11 SLOSHING RESPONSE OF WATER IN ANNULAR TANK (INNER RADIUS =480 IN, OUTER RAD=720 IN, DEPTH OF WATER=240 IN) UNDER ARTIFICIAL EARTHQUAKE ACCELEROGRAM C1

XBL 7812-13905

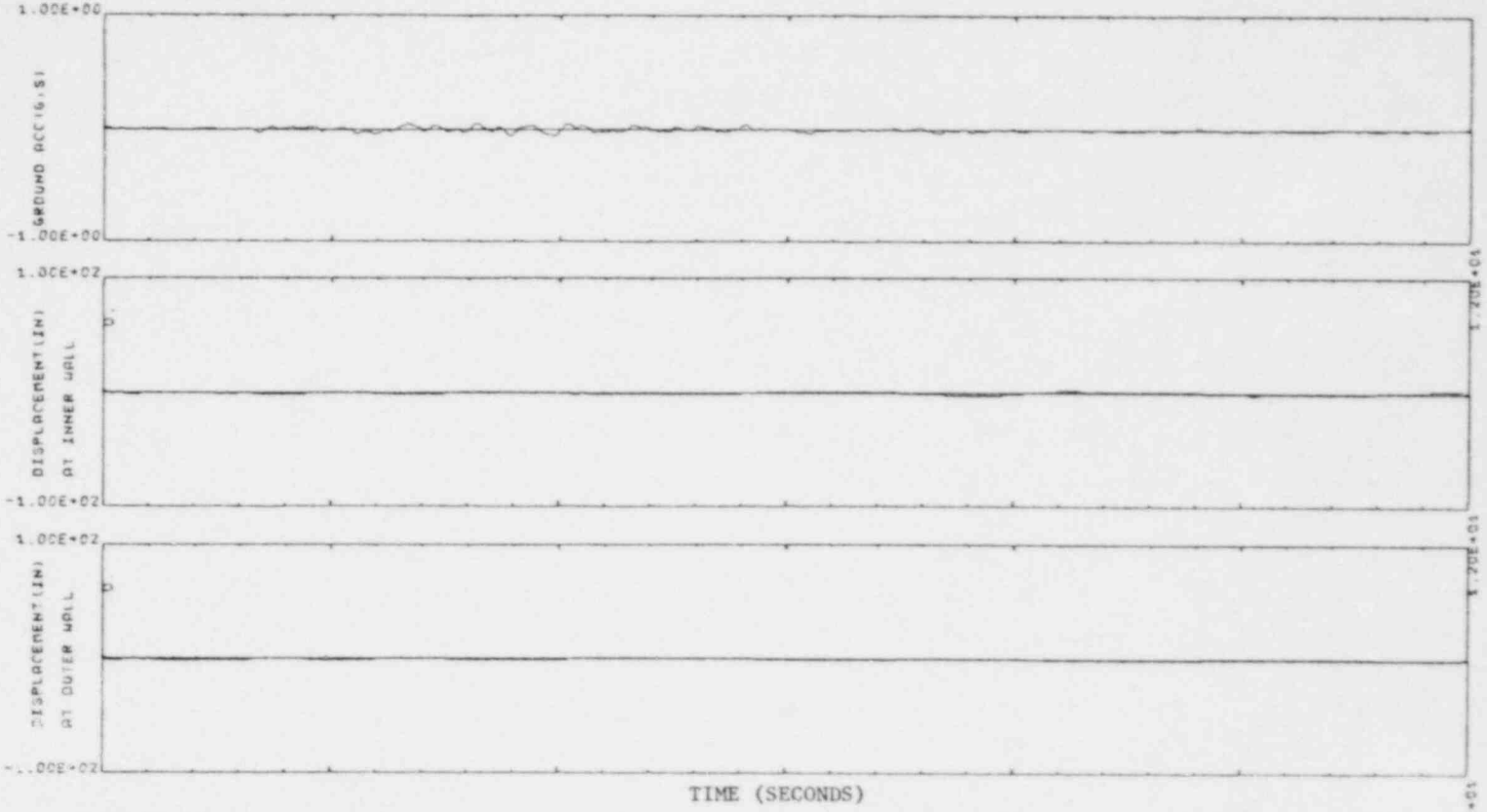

FIG. 3-12 SLOSHING RESPONSE OF WATER IN ANNULAR TANK (INNER RADIUS =480 IN, OUTER RAD=720 IN, DEPTH OF WATER=240 IN) UNDER ARTIFICIAL EARTHQUAKE ACCELEROGRAM C2

XBL 7812-13906

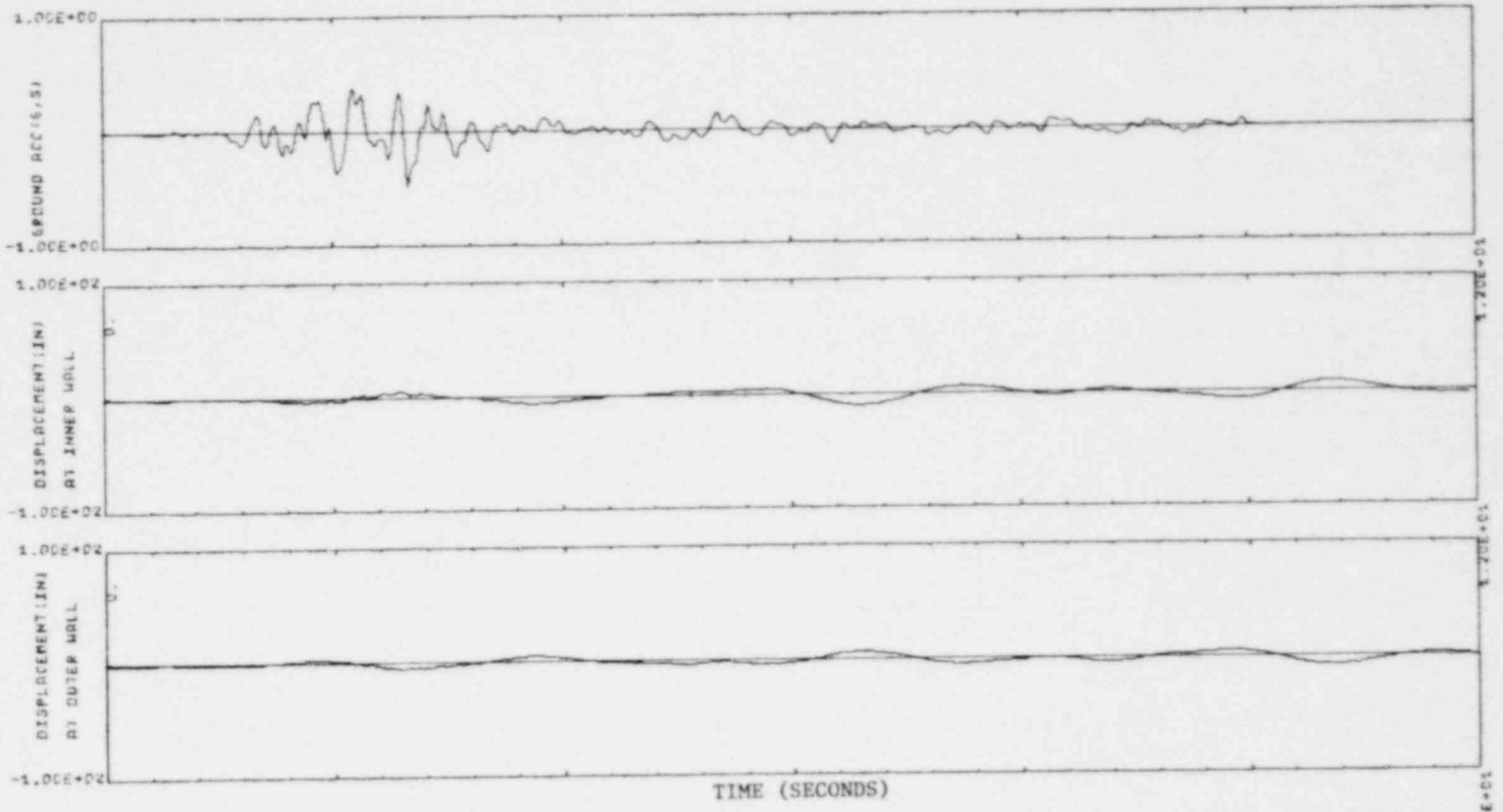

FIG. 3-13 SLOSHING RESPONSE OF WATER IN ANNULAR TANK(INNER RADIUS =480 IN, OUTER RAD=720 IN, DEPTH OF WATER=240 IN) UNDER ARTIFICIAL EARTHQUAKE ACCELEROGRAM D1

XBL 7812-13907

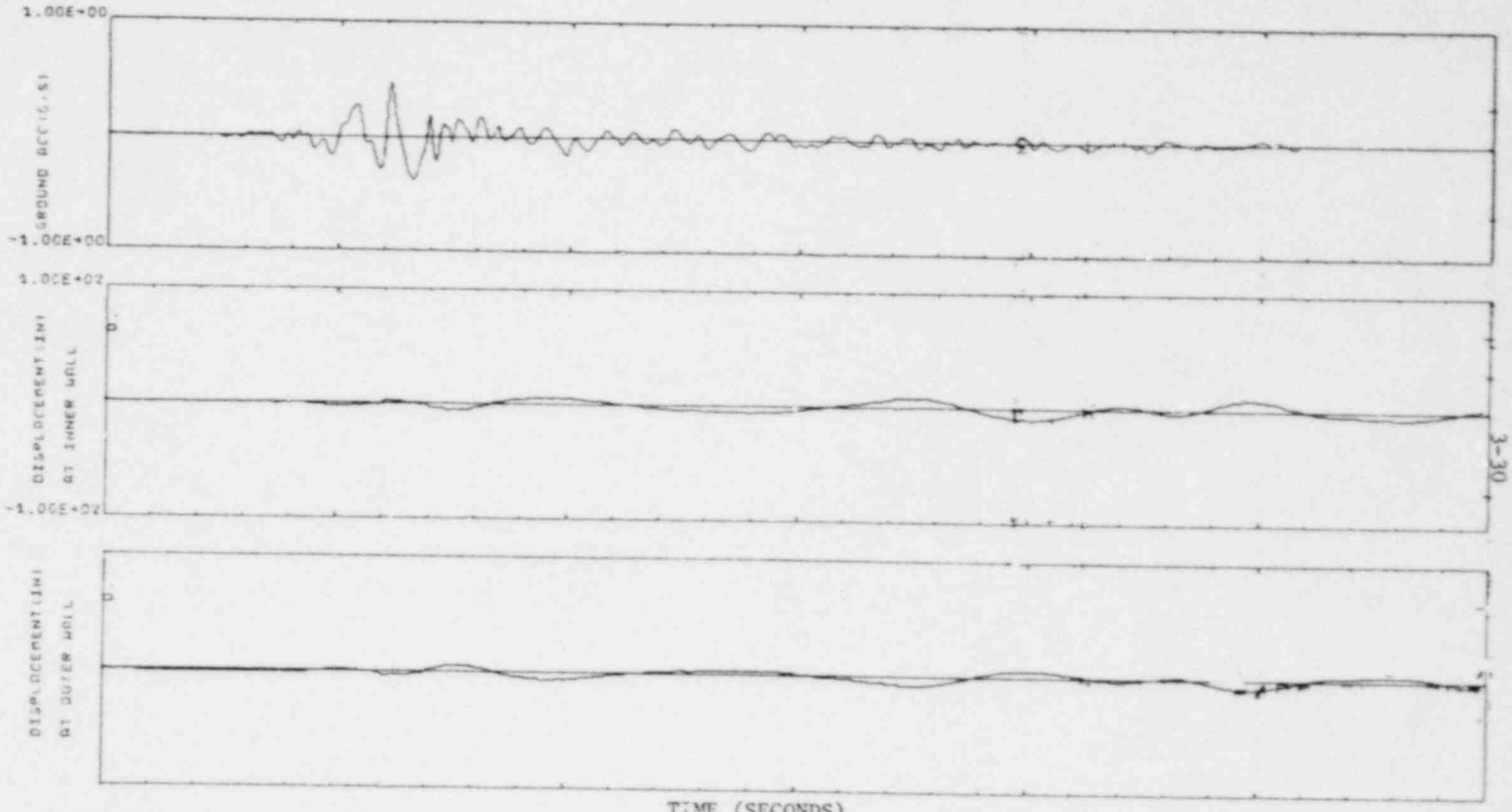

FIG. 3-14 SLOSHING RESPONSE OF WATER IN ANNULAR TANK (INNER RADIUS =480 IN, OUTER RAD=720 IN, DEPTH OF WATER=240 IN) UNDER ARTIFICIAL EARTHQUAKE ACCELEROGRAM D2

XBL 7812-13908

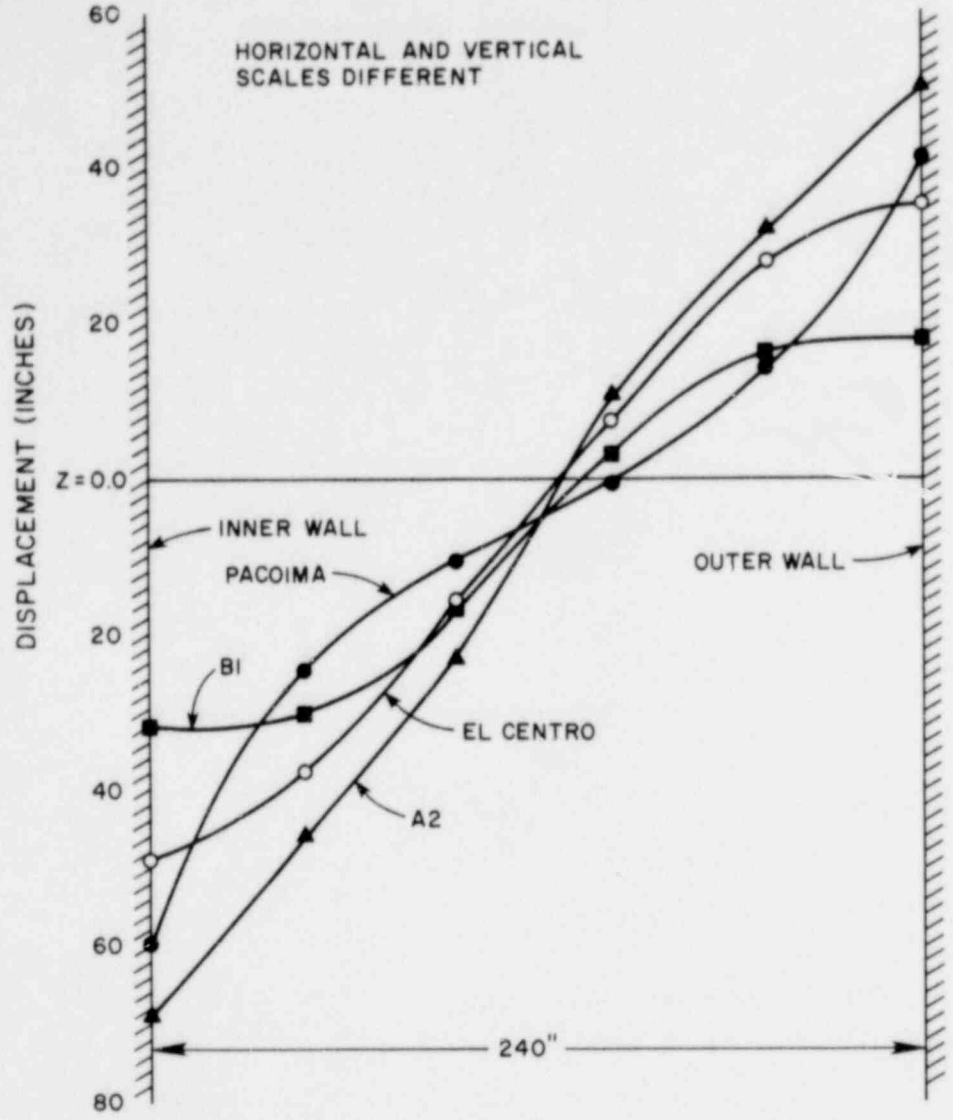

FIG. 3-15 PROFILE OF WATER SURFACE AT SECTION A-A (FIG. 1-1) AT THE TIME OF MAXIMUM DISPLACEMENT IN PROTOTYPE

XBL 7812-13909

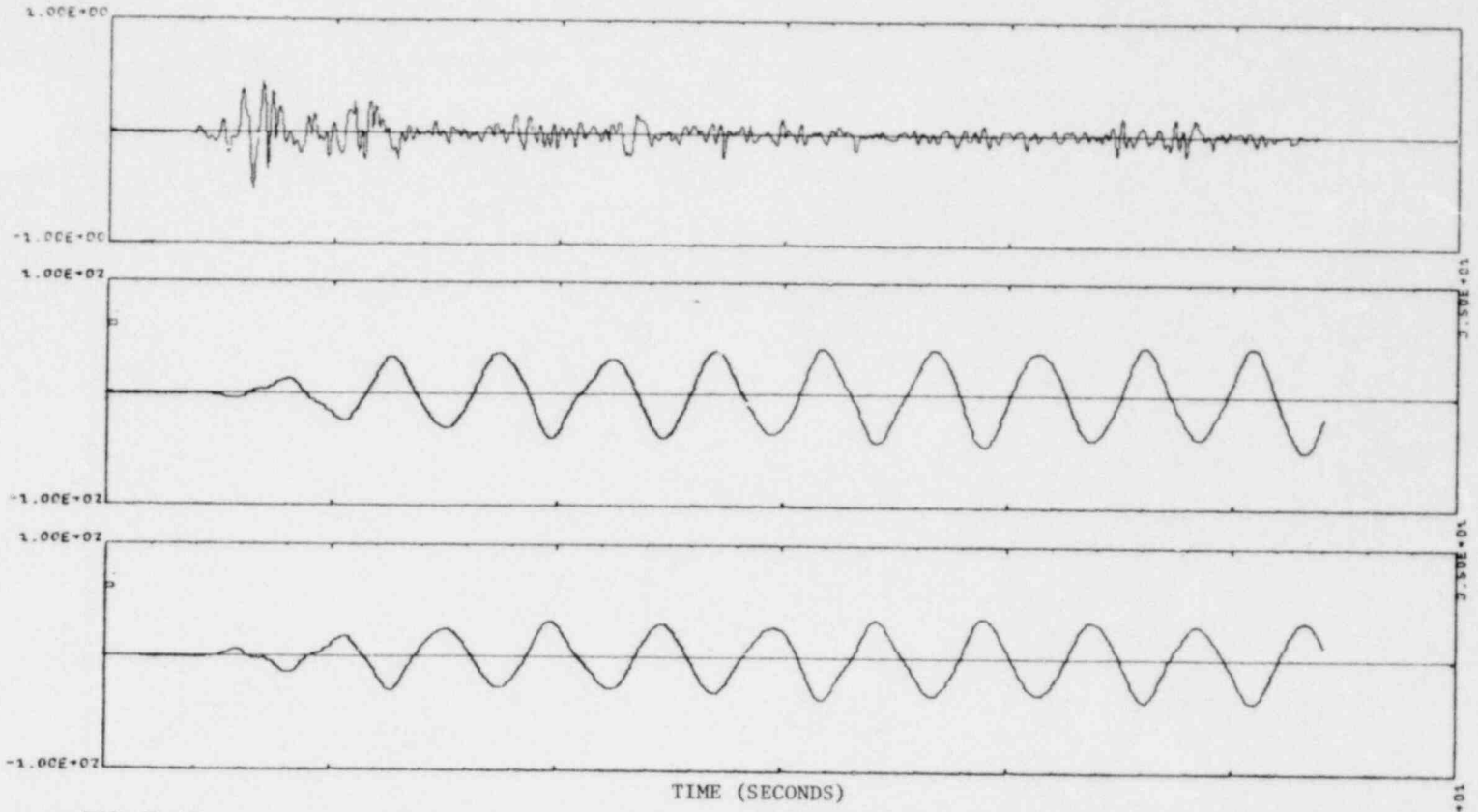

FIG. 3-16 SLOSHING RESPONSE OF WATER IN ANNULAR TANK (INNER RADIUS =480 IN, OUTER RAD=720 IN, DEPTH OF WATER=240 IN) UNDER ELCENTRO EARTHQUAKE (1940) TIME SCALE=1.

XBL 7812-13910

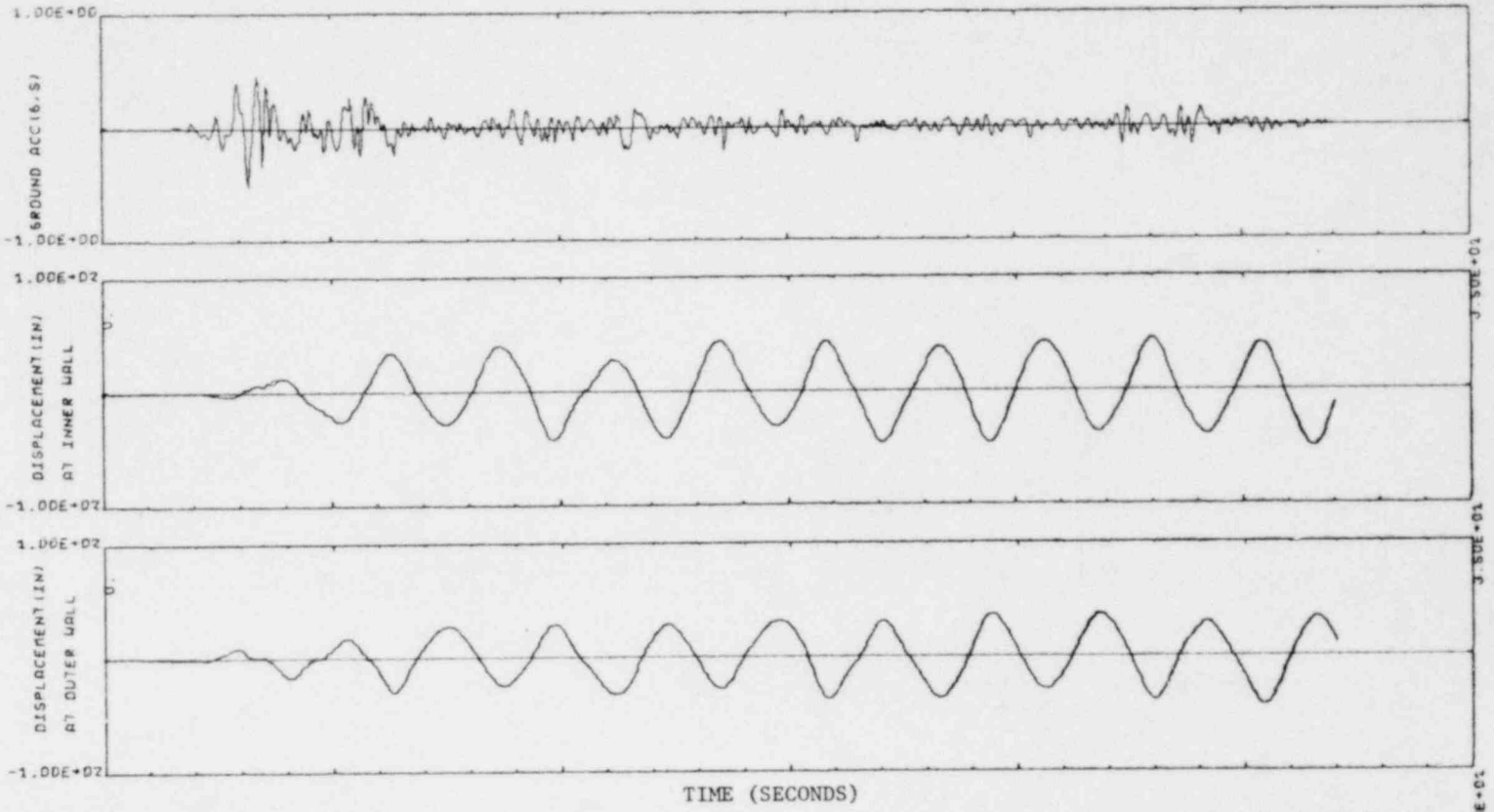

FIG. 3-17 SLOSHING RESPONSE OF WATER IN ANNULAR TANK(INNER RADIUS =480 IN, OUTER RAD=720 IN, DEPTH OF WATER=720 IN) UNDER ELCENTRO EARTHQUAKE ACCELEROGRAM(1940)

XBL 7812-13911

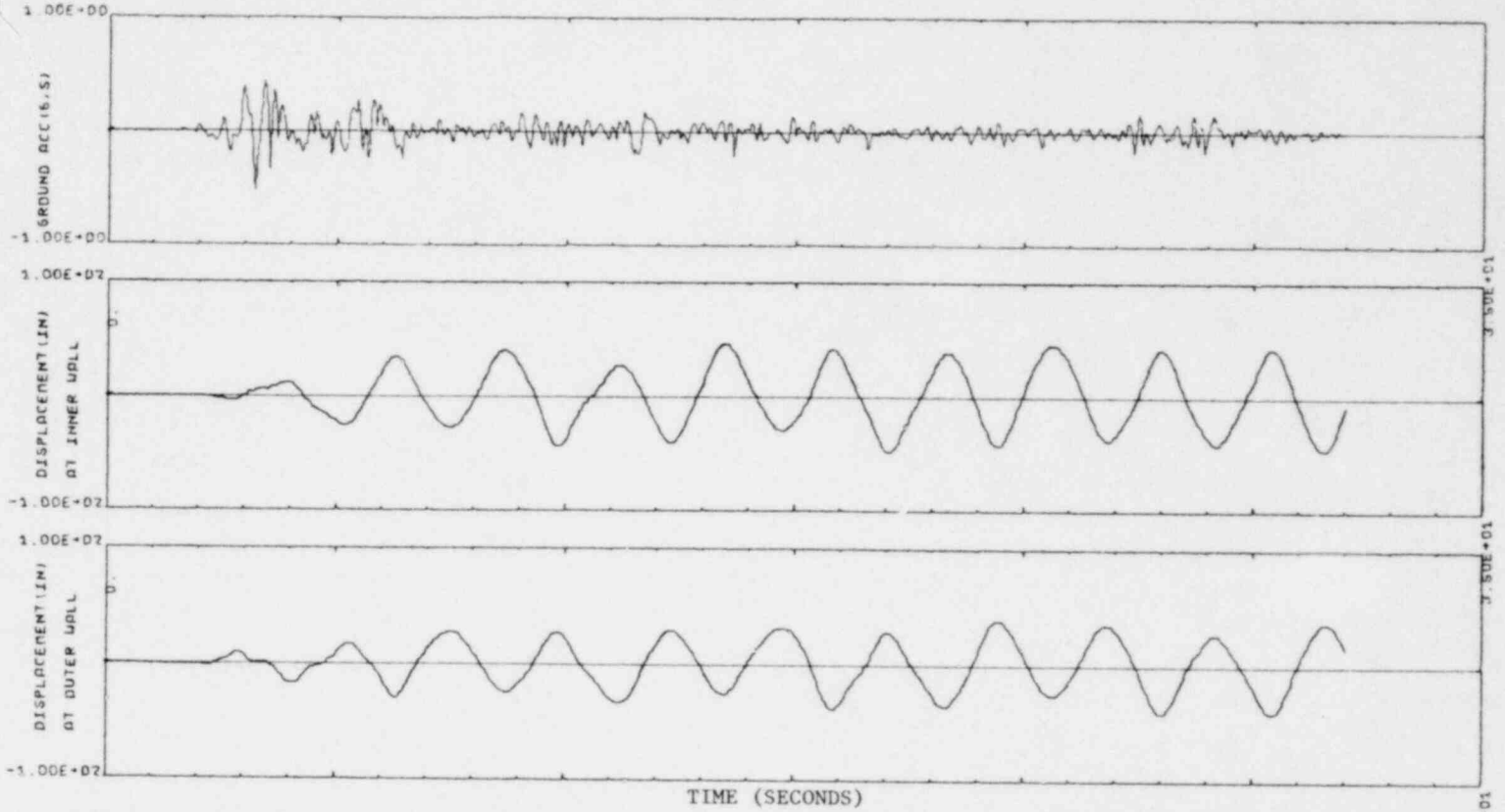

FIG. 3-18 SLOSHING RESPONSE OF WATER IN ANNULAR TANK (INNER RADIUS =480 IN, OUTER RAD=720 IN, DEPTH OF WATER=960 IN) UNDER ELCENTRO EARTHQUAKE ACCELEROGRAM (1940)

XBL 7812-13912

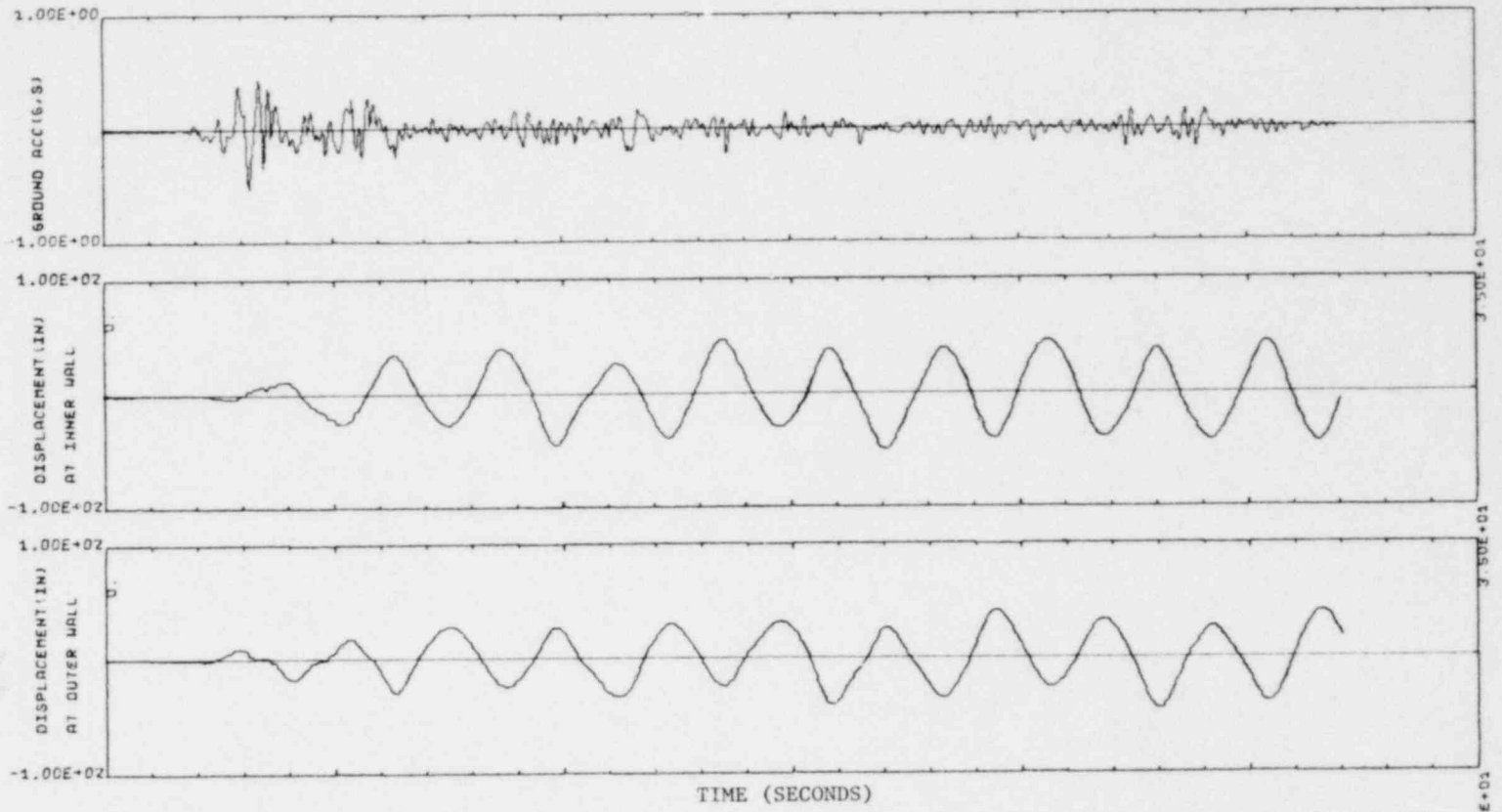

FIG. 3-19 SLOSHING RESPONSE OF WATER IN ANNULAR TANK(INNER RADIUS =480 IN, OUTER RAD=720 IN, DEPTH OF WATER=1440 IN) UNDER ELCENTRO EARTHQUAKE ACCELEROGRAM(1940)

XBL 7812-13913

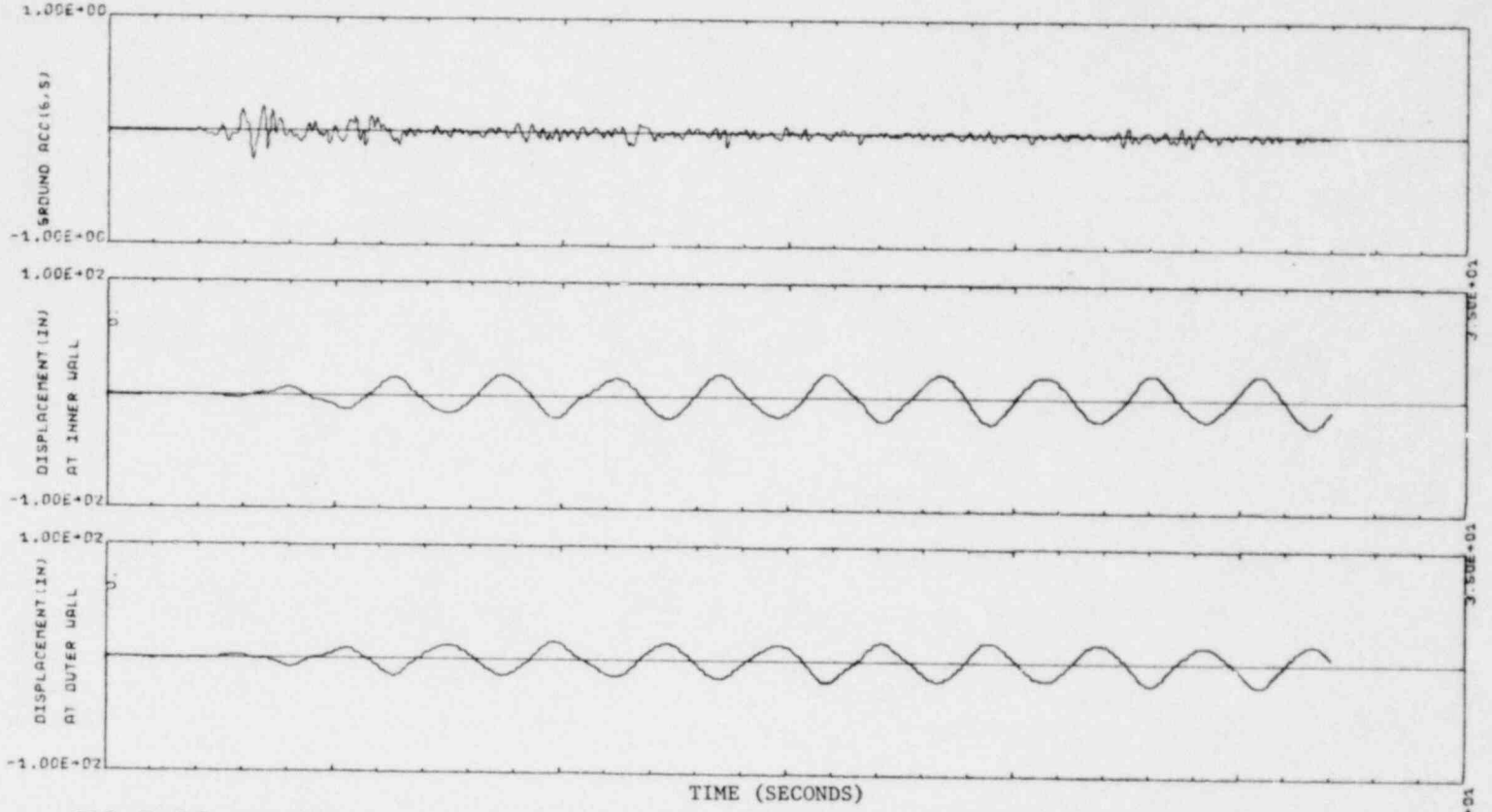

FIG. 3-20 SLOSHING RESPONSE OF WATER IN ANNULAR TANK (INNER RADIUS =480 IN, OUTER RAD=720 IN, DEPTH OF WATER=240 IN) UNDER ELCENTRO EARTHQUAKE ACCELEROGRAM (1940)

XBL 7812-13914

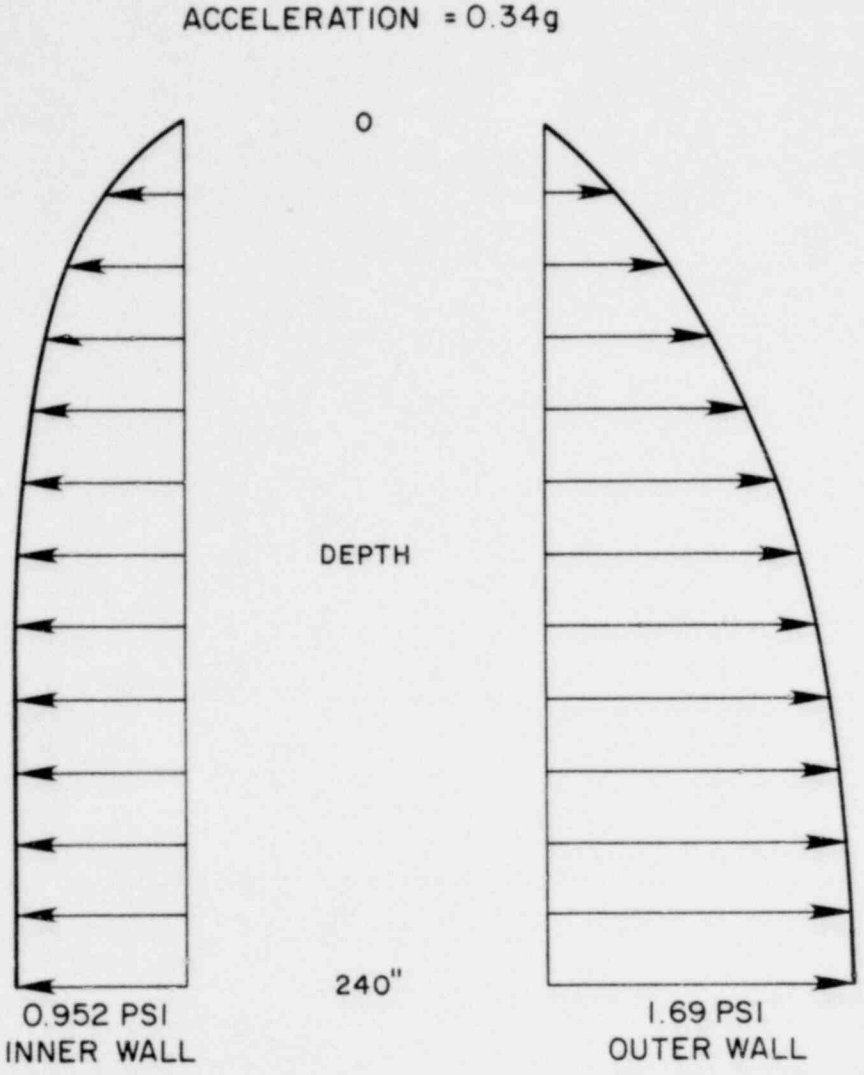

FIG. 3-21 PRESSURE DISTRIBUTION IN PROTOTYPE (a_{MAX}=0.338g)

XBL 782-7208

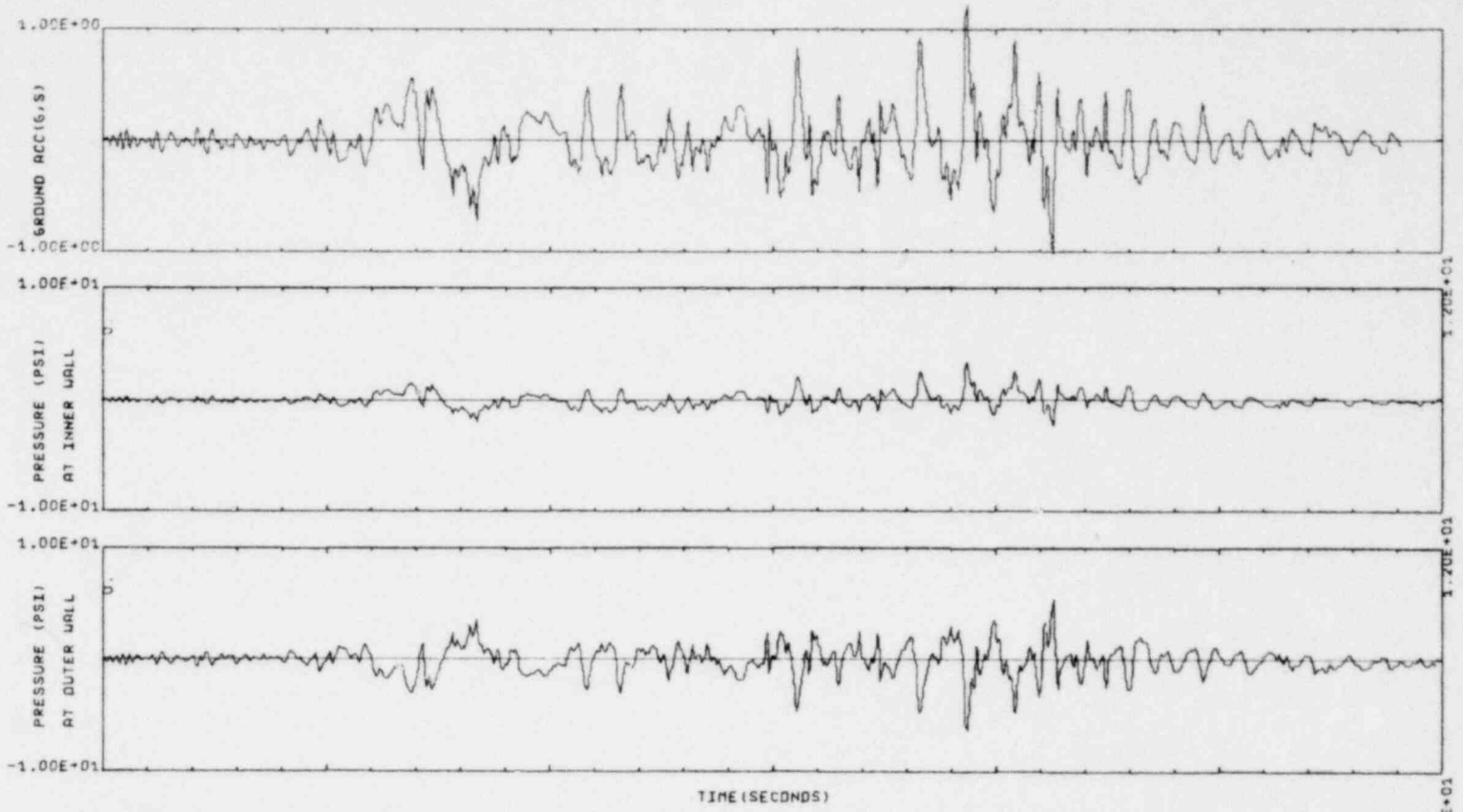

FIG. 3-22 PRESSURE RESPONSE OF WATER IN ANNULAR TANK(INNER RADIUS =480 IN, OUTER RAD=720 IN,DEPTH OF WATER=240 IN) UNDER PACOIMA DAM ACCELEROGRAM(S16E) 1971

XBL 7812-13931

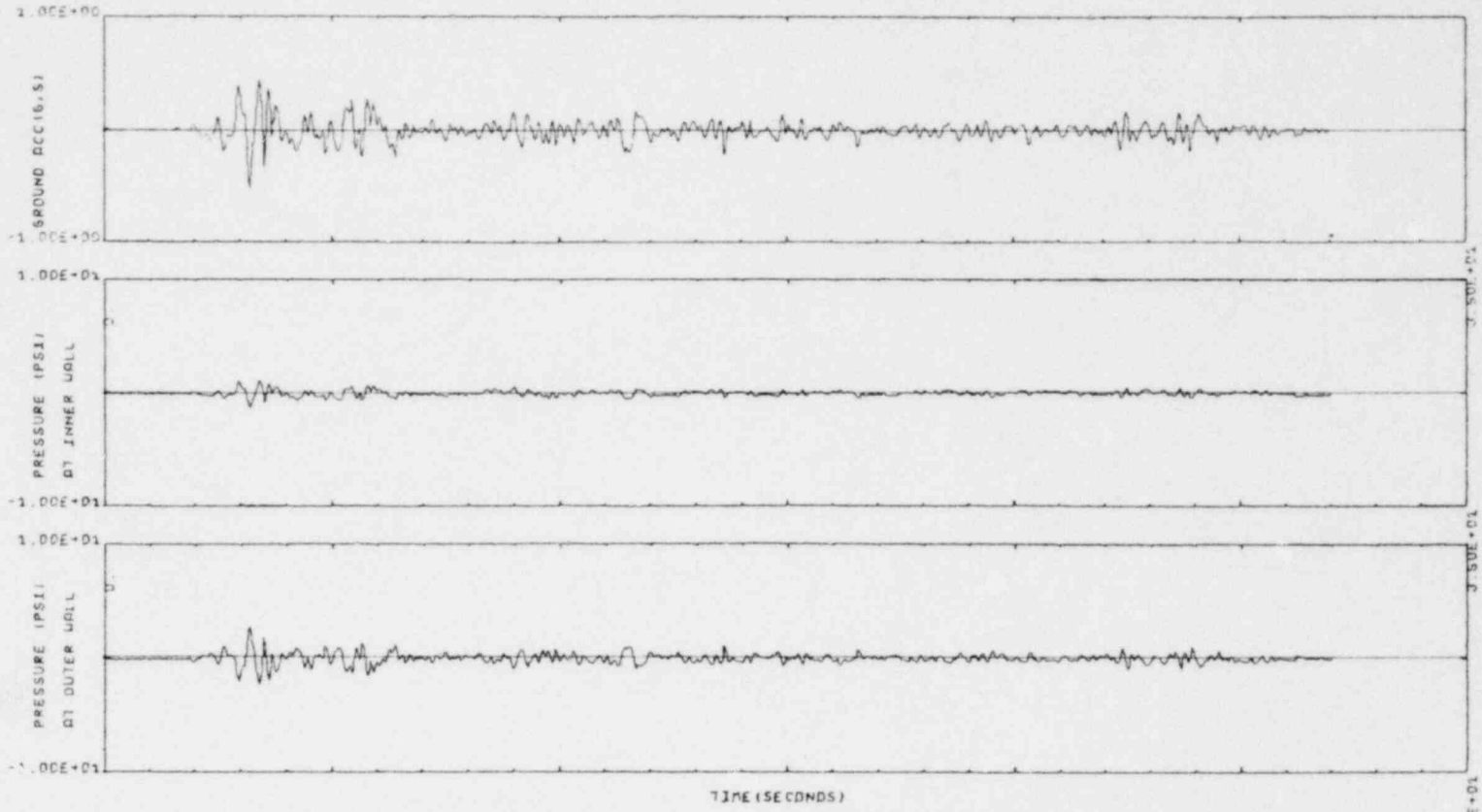

FIG. 3-23 PRESSURE RESPONSE OF WATER IN ANNULAR TANK(INNER RADIUS =480 IN, OUTER RAD=720 IN,DEPTH OF WATER=240 IN) UNDER ELCENTRO EARTHQUAKE(1940)TIME SCALE=1

XBL 7812-13930

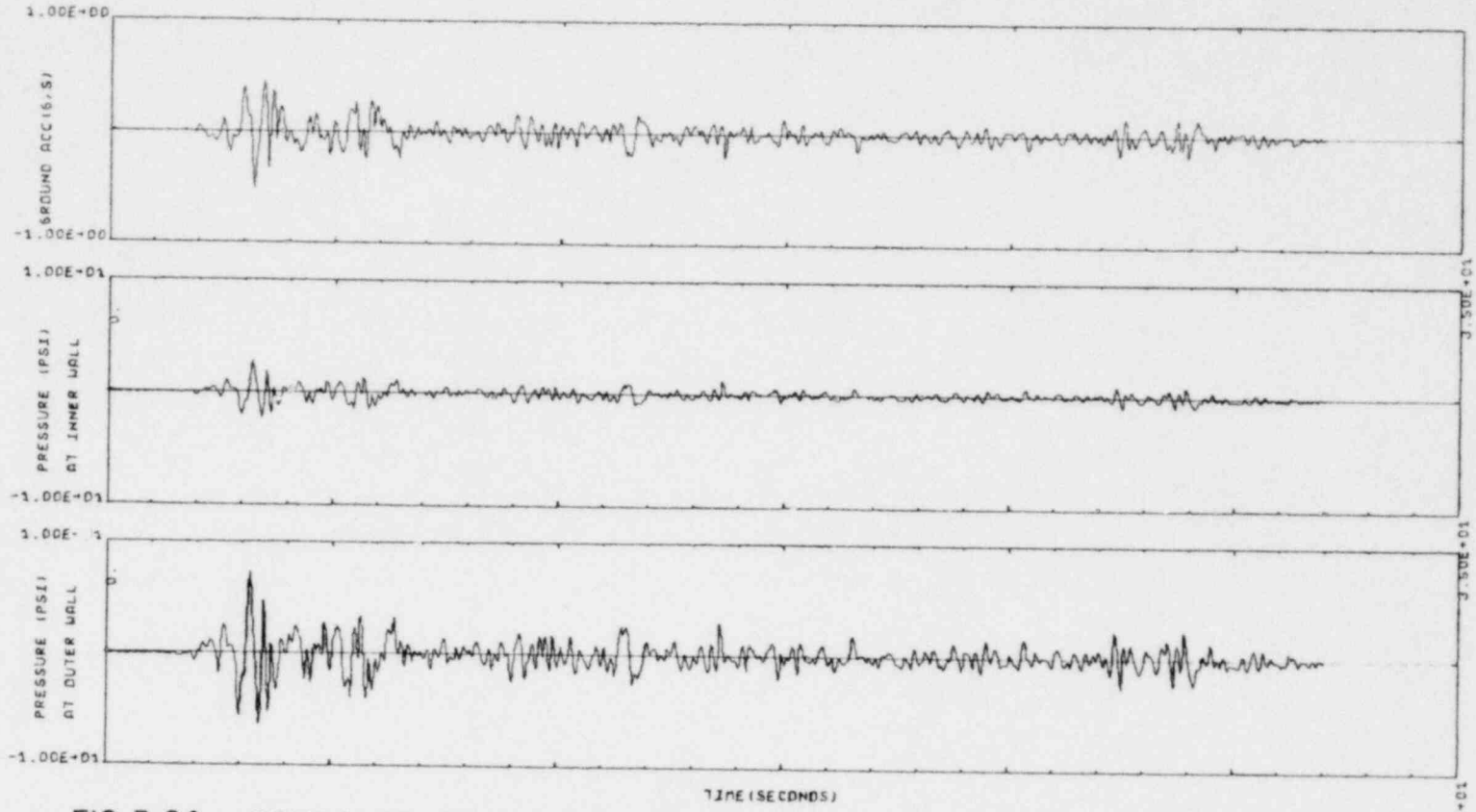

FIG. 3-24 PRESSURE RESPONSE OF WATER IN ANNULAR TANK(INNER RADIUS =480 IN, OUTER RAD=720 IN, DEPTH OF WATER=720 IN) UNDER ELCENTRO EARTHQUAKE(1940) TIME SCALE=1

XBL 7812-13929

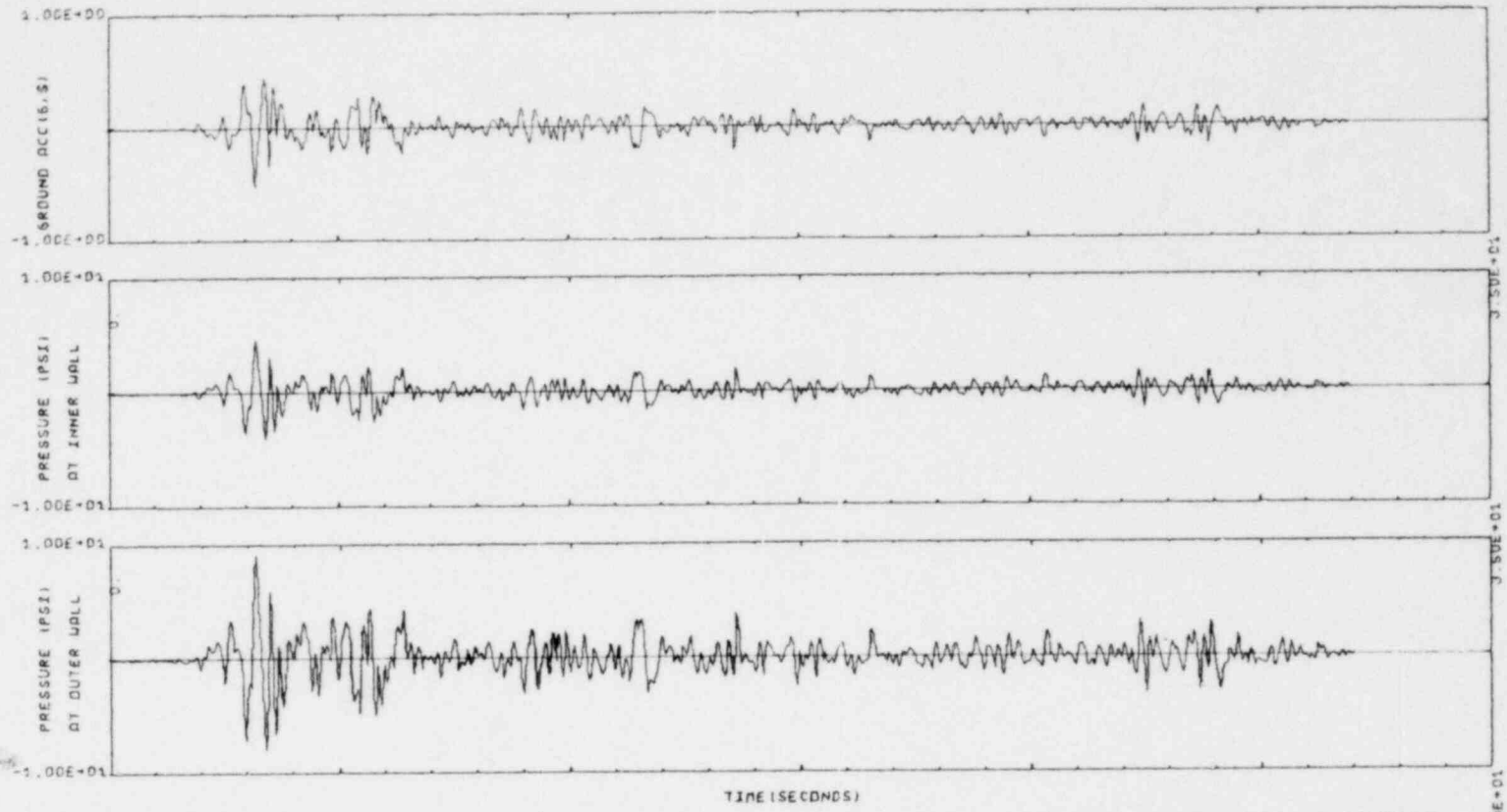

FIG. 3-25 PRESSURE RESPONSE OF WATER IN ANNULAR TANK (INNER RADIUS =480 IN, OUTER RAD=720 IN, DEPTH OF WATER=960 IN) UNDER ELCENTRO EARTHQUAKE (1940) TIME SCALE=1

XBL 7812-13928

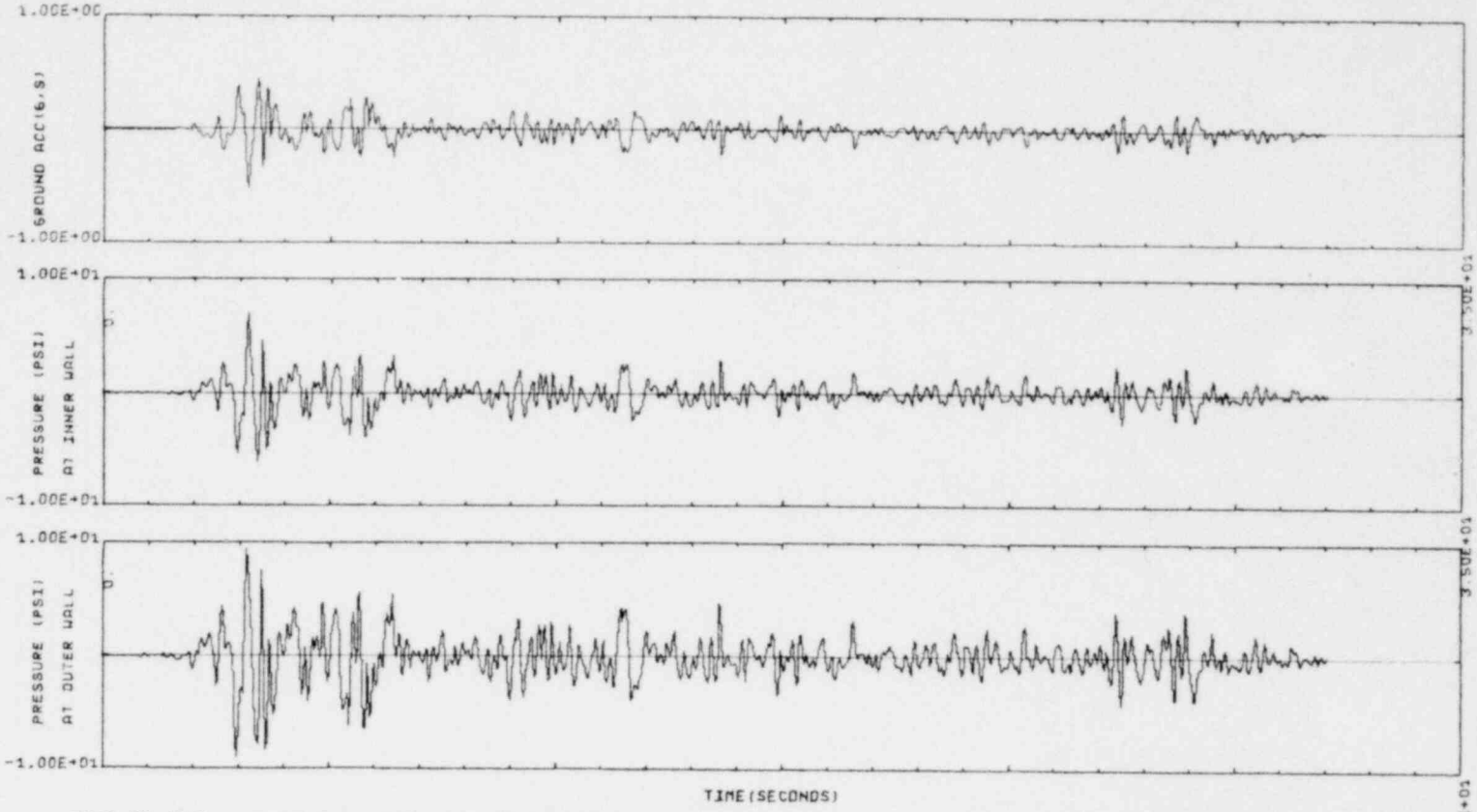

FIG. 3-26 PRESSURE RESPONSE OF WATER IN ANNULAR TANK (INNER RADIUS =480 IN, OUTER RAD=720 IN, DEPTH OF WATER=1440 IN) UNDER ELCENTRO EARTHQUAKE (1940) TIME SCALE=1

XBL 7812-13927

4. SMALL SCALE MODEL STUDIES AND COMPARISON WITH COMPUTER RESULTS

4.1 Introduction

Small scale model tests were conducted primarily

- To help understand the basic sloshing phenomenon on a small readily available 4 × 3 ft shaking table.
- To compare the test results with the computer results from the program SLOSH which was being developed simultaneously.

This testing program helped greatly for both the purposes mentioned above. Based upon the visual observations regarding tangential and radial motion of particles in certain modes, an approximate analysis was developed (see Chapter 3) to predict the sloshing frequencies in annular tanks. This approximate analysis is discussed in Section 2.8.

Tests were carried out on a 1/80th scale model shown in Fig. 4-1. Natural frequencies and water displacements were measured and the test results were compared with the computer results; a good agreement was found between them.

Tests were also performed simultaneously on a small tank which had the same outer diameter as the true scale model but the inner diameter was smaller. These tests were made to study the characteristics of damping and linearity with variation in the value of K.

The small shaking table was only capable of producing harmonic motions, therefore, these tests were carried out under harmonic motions only, and the response under actual earthquake ground motions was left for the larger model on the 20 × 20 ft shaking table which can reproduce actual earthquake accelerograms. Dynamic pressure measurements, being too low in the small model were left for the larger model.

4.2 Model Description

Dimensions of the 1/80 scale model are shown in Fig. 4-1. Inner and outer radii are 6 in. and 9.09 in. respectively. Height of the model is 9 in., but the normal depth of water corresponding to the prototype depth is 3 in. This represents a typical prototype with a = 60 ft, b = 40 ft, and h = 20 ft. Small discrepancy in the outer radii of the model and the prototype was due to fabrication problems.

The model was constructed out of ½-inch-thick plastic and is shown attached to the shaking table in Fig. 4-2. One-half-inch-thick plastic was used to ensure the rigid boundary conditions and it was estimated that the displacements of the tank walls, relative to the base, would be negligible. This true scale model is designated Model 1 in Fig. 4-2. The plastic model designated as Model 2 in Fig. 4-2 has the same outside diameter as Model 1 but the inside diameter is 6 in. instead of 12 in. Model 2 was basically constructed to study the effects of variation of K on the linearity range.

4.3 Instrumentation

Water displacements at each point were measured by means of two parallel stainless wires running through the depth of water and attached to the bottom of the tank. These two wires are insulated from each other at the bottom of the tank and the resistance across the wires is dependent upon the water depth h in the tank (see Fig. 1-3 for the wires).

The stainless steel wires were 0.03 in. in diameter and were spaced 0.25 in. apart. The top end of the wires was connected in a four-arm bridge

circuit across 1Ω resistance as shown in a schematic diagram of Fig. 4-3. Steel wires were connected across a low resistance (1Ω) so that the bridge circuit would remain linear for fairly large variations in the depth of water. Input to the bridge circuit was given by means of a Valedyne carrier demodulator as seen in Figs. 4-2 and 4-3. Carrier demodulator had to be used in order to avoid electrolysis of water.

The bridge was initially balanced when the water was at rest and any variation of water depth in the tank thus caused a change in the resistance across the wires, unbalancing the bridge and giving an output across AC (Fig. 4-3). Thus a continuous output across AC could be measured and related to the water depth. Calibration was done by changing the depth of water by a known amount and measuring the voltage output across AC. During sloshing experiments the output across AC was continuously plotted by means of an oscillograph connected to the bridge across AC, as shown in Figs. 4-2 and 4-3.

Models 1 and 2 both were instrumented with two displacement gages (steel wires). Each displacement gage was located at a distance of 0.2 in. from the walls and along the axis of the shaking table motion (see Fig. 1-3).

Acceleration of the shaking table was measured by an accelerometer (see Fig. 1-3) attached to the table and the output was connected to the oscillograph via an amplifier for a continuous record. As a further check on the accuracy of the accelerometer, the displacements of the shaking table were also recorded from the MTS control panel and the accelerations were computed from displacements knowing the frequency of the sinusoidal motion.

The frequency of the shaking could be determined either from the oscillographs or directly from the function generator (Fig. 4-2).

4.4 Shaking Table

The shaking table (Fig. 4-2) consists of a 4 × 3 ft aluminum plate which is ½-in. thick and is reinforced by 4 × 2 inch channel sections spaced 1 ft apart. The table is supported on four linear roller bearings and is driven horizontally by a 50 kip hydraulic actuator. The table has 3/8-in. tapped holes at 8-in. spacing through which the structure can be fixed to the table.

The hydraulic actuator is controlled electronically via a servo-valve as shown in Fig. 4-2. The servo-valve has a 20 gpm capacity and normally operates at a pressure of 3000 psi. The hydraulic actuator which drives the shaking table has a capacity of ±2.5 inches.

The electronic control system for the servo-valve consists of an MTS Systems Corporation's supplied console (see Fig. 4-2) which acts as an amplifier for the input signal and compares it with the feedback signal. The input signal is generated by a function generator (shown in Fig. 4-2) which can generate harmonic signals over a wide range of frequencies.

The input signal as generated by the function generator is fed to the servo-valve via MTS control system's amplifiers. Servo-valve controls the flow and pressure of oil to the hydraulic actuator and drives it according to the input signal. Servo-valve also sends a feedback signal to the MTS control console which compares the feedback signal with the input signal, and the MTS system stops automatically if there is any significant discrepancy between the input and feedback signals.

4.5 Test Set-up and Testing Procedure

Test set-up is shown in Fig. 4-2. Models 1 and 2 were fixed to the shaking table such that the displacement meters lie at the points where maximum water displacements were expected. The displacement meters were connected in the four-arm bridge and the output signal was wired to the oscillograph through the amplifier of the carrier demodulator for a continuous record of the water displacements. The accelerometer was also connected to the oscillograph through the amplifier.

Before starting the actual experiment, the displacement meters were carefully calibrated. The depth of water in the tanks was brought to a certain level and the bridge circuit was balanced. Then water was added to the tanks at a constant flow rate and a continuous plot of the signal was obtained on the oscillograph to make sure that the plot was a straight line within the range of maximum and minimum displacements expected in the tank. A straight-line plot ensured the linearity of the bridge circuit. The oscillograph output was then related to the change in water depth in the tank and scale was established between the surface water displacements and the oscillograph output.

After calibration of the displacement meters and the accelerometer, water depth in the tanks was brought up to the required level and the shaking table was given a sinusoidal input at a pre-selected frequency. The amplitude of the table acceleration was brought up slowly to the required level with the help of MTS console. The frequency of the table motion could be changed continuously with the help of the function generator and this procedure was adopted to search out the sloshing frequencies.

Table acceleration and water displacements were recorded on the oscillograph whenever desired. Frequency of the sinusoidal motion was

directly read from the function generator and the amplitude of the displacement of the hydraulic ram was also recorded directly from the MTS control which would be the same as the amplitude of the shaking table. Thus knowing the displacement amplitude and the frequency of the motion, the acceleration of the table could be determined directly and was a further check on the accuracy of the acceleration measured from the oscillograph as recorded from the accelerometer.

It was learned during the initial part of testing that the two displacement meters located in the same tank become coupled with each other through water, and since they are located quite close to each other, this caused some error due to interaction, especially when water displacements were out of phase. In subsequent testing, therefore, only one displacement meter was connected in each tank except when the mode shape was required.

4.6 Determination of Natural Frequencies and Mode Shapes

To determine the natural sloshing frequencies, table was excited at a low but roughly constant amplitude of acceleration, and the frequency of the sinusoidal motion was slowly increased until resonance occurred and a marked increase in the amplitude of the sloshing water was observed. The frequencies at which resonance occurred were recorded as these represent the natural frequencies of sloshing. As the table motion was horizontal only, the antisymmetric modes were excited.

Mode numbers 1 (see Fig. 4-4 for Mode 1) and 2 were very easy to produce and the amplitude of sloshing becomes very high even with extremely small accelerations. Mode number 3 was rather hard to excite on account of its rather symmetrical shape about a vertical axis passing through the

middle of the annulus (see Fig. 3-1). Similarly, mode numbers 5, 7, 9, ... and so on will be hard to excite and therefore would contribute little to the overall response under earthquake-type of accelerograms.

Mode numbers 4, 6, 8, ... and so on can be excited easily but the amplitude of mode shapes above mode number 6 again becomes rather small and the contribution to water displacements by higher modes would be rather small. This fact was verified by the computer analysis which showed that under earthquake accelerograms, the major share of the response comes through the first and second modes. Mode number 3 contributes very little and mode number 4 contributes significantly, and modes higher than 4 contribute very little to the sloshing response.

Table 4-1 shows the measured and computed frequencies for Models 1 and 2. It will be seen that whereas the numerical difference between the first and the second natural periods is rather large, the difference between the subsequent consecutive periods becomes small. Table 4-1 gives the sloshing frequencies for $h = 3$ in. and $h = 5$ in., where h is the depth of water in the tank and it can be seen again that changing the depth of water from 3 in. to 5 in. does not cause any appreciable change in the natural frequencies except the first one.

During the course of testing it was observed that the particle motion was tangential in the first antisymmetric mode and radial in all the higher modes in Model 1. This can be explained on the basis of water surface gradients. Looking at Fig. 3-1, it can be observed that there is almost zero slope in the radial direction and the slope in the tangential direction will be much higher (because the displacements vary with $\cos\theta$) and therefore the movement of particles will be in a tangential direction. This, however, is not true for the second or higher modes (see

TABLE 4-1. Test and analytical frequencies of Models 1 and 2.

Mode number	Natural Sloshing Frequencies (Hz)			
	Model 1		Model 2	
	Test	Theory	Test	Theory
	for h = 3 in.			
1	0.70	0.70	0.90	0.88
2	3.20	3.17	2.30	2.31
3	4.50	4.47	3.20	3.22
4	5.50	5.47	3.90	3.92
	for h = 5 in.			
1	0.90	0.87	1.10	1.07
2	3.20	3.18	2.40	2.37
3	4.50	4.50	3.20	3.22
4	5.50	5.51	3.90	3.91

Fig. 3-1) where the gradients are much higher in the radial direction compared to those in the tangential direction and therefore the particle motion should be in the radial direction for these modes. Based upon this observation, an approximate analysis has been presented to predict the natural frequencies in annular-circular tanks (see Section 2.8) with comparatively higher values of K.

It was also observed that when the water was sloshing in the first and second natural modes, it could become unstable very easily (due to slight imperfections) and would start sloshing along an axis not aligned with the axis of ground excitation. This instability problem may not, however, be important for sloshing under earthquake accelerograms.

Test data regarding the mode shapes are shown in Fig. 4-5 along with the predicted mode shapes. Test data represents only two points since there were only two water measurement gauges near the tank walls. The data in Fig. 4-5 relates to Model 1 only.

4.7 Determination of Damping

Damping of the sloshing mass of water was determined by exciting the water in its first natural sloshing mode and then recording the free vibration time history as the amplitude of the motion dies down. Two such typical plots for Models 1 and 2 are shown in Fig. 4-6. The depth of water in both cases was 3 in. and frequency of vibration was 0.7 Hz and 0.9 Hz for Models 1 and 2 respectively. Similar plots were obtained for both models for depth of water equal to 5 in.

Using decay curves of the type shown in Fig. 4-6, damping was determined as follows.

Let A_1 be the amplitude of sloshing at a particular time, and A_2 be the amplitude after m consecutive vibrations. Then for a lightly damped system, damping β can be determined from the following formula:

$$\beta = \log_e \frac{\left(\frac{A_1}{A_2}\right)}{(2\pi m)}$$

The values of the damping for Models 1 and 2 for h = 3 in. were 0.84% and 0.48% of the critical damping respectively. The corresponding values for h = 5 in. were 0.65% and 0.36% respectively for Models 1 and 2. It can be seen that the damping decreases as the depth is increased, as would be expected. It can also be expected that as the tank size is increased the damping will be reduced and very little amount of damping can be expected in a prototype structure.

4.8 Determination of Water Displacements Under Sinusoidal Ground Motions

Water displacements were measured only at the inner wall along the axis of ground motion in each model. The shaking table was given a sinusoidal acceleration at a predetermined frequency; the amplitude was brought up to the required level and the table was allowed to run for about 30 to 60 seconds until the response of the water became steady. When the sloshing response became steady, the oscillograph was turned on to have a continuous plot of the water displacements and table acceleration. Such a typical plot is shown in Fig. 4-7. The upper plot in Fig. 4-7 shows the table acceleration and the lower curves indicate the displacement response at the inner walls of Models 1 and 2. It is clear from this

figure that the response is steady state.

Using such plots as shown in Fig. 4-7 for each test, the amplitudes of ground acceleration and water displacements were determined. Amplitude of the ground acceleration was also determined from the recorded displacement amplitude as read directly on the MTS console as a double check. Frequency of the motion was recorded from the function generator. Tests were made for various frequencies and level of ground accelerations as shown in Table 4-2. This table shows the frequency and the amplitude of acceleration of the sinusoidal motion of the shaking table along with the measured and predicted values of the displacements at the inner walls of Models 1 and 2.

The data given for Model 1 in Table 4-2 can be applied to the prototype structure using the laws of simlitude. Let L_r = Model/Prototype scale ratio.

From dimensional analysis, it can be shown that if the frequencies of sinusoidal ground motion are scaled by a factor of $\sqrt{L_r}$, then the displacements in the prototype can be obtained by multiplying the model displacement values by a factor $1/L_r$.

4.9 Comparison of Test and Analytical Results

4.9.1 Frequencies and mode shapes

Comparison between the test and predicted frequencies for Models 1 and 2 is shown in Table 4-1. The results are given for water depths equal to 3 in. and the frequencies are given in Hz. It can be seen in Table 4-1 that the agreement between the test and analytical

TABLE 4-2. Sloshing response of water in Models 1 and 2 under sinusoidal ground accelerations (h = 3 in.).

Frequency (Hz)	Acceleration (g)	Maximum Displacement at Inner Wall (Inches)					
		Model 1			Model 2		
		Test	Theory	Test / Theory	Test	Theory	Test / Theory
0.6	0.00195	0.047	0.051	1.08	0.013	0.014	1.08
0.6	0.00390	0.103	0.102	0.99	0.026	0.028	1.08
0.6	0.00490	0.138	0.128	0.93	0.034	0.035	1.03
0.6	0.00585	0.167	0.153	0.92	0.040	0.042	1.05
1.2	0.00780	0.042	0.045	1.07	0.073	0.080	1.09
1.2	0.0156	0.087	0.090	1.03	0.150	0.160	1.06
1.2	0.0234	0.128	0.135	1.05	0.224	0.240	1.07
1.2	0.0312	0.184	0.180	0.98	0.308	0.321	1.04
2.0	0.0212	0.070	0.070	1.00	0.214	0.234	1.09
2.0	0.0265	0.081	0.087	1.07	0.275	0.293	1.06
2.0	0.0319	0.101	0.105	1.04	0.344	0.353	1.03
2.0	0.0424	0.137	0.139	1.01	0.450	0.469	1.04
2.0	0.0530	0.168	0.174	1.04	0.580	0.586	1.01
3.7	0.0146	0.054	0.047	0.87	0.036	0.039	1.08
3.7	0.0291	0.110	0.094	0.86	0.072	0.079	1.10
3.7	0.0437	0.160	0.140	0.88	0.112	0.118	1.05
3.7	0.0582	0.217	0.186	0.86	0.150	0.157	1.05
3.7	0.0742	0.271	0.237	0.88	0.196	0.201	1.03

results is very good and within acceptable limits of experimental error.

Comparison between the test and analytically predicted mode shapes is shown in Fig. 4-5 for Model 1. The experimental values are given at only two points near the tank walls and the comparison has been made for mode shapes 1 and 2 only. It can be seen that the agreement between the test and predicted values is excellent for the first mode but slightly off for second mode shape. The reason for the discrepancy in the second mode was attributed to interaction between the displacement meters because of the fact that the water displacements are in opposite phase. This interaction problem does not cause any measurement errors in the first mode because in this case the water motion is in phase and of the same amplitude at the inner and outer walls and this matches exactly the conditions under which the calibration of the displacement meters was done.

4.9.2 Forced harmonic response

Test and analytical results of water displacements at the inner wall of Models 1 and 2 are shown in Table 4-2 for sinusoidal ground motions. All tests represent a steady-state response and the water depth was always 3 in. Table 4-2 shows the frequencies and amplitude of sinusoidal ground motion. The amplitude of the ground motion is given in terms of acceleration in g's and frequency is given in Hz. In addition to the test and predicted values of displacements of water surface (given in inches), Table 4-2 also shows the ratios between the test and theoretical displacement values indicating error on the basis of test values. It should be remembered that the steady-state sloshing response under harmonic ground acceleration will also be harmonic with the same frequency as the ground excitation

frequency. Thus the water displacement values given in Table 4-2 represent the sloshing amplitude.

In Table 4-2, it can be seen that the agreement between the test and analytical results is generally within 10% except for a few values of Model 1. It can also be seen that in Model 2 the test results are always lower than the analytical results, but this is not true for Model 1 indicating that damping (viscosity) is probably not the major source of discrepancy between the two results. If it were so, then test results should always be lower compared with the analytical results which neglect the viscosity (damping) of water.

Figures 4-8 and 4-9 show the comparison of test and analytical water displacements (time-history plots) at the inner wall of Models 1 and 2 respectively. The comparison is shown by superimposing the test results (dotted line) over the analytical results (solid line) by the middle curves in Figs. 4-8 and 4-9. Ground motion frequency and acceleration amplitude was 1.2 Hz and 0.0312 g, respectively, and is represented by the upper curves in Figs. 4-8 and 4-9. It can be seen that the agreement between the test and computer results is good in this case and is within 4% as may be seen in Table 4-2.

Figure 4-10 shows the variation of sloshing response displacements at inner walls of Models 1 and 2 under sinusoidal ground accelerations of frequency 2 Hz and varying amplitude of motion. Figure 4-10 shows both the test and analytical values as given in Table 4-2. It can be seen that the displacements increase linearly with an increase in the ground motion amplitude within the limits indicated in Fig. 4-10. It is clear that the test values agree well with the theoretical linear line, indicating that the sloshing response is in fact quite linear in the range of Fig. 4-10.

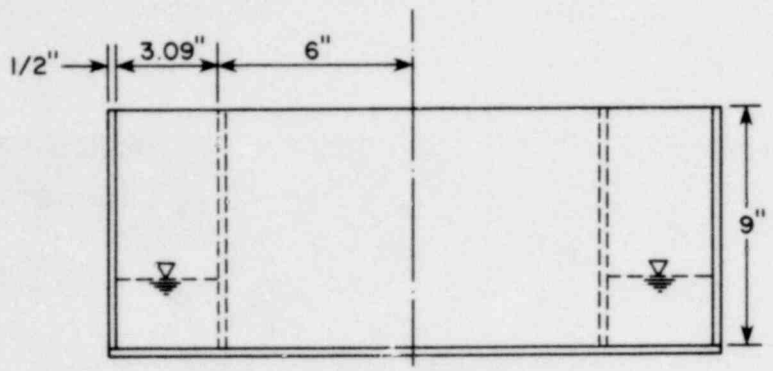

ELEVATION

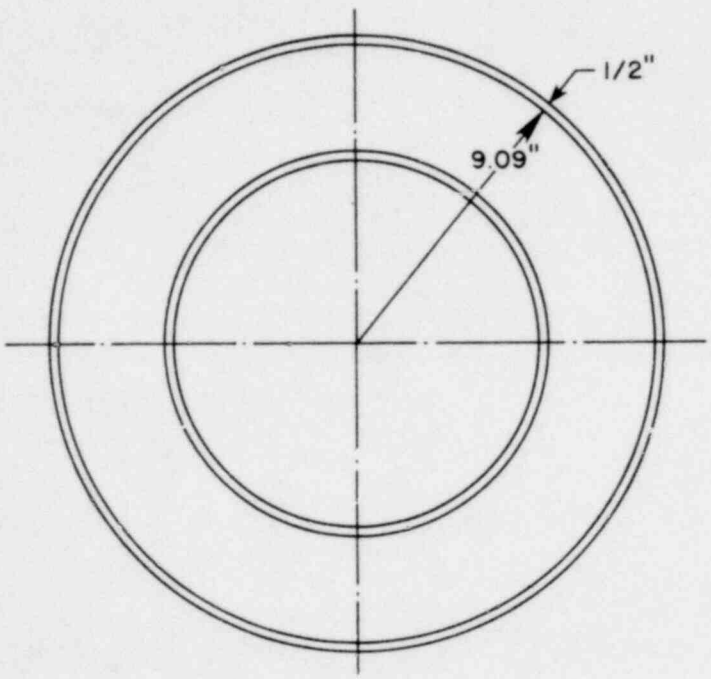

PLAN

FIG. 4-1 DIMENSIONS OF 1/80 SCALE MODEL

XBL 7812-13932

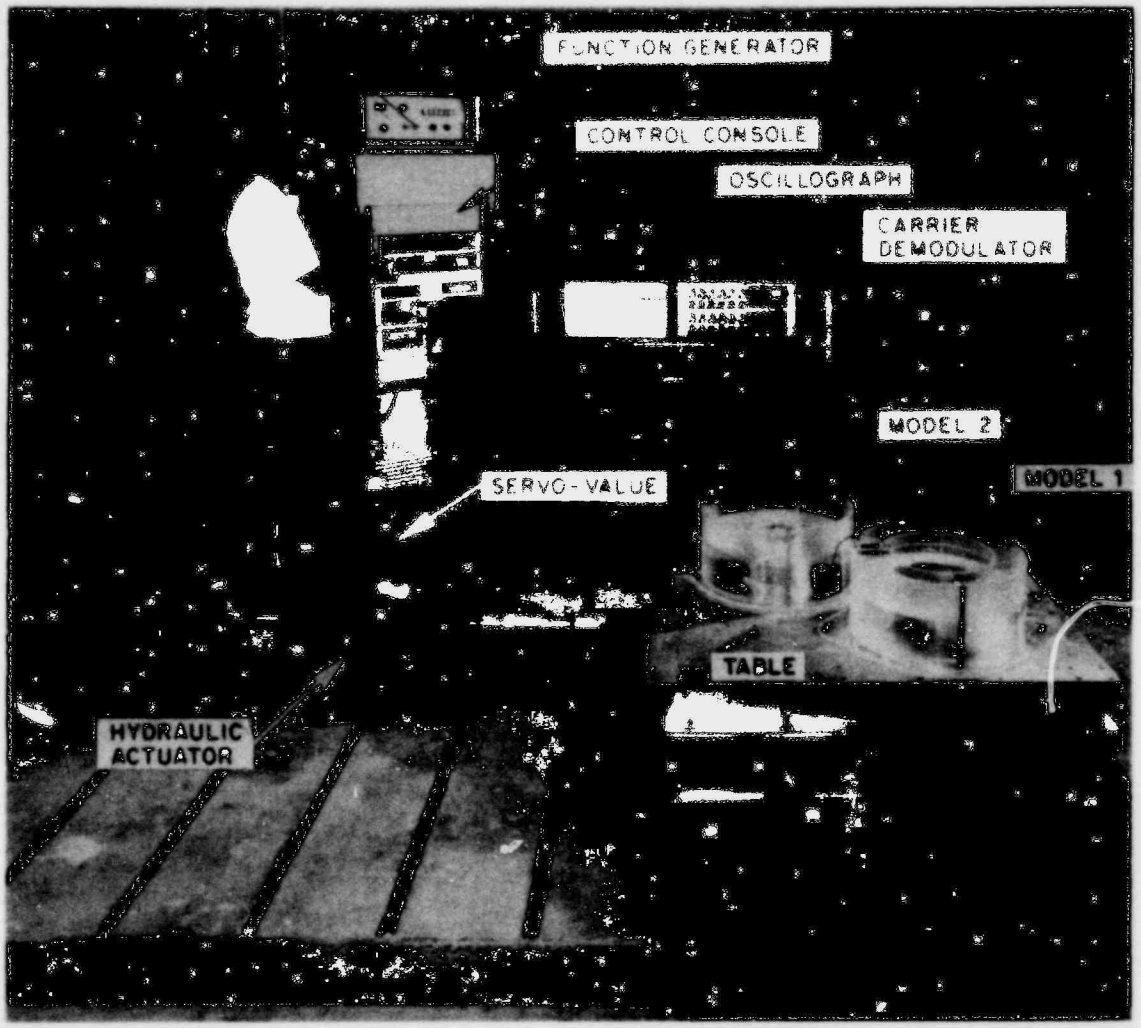

CBB 762-1195A

FIG. 4-2 TEST SET-UP FOR SMALL SCALE MODEL TESTS

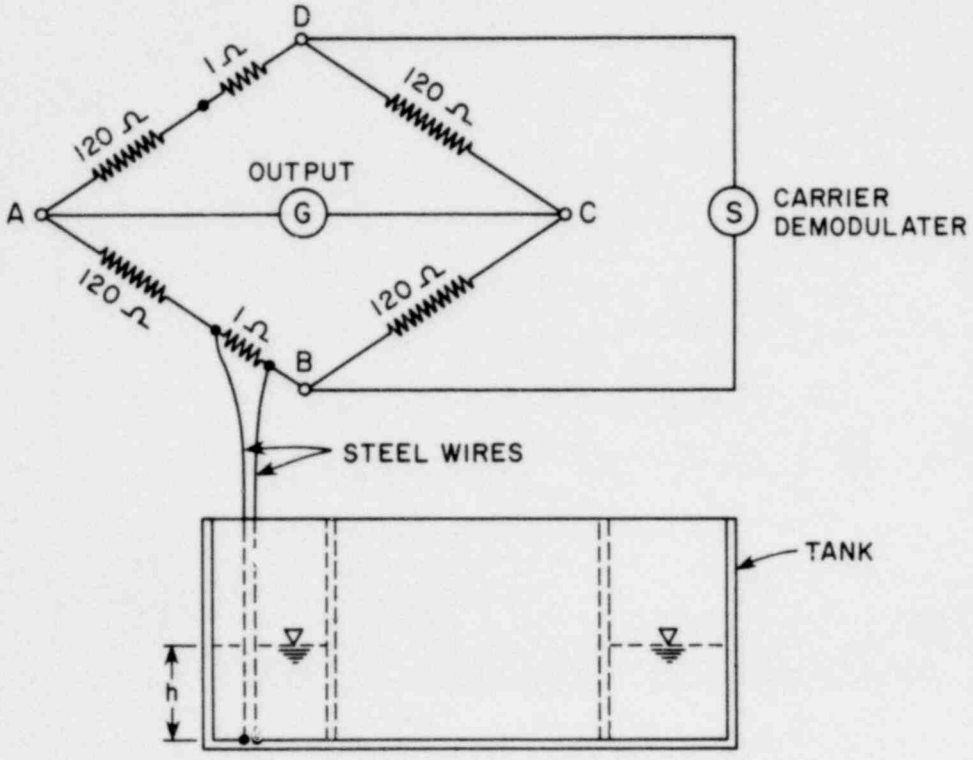

FIG. 4-3 SCHEMATIC DIAGRAM FOR DISPLACEMENT GAGE

XBL 7812-13933

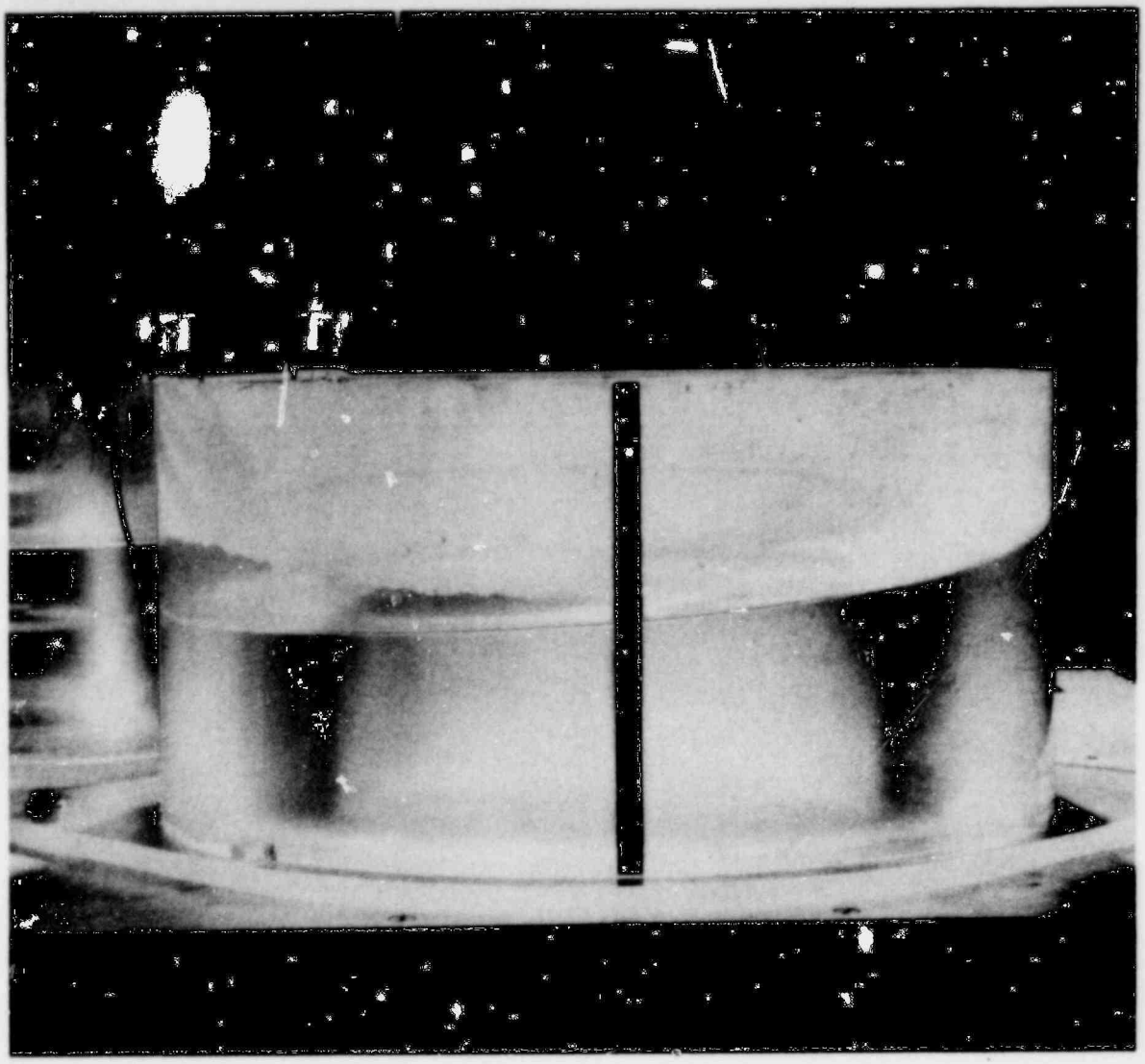

CBB 762-1193A

FIG. 4-4 MODEL 1 SHOWING THE FIRST SLOSHING MODE

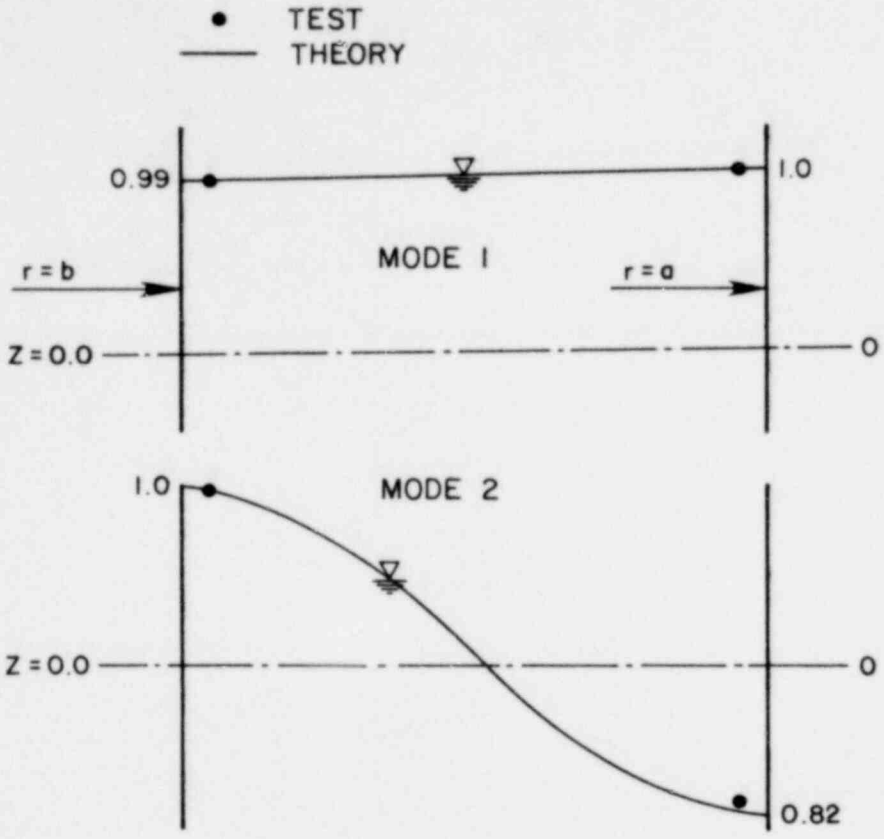

FIG. 4-5 COMPARISON OF TEST AND ANALYTICAL MODE SHAPES (MODEL I)

XBL 7812-13934

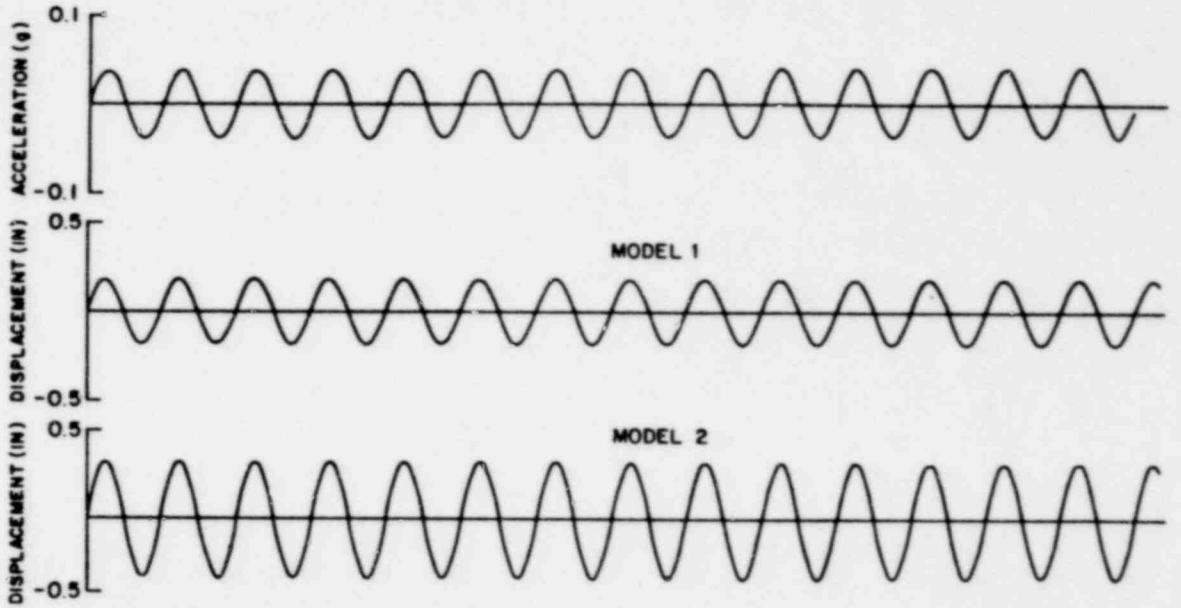

FIG. 4-7 SLOSHING DISPLACEMENTS AT INNER WALL OF MODELS 1 AND 2 (TEST) UNDER SINUSOIDAL ACCELERATIONS OF FREQUENCY 1.2 H_z AND AMPLITUDE 0.0312g

XBL 7812-13935

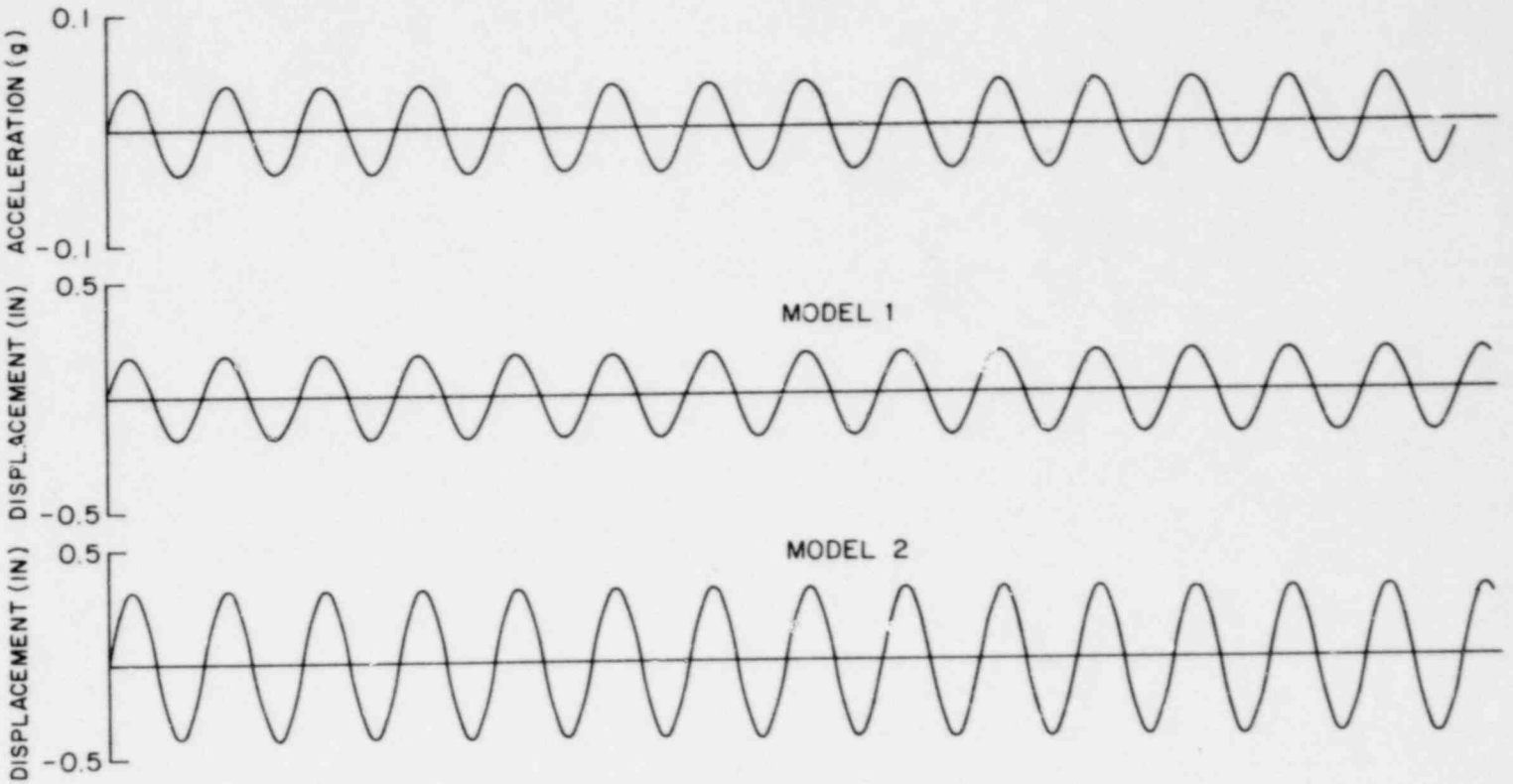

FIG. 4-7 SLOSHING DISPLACEMENTS AT INNER WALL OF MODELS 1 AND 2 (TEST) UNDER SINUSOIDAL ACCELERATIONS OF FREQUENCY 1.2 H_z AND AMPLITUDE 0.0312g

XBL 7812-13936

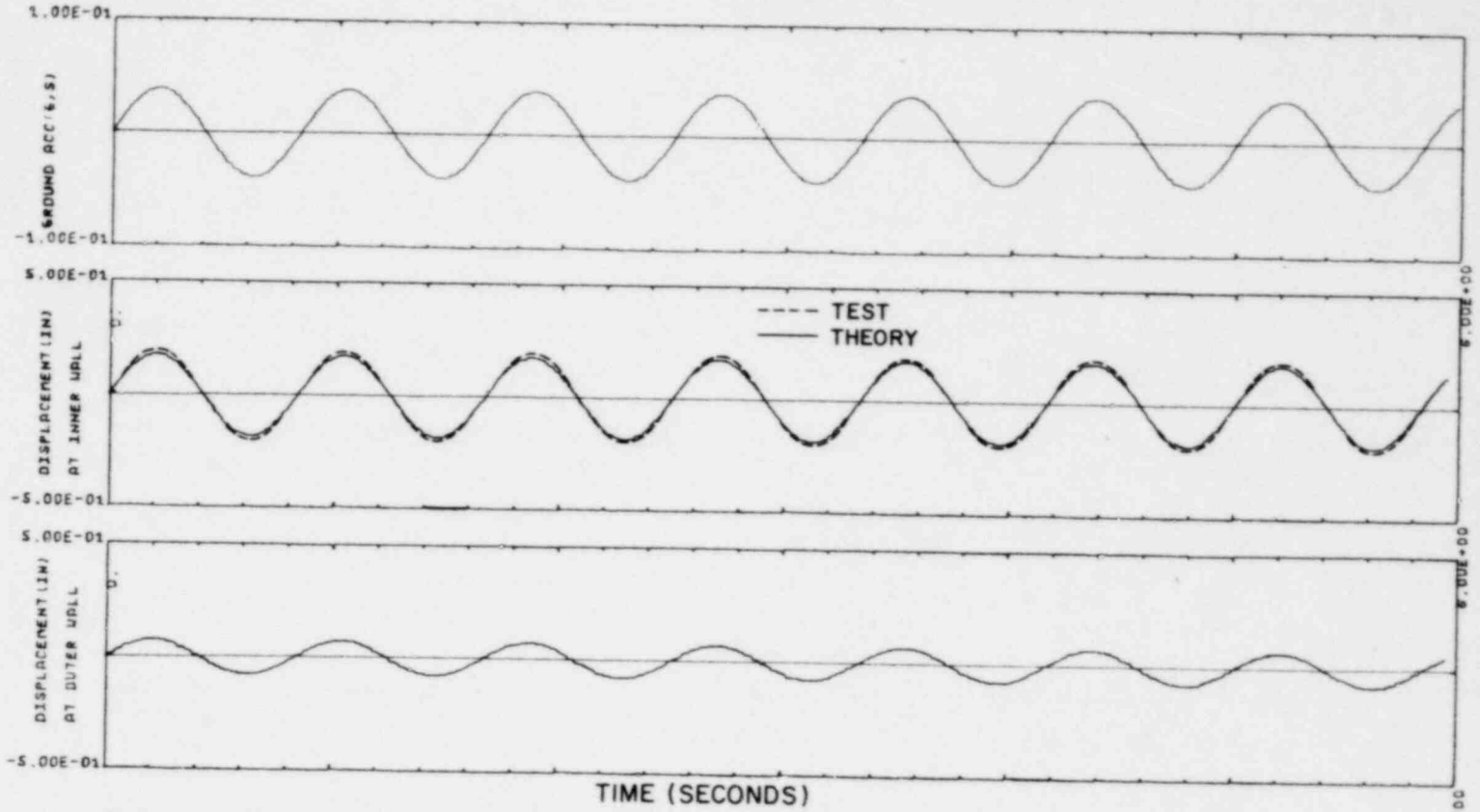

FIG. 4-8 SLOSHING RESPONSE OF WATER IN ANNULAR TANK(INNER RADIUS =6.0 IN, OUTER RAD=9.0 IN, DEPTH OF WATER=3.0 IN) UNDER HARMONIC GROUND ACCEL. OF AMPLITUDE-0.03126, FREQ.=1.20HZ

XBL 7812-13938

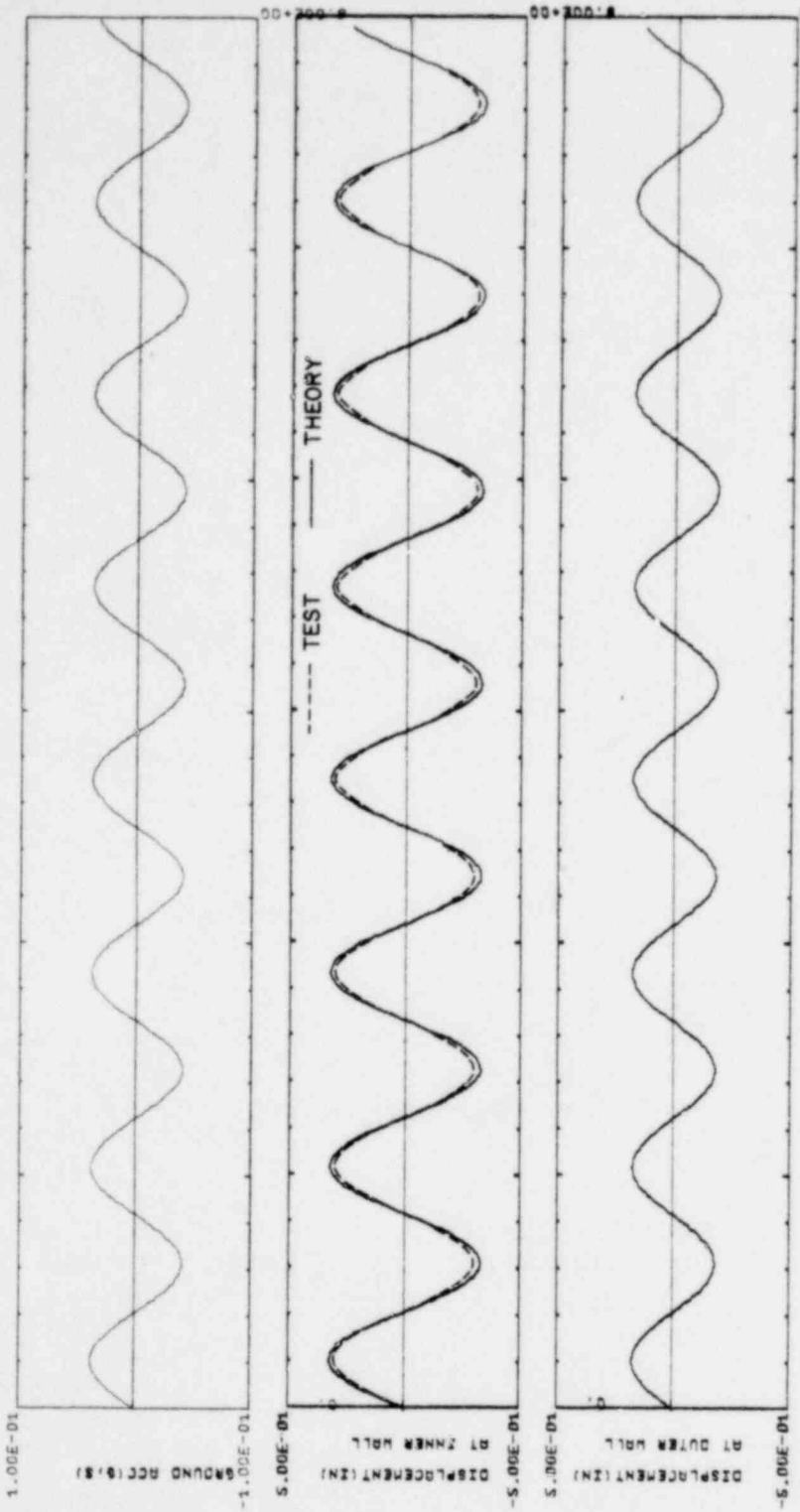

FIG.4-9 SLOSHING RESPONSE OF WATER IN ANNULAR TANK(INNER RADIUS =3.0 IN, OUTER RAD=9.0 IN, DEPTH OF WATER=3.0 IN) UNDER HARMONIC GROUND ACCEL. OF AMPLITUDE=0.03126,FREQ.=1.20HZ

XBL 7812-13937

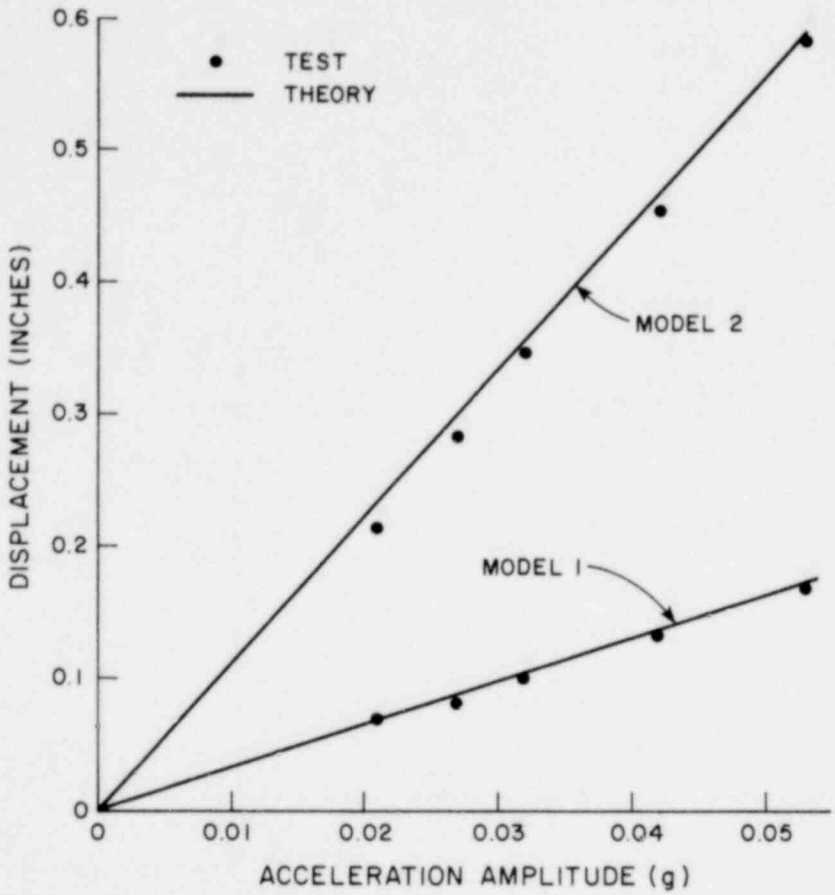

FIG. 4-10 VARIATION OF SLOSHING DISPLACEMENT AT INNER WALL UNDER SINUSOIDAL GROUND MOTION OF FREQUENCY 2 H_z

XBL 7812-13939

5. LARGE SCALE MODEL TESTS AND COMPARISON OF COMPUTER AND TEST RESULTS

5.1 General

The purpose of these tests was to check the accuracy of the analytical model and to determine the range in which the linear solution is satsifactory. These tests were conducted under simulated earthquake ground motions on the 20 × 20 ft shaking table located at the Earthquake Engineering Research Center, University of California, Berkeley. The test model consisted of an 8-ft-diameter steel tank and the quantities measured included the water surface displacements and dynamic pressures. The effect of the vertical ground acceleration on the sloshing response was also studied in these tests.

Tests were carried out with and without a damping mechanism present in the tank and the value of damping was determined in both cases. Details of the model, instrumentation, testing procedure, and comparison with the analytical results are presented in this chapter.

5.2 Model Description and Instrumentation

Figure 5-1 shows a 1/15th scale model of a pressure-suppression pool used in boiling-water reactors. The external and internal radii of the model were 48 in. and 33.2 in., respectively, and the height was 48 in.

The model was made of steel with 1/4-in.-thick walls which were welded to a 3/4-in.-thick base plate. The tank walls were stiffened in the vertical and horizontal directions by means of 3/16 × 2 × 2-in.-angle iron as may be seen in Fig. 5-1. The tank was provided with nine observation

windows in one-half of the tank. Each observation window was 8 × 40-in. and was fitted with 1-in.-thick lucite, having grid lines to indicate the relative motion of water. The observation windows were used to make a movie showing the water motion.

The tank was instrumented with six water displacement gages and three pressure gages. The location of the water gages is shown in Fig. 5-2. Figure 5-4 is a close-up view of water gages 4 and 5. Note that in Fig. 5-4 there is also a water gage in between gages 4 and 5 but it was disconnected to overcome interaction problems. These water gages work on the same principle as explained in Chapter 4.

The location of the pressure gages is shown in Fig. 5-3. A close-up view of the location of gage numbers 1 and 2 can also be seen in the photograph of Fig. 5-5. At location number 1, the pressure gage has been removed while location number 2 shows both the gage and the adapter (Fig. 5-5). These pressure gages are of a piezoelectric type and measure the dynamic pressures.

5.3 Internal Damping System

Since the internal damping of the water system is very low, it was considered highly desirable to study the effect of introducing an artificial damping mechanism which would create turbulence and thus increase energy loss. The design chosen for this internal damping mechanism is shown in Fig. 5-6. This design was based both on the initial observations in the small scale model studies, and also on computer analysis of the sloshing behavior of water in such annular tanks under actual earthquake ground motions. It was pointed out in Chapter 4 that the motion of the water

particles in the first and second antisymmetrical modes is tangential and radial respectively. The computer analysis showed that the second mode is the dominant mode of sloshing in such annular tanks under earthquake accelerograms (see Chapter 3) with significant contribution from the first mode.

Based upon the observation mentioned above the design shown in Fig. 5-6, which consists of a circular screen and four radial sections, was selected. The diameter of the circular screen was 6 ft, 9 in. and the screen was 3 ft high. The screen was made up of 3/64-in.-thick aluminum sheet with 1/8-in.-diameter holes. The ratio of the open area to the closed area was roughly 3 to 2. The circular portion of the screen was designed to offer resistance to the radial motion (i.e., to second mode sloshing) of the water, whereas the four radial sections of the screen were designed to reduce the water motion in the tangential direction (i.e., to first mode sloshing). The circular screen was stiffened by means of vertical strips of aluminum which were then fastened to the tank walls at the top and bottom by means of horizontal strips (see Figs. 5-1 and 5-6). Figure 5-1 shows the damping system placed and fastened inside the tank.

5.4 Shaking Table and Associated Systems

The shaking table is located at the University of California Richmond Field Station. It has plan dimensions of 20 ft × 20 ft, with one horizontal and the vertical degrees of freedom. It may be used to subject structures weighing up to 100 kips to motions of about twice the intensity of the N-S component of El Centro (1940) earthquake.

Figure 5-7(a) shows the shaking table with the tank model prestressed to it. The shaking table is constructed with a combination of reinforced and prestressed concrete and may be considered as a 1-ft-thick, 20-ft-square plate stiffened with heavy ribs. The table, which weighs 100 kips, is driven horizontally by three 50-kip hydraulic actuators and vertically by four 25-kip hydraulic actuators. The horizontal and vertical actuators are 10-ft, 6-in. and 8-ft, 8-in. long, and are equipped with 200 gpm and 90 gpm servo-valves, respectively. These actuators are located in a pit beneath the table.

When the table is in operation, the air within the pit and beneath the shaking table is pressurized so that the total dead weight of the table and test structure is carried by the pressurized air. Because the dead weight is balanced by air pressure, the four vertical actuators can accelerate the table to a maximum of 1 g vertically. The three horizontal actuators can accelerate the table up to 1.5 g horizontally. The actuator forces are reacted by a massive reinforced concrete foundation weighing 1,580 kips.

The electronic MTS control system for the shaking table is shown in Fig. 5-7(b) and controls five degrees of freedom of the table. The sixth degree of freedom, which is one of the horizontal translations, is controlled by a sliding mechanism. Normally the pitch, roll and yaw (twist) command signals are zero, and the horizontal and vertical command signals represent translational and displacement time histories of an earthquake record.

Associated with the table is a data acquisition and processing system which is based on a NOVA-1200 minicomputer operating in conjunction

with a Diablo-31 moving-head magnetic disc unit (see Fig. 5-8). The data acquisition and processing system is used for three main purposes:

1) Generation of command signals in the form of displacement time histories
2) Acquisition of data from up to 128 transducers that monitor the behavior of the test structure and shaking table during a test
3) Processing of test data

The shaking table command signals must be in the form of displacement time histories and the NOVA computer is used to derive this from the acceleration records. The original acceleration time histories may be fed to the computer by means of the teletype keyboard or the teletype paper tape reader. The time histories of the required earthquake are checked to see if the maximum values of acceleration, velocity or displacement will exceed the limits on the shaking table motion. After satisfactory displacement time histories are available for both the horizontal and vertical command signals, they are fed via a digital-to-analog converter to an analog tape recorder. The signals are stored there until they are required for a test, and at that time are fed to the MTS Control Console.

During a test the minicomputer is dedicated to the collection of data. Analog signals originating in accelerometers, LVDT's, etc, are fed to amplifiers, multiplexers, and an analog-to-digital converter housed in the Neff System 620. It is possible to sample up to 128 analog channels at a rate of 100 samples per second per channel. The sampled data is stored initially on the disc, and if permanent storage is desired, the data is transferred to the nine-track Wang digital-magnetic tape

recorder. The computer is also used to process test data stored on the disc or on the magnetic tape recorder, as well as to plot the complete time history of the signal of any channel on the Versatec printer/plotter.

5.5 Test Set-up

The tank model was prestressed to the shaking table by means of five 1¼-in-diameter steel rods located at the four corners and in the center of the tank. Water displacement gages and the pressure gages were connected to the data acquisition system of the shaking table and a careful calibration was done.

Linearity of the water displacement gages was established by varying the water level in the tank. Under normal conditions of operation, the water depth in the tank should be 16 in. (corresponding to the 20-ft depth in prototype) and therefore to ensure a sufficient linear range of water displacement gages, the water depth in the tank was increased to 20 in. initially and then water was pumped out of the tank at a constant rate to a depth of 12 inches. A visicorder trace was obtained between the water gage output and time which were straight lines indicating that the water displacement gages are linear.

Water displacement gages were calibrated to give the displacements directly in inches and the pressure gages gave the pressures in psi. Before the start of actual tests, water depth was brought to the required level of 16 inches and each test was started with zero initial conditions. Tests were also done with twice the normal depth of water and the linearity of the water gages was again checked by varying the depth of water in the tank between 36 inches and 28 inches.

5.6 Testing Procedure

Tests were conducted for sinusoidal motions as well as actual earthquake accelerograms. The time scale of the earthquake records was reduced by a factor of $\sqrt{15}$ to correctly represent the similitude requirements.

Before starting each test, the water in the tank was brought to a standstill and the shaking table was given the appropriate motion; the resulting data was digitized at a rate of 100 samples per second and stored temporarily on the disc. The digitized data included the water displacement, dynamic pressures and the horizontal and vertical displacements and acclerations of the shaking table. This digitized acceleration data were used to carry out the computer analysis for comparison with the test data regarding the water surface displacements and dynamic pressures.

At the end of each test, maximum and minimum values of the response quantities and the shaking table data were printed out for a spot check to see if everything was working properly. In certain cases when it was felt necessary, versatic plots were also obtained shortly after the test, but this was not done for every test as it was a rather slow process. Later on the data was transferred to a magnetic tape for permanent record and for subsequent processing and plotting of the data on the CDC-6400 computer.

The normal length of digitized records was about 10 seconds for each test except the tests which were conducted for determining the damping. The procedure of testing was also somewhat different in these tests. In the damping tests, the table was moved sinusoidally to excite the

fundamental sloshing mode and then it was stopped when sufficient sloshing response was built up. A 50-second decay curve was used to determine the effective damping.

5.7 Sequence of Tests

The series of tests which were carried out on the 8-ft-diameter tank can be classified into two main categories:

A) Tests without internal damping mechanism

B) Tests with internal damping mechanism.

In both series A) and B), tests were conducted at water depths of 16 inches and 32 inches. In these tests, 16 in. represents the scaled water depth at which a typical pressure-suppression pool of water in boiling water reactors is operated. The purpose of the tests at double the normal depth was to study the effect of the variation of water depth on the sloshing response.

Test series A) and B) can be subdivided into the following categories:

1) Free sloshing tests to determine the damping and to study the variation in damping with variation in water depth.

2) Sloshing tests under El Centro earthquake of 1940: These tests were carried out for various intensities of maximum ground acceleration ranging from 0.2 g to 0.6 g which were useful in determining the range of linearity. (Note the recorded maximum acceleration in this case is 0.32 g.)

Tests under El Centro earthquake were repeated with and without

the presence of the actually recorded vertical ground motion. This was found helpful in establishing the fact that vertical ground motions do not significantly affect the sloshing response.

3) Sloshing tests under Parkfield earthquake (1966): Tests for Parkfield accelerogram were also conducted for various intensities of ground acceleration ranging from 0.3 g to 0.9 g. These tests were carried out to study a change in the characteristics of sloshing response with a different earthquake record. It will be seen later (in the next section) that the sloshing mode in 2) and 3) are essentially the same.

5.8 Test Data

A summary of the test data is presented in this section, including damping values, a summary of the extreme values, and time-history plots of some selected data.

5.8.1 Damping values

Table 5-1 summarizes the damping values for the 8-ft steel tank model. These values which represent the percent of the critical damping were calculated using the digitized data from the free vibration tests on the model. The damping values are 0.4% and 0.2% for water depths of 16 inches and 32 inches, respectively, when there was no internal damping mechanism present. These damping values are applicable to the model only and it is anticipated that the damping values for the prototype will be smaller. It is interesting to note that the damping value for the small

TABLE 5-1. Damping values for sloshing in 8-ft-diameter steel tank.

Water depth = 16 inches		Water depth = 32 inches	
Without screen	With screen	Without screen	With screen
0.4%	4.5%	0.2%	3.4%

lucite model (Chapter 4) was 0.84% compared to 0.4% in the 8-ft model, although the 8-ft steel tank model had a rougher surface compared to that of the lucite model.

The damping values for the large-scale model in the presence of the damping screens increased considerably and are 4.5% and 3.4% for 16-in. and 32-in. depths, respectively (see Table 5-1).

5.8.2 Extreme values

Table 5-2 gives the extreme values for all the tests carried out in this study on the 8-ft model. This table shows the test number, the name of the earthquake, maximum horizontal and vertical ground acceleration (in g's), water depth in the tank (in inches), maximum and minimum (i.e., maximum upward and downward displacements), surface water displacements (in inches) at water gage locations 1, 5, 2, 4, and maximum dynamic pressures (in psi) at pressure gage locations 1, 2 and 3. Note that W-1 means water displacement at water gage location 1, and P-1 means dynamic pressure at pressure gage location 1, etc.

Water displacements at locations 3 and 6 are not given in Table 5-2 because they are normally close to zero as expected (under perfect symmetrical conditions, they should be zero for horizontal ground excitation).

TABLE 5-2. Extreme values for Test Series A (without damping mechanism).

Test No. (1)	Earthquake (2)	Ground Acceleration (g) Horiz. (3)	Ground Acceleration (g) Vert. (4)	Water depth (in) (5)	Water Displacements maximum/minimum (inches) W-1 (6)	W-5 (7)	W-2 (8)	W-4 (9)	Dynamic Pressures maximum (psi) P-1 (10)	P-2 (11)	P-3 (12)
171276.1	El Centro	0.18	0.	16	0.7/0.7	0.7/0.6	0.8/0.7	0.9/0.9	0.081	0.076	0.034
.2	El Centro	0.33	0.	16	1.5/1.3	1.3/1.1	1.9/1.4	1.9/1.6	0.140	0.113	0.061
.3	El Centro	0.48	0.	16	2.7/2.0	2.3/1.8	2.9/2.2	3.8/2.5	0.190	0.161	0.068
.4	Parkfield	0.30	0.	16	0.8/0.7	0.6/0.6	0.8/0.8	0.9/0.7	0.115	0.092	0.054
.5	Parkfield	0.58	0.	16	1.7/1.2	1.3/1.1	2.0/1.5	1.8/1.4	0.215	0.181	0.087
.6	Parkfield	0.87	0.	16	2.8/1.9	2.2/1.6	2.9/2.1	2.8/2.1	0.295	0.246	0.138
201276.3	El Centro	0.00	0.11	16	0.0/0.0	0.0/0.0	0.1/0.0	0.0/0.0	0.062	0.044	0.059
.4	El Centro	0.08	0.00	16	0.3/0.3	0.4/0.4	0.5/0.4	0.5/0.5	0.038	0.038	0.021
.5	El Centro	0.08	0.10	16	0.4/0.3	0.4/0.4	0.5/0.5	0.5/0.5	0.088	0.058	0.102
.6	El Centro	0.15	0.10	16	0.7/0.5	0.6/0.6	0.8/0.7	0.8/0.9	0.110	0.076	0.100
.7	El Centro	0.22	0.10	16	0.8/0.8	0.9/0.8	1.4/1.0	1.2/1.2	0.127	0.091	0.100
.8	El Centro	0.23	0.21	16	0.7/0.8	0.9/0.7	1.3/1.1	1.2/1.1	0.223	0.158	0.220
.9	El Centro	0.29	0.14	16	1.1/1.1	1.3/1.1	1.9/1.4	1.8/1.5	0.125	0.110	0.097
.10	El Centro	0.29	0.30	16	1.1/1.0	1.2/1.0	1.8/1.4	1.7/1.5	0.217	0.152	0.209
.11	El Centro	0.44	0.14	16	2.0/1.6	2.0/1.6	2.8/2.1	3.1/2.3	0.175	0.145	0.125
.12	El Centro	0.41	0.30	16	1.8/1.5	1.8/1.7	2.8/1.9	2.9/2.2	0.249	0.178	0.218
.13	El Centro	0.43	0.44	16	1.7/1.5	1.8/1.7	2.6/2.0	2.9/2.2	0.373	0.261	0.322
.14	El Centro	0.65	0.15	16	5.2/2.9	4.6/3.4	7.5/4.9	7.1/4.7	0.266	0.227	0.166
.15	El Centro	0.65	0.30	16	4.4/3.3	4.6/3.1	7.9/6.9	7.3/5.6	0.277	0.211	0.218
.16	El Centro	0.55	0.14	16	3.7/2.4	3.7/2.8	6.1/3.8	5.6/4.0	0.219	0.182	0.139

continued . . .

TABLE 5-2 (continued)

Test No. (1)	Earthquake (2)	Ground Acceleration (g) Horiz. (3)	Ground Acceleration (g) Vert. (4)	Water depth (in.) (5)	Water Displacements maximum/minimum (inches) W-1 (6)	W-5 (7)	W-2 (8)	W-4 (9)	Dynamic Pressures maximum (psi) P-1 (10)	P-2 (11)	P-3 (12)
201276.17	El Centro	0.55	0.29	16	3.5/2.5	3.5/2.4	5.6/3.6	5.6/3.5	0.299	0.218	0.213
.18	El Centro	0.08	0.0	16	0.4/0.4	0.4/0.4	0.5/0.5	0.5/0.6	0.031	0.027	0.025
.19	El Centro	0.13	0.0	16	0.6/0.6	0.7/0.7	0.9/0.8	0.8/0.9	0.055	0.043	0.022
.20	El Centro	0.21	0.0	16	0.8/0.8	0.9/0.8	1.3/1.1	1.3/1.2	0.091	0.077	0.048
.21	El Centro	0.31	0.0	16	1.3/1.2	1.4/1.2	1.9/1.5	1.9/1.6	0.124	0.112	0.053
.22	El Centro	0.38	0.0	16	1.9/1.5	1.9/1.6	2.6/1.9	2.8/2.1	0.147	0.127	0.067
.23	El Centro	0.46	0.0	16	2.8/2.1	2.8/2.2	3.7/2.7	4.6/3.1	0.194	0.170	0.080
211276.1	El Centro	0.24	0.0	16	0.9/0.9	0.9/0.8	1.2/1.0	1.2/1.2	0.096	0.086	0.032
.2	El Centro	0.44	0.0	16	2.2/1.7	2.1/1.8	2.5/2.0	3.4/2.3	0.164	0.149	0.063
.3	El Centro	0.56	0.0	16	4.3/2.7	3.5/3.0	5.8/4.5	6.0/4.0	0.207	0.184	0.088
.4	Parkfield	0.39	0.0	16	1.0/0.8	0.9/0.8	1.2/1.0	1.2/1.1	0.152	0.130	0.059
.5	Parkfield	0.60	0.0	16	1.7/1.5	1.4/1.3	2.2/1.8	2.1/1.6	0.251	0.215	0.093
.6	Parkfield	0.76	0.0	16	2.2/1.7	1.8/1.4	2.9/2.2	2.9/1.9	0.306	0.264	0.116
.7	Parkfield	0.87	0.0	16	2.6/1.7	2.1/1.6	3.0/3.0	2.8/2.2	0.351	0.296	0.109
.8	El Centro	0.39	0.26	16	1.6/1.4	1.9/1.5	2.1/1.7	2.6/2.0	0.185	0.129	0.135
.9	El Centro	0.54	0.39	16	3.5/2.5	3.3/2.6	4.5/2.8	4.9/3.3	0.310	0.220	0.188
.10	El Centro	0.20	0.0	32	0.8/0.9	0.8/0.8	1.2/1.0	1.0/1.0	0.179	0.178	0.065
.11	El Centro	0.29	0.0	32	1.3/1.2	1.2/1.2	1.8/1.4	1.5/1.3	0.236	0.237	0.079
.12	El Centro	0.39	0.0	32	1.9/1.6	1.7/1.6	2.5/1.8	2.2/1.7	0.294	0.295	0.093
.13	El Centro	0.47	0.0	32	2.8/2.0	2.6/1.9	3.5/2.3	3.6/2.2	0.354	0.350	0.118

continued . . .

TABLE 5-2 (continued)

Test No. (1)	Earthquake (2)	Ground Acceleration (g) Horiz. (3)	Ground Acceleration (g) Vert. (4)	Water depth (in.) (5)	Water Displacements maximum/minimum (inches) W-1 (6)	W-5. (7)	W-2 (8)	W-4 (9)	Dynamic Pressures maximum (psi) P-1 (10)	P-2 (11)	P-3 (12)
211276.14	El Centro	0.54	0.0	32	3.8/2.9	3.9/2.9	5.3/3.4	5.6/3.2	0.426	0.422	0.172
.15	Parkfield	0.39	0.0	32	1.1/0.9	0.8/0.9	1.2/1.1	1.0/0.9	0.303	0.294	0.104
.16	Parkfield	0.60	0.0	32	1.9/1.5	1.5/1.4	2.4/1.7	1.8/1.4	0.470	0.458	0.165
.17	Parkfield	0.86	0.0	32	2.9/1.9	1.7/1.7	3.8/2.8	2.1/1.8	0.629	0.615	0.219
		Extreme Values for Test Series B (with damping mechanism)									
291276.1	El Centro	0.22	0.0	16	0.4/0.8	0.6/0.7	0.6/0.7	0.5/0.9	0.095	0.085	0.035
.2	El Centro	0.32	0.0	16	0.5/1.0	0.7/0.8	0.8/1.0	0.7/1.0	0.126	0.111	0.044
.3	El Centro	0.41	0.0	16	0.7/1.2	1.0/0.8	1.0/1.1	0.9/1.1	0.149	0.134	0.053
.4	El Centro	0.48	0.0	16	0.8/1.3	1.2/0.9	1.2/1.2	1.1/1.3	0.170	0.147	0.077
.5	El Centro	0.57	0.0	16	1.0/1.5	1.3/1.1	1.3/1.4	1.2/1.7	0.228	0.198	0.082
.6	El Centro	0.67	0.0	16	1.2/1.7	1.5/1.2	1.7/1.5	1.5/1.8	0.266	0.230	0.108
.7	El Centro	0.39	0.23	16	0.7/1.2	1.0/0.9	1.0/1.2	0.9/1.2	0.160	0.120	0.122
.8	El Centro	0.57	0.40	16	1.0/1.6	1.4/1.1	1.5/1.5	1.3/1.6	0.300	0.200	0.224
.9	Parkfield	0.36	0.0	16	0.7/0.7	0.6/0.7	0.7/0.8	0.8/0.7	0.130	0.115	0.058
.10	Parkfield	0.53	0.0	16	1.0/0.9	0.8/0.8	1.0/1.1	1.2/0.9	0.210	0.167	0.097
.11	Parkfield	0.62	0.0	16	1.1/1.0	0.9/0.9	1.1/1.2	1.4/1.0	0.239	0.200	0.126
.12	Parkfield	0.76	0.0	16	1.2/1.2	1.1/1.1	1.3/1.4	1.7/1.1	0.300	0.225	0.126
.13	Parkfield	0.87	0.0	16	1.4/1.4	1.2/1.1	1.6/1.5	1.8/1.2	0.320	0.263	0.145

continued . . .

TABLE 5-2 (continued)

Test No. (1)	Earthquake (2)	Ground Acceleration (g) Horiz. (3)	Ground Acceleration (g) Vert. (4)	Water depth (in.) (5)	Water Displacements maximum/minimum (inches) W-1 (6)	W-5 (7)	W-2 (8)	W-4 (9)	Dynamic Pressures maximum (psi) W-1 (10)	P-2 (11)	P-3 (12)
291276.16	El Centro	0.31	0.0	32	0.7/0.9	0.8/0.7	0.8/0.9	0.7/0.9	0.228	0.212	0.074
.17	El Centro	0.38	0.0	32	0.8/1.1	1.0/0.9	1.0/1.1	0.9/1.1	0.288	0.287	0.116
.18	El Centro	0.57	0.0	32	1.1/1.5	1.4/1.0	1.4/1.4	1.2/1.5	0.408	0.396	0.181
.19	El Centro	0.71	0.0	32	1.3/1.7	1.5/1.2	1.8/1.5	1.3/1.7	0.497	0.503	0.238
.20	Parkfield	0.40	0.0	32	0.7/0.7	0.7/0.7	0.7/0.8	0.8/0.6	0.298	0.297	0.100
.21	Parkfield	0.59	0.0	32	0.8/1.3	1.0/1.1	0.9/1.5	1.2/1.0	0.487	0.440	0.167
.22	Parkfield	0.84	0.0	32	1.5/1.6	1.3/1.4	1.7/1.7	1.8/1.2	0.640	0.600	0.210

5.8.3 Time-history plots

Figures 5-9 through 5-26 are the Calcomp plots showing the time-history response at water gage locations 1, 2, 4 and 5, which were obtained from the digitized data kept on the magnetic tape. These representative test results are given to support the general observations of Section 5-11.

Figures 5-9 through 5-12 show the sloshing response of water under El Centro earthquake (1940) for various ground intensities ranging from 0.24 g to 0.60 g. By comparing these figures, it can be seen that the response clearly becomes nonlinear at 0.6 g.

Figures 5-13 through 5-16 show the sloshing response of water in the annular tank model when subjected to the Parkfield earthquake (1966). Maximum ground accelerations vary from 0.39 g to 0.87 g and the vertical ground accelerations are zero. It can be seen that the response under Parkfield accelerogram is much lower compared with that under the El Centro earthquake (for a given intensity of maximum acceleration) because of the smaller duration of the Parkfield earthquake and different frequency contents. Water displacements under Parkfield earthquake are only about 50% of those under El Centro earthquake, but the dominant mode of vibration is the same in both cases.

Figures 5-17 and 5-18 show the sloshing response under El Centro earthquake and include both the horizontal and the vertical ground motions. Comparison of Figs. 5-17 and 5-18 with Figs. 5-11 and 5-12, respectively, shows that addition of the vertical ground motion has small effect even in the nonlinear range of sloshing.

Figures 5-19 through 5-21 show the sloshing response under El Centro when the depth of water in the model is changed to 32 inches (twice the

normal operating depth). Comparison of Figs. 5-19, 5-20 and 5-21 with Figs. 5-10, 5-11 and 5-12, respectively, reveals that the water surface displacement remains virtually unaffected by the change in water depth.

Figures 5-22 through 5-25 show the time histories of water surface displacements under El Centro earthquake with the internal damping system (damping screens) present in the tank model. Comparing Figs. 5-22, 5-23 and 5-24 with Figs. 5-10, 5-11 and 5-12, respectively, it can be seen that the presence of damping screens both reduces the maximum response and shortens the decay time as would be expected. It is interesting to note that in the absence of damping mechanism (Figs. 5-11 and 5-12), the sloshing response actually grows after the end of the earthquake and the maximum displacements actually occur well after the ground motion has already stopped. Comparison of Figs. 5-24 and 5-25 show that vertical ground acceleration has no effect on the response.

Figure 5-26 shows the sloshing response under Parkfield earthquake with the damping mechanism present in the tank model. Comparison of Fig. 5-26 with Fig. 5-16 shows the response with and without damping screens for the same ground motion intensity.

Figures 5-27 through 5-30 are the time-history plots of the pressure response at pressure gauge locations 1, 2 and 3 under El Centro earthquake. Figures 5-27 and 5-28 show the pressure response with and without the damping screen indicating no change in the impulsive pressures at the walls. Figure 5-29 shows the effect of vertical ground motion on the pressures. Note that the dynamic pressures are directly affected whereas the water displacements are note affected in any significant way as noted earlier. Figure 5-30 is the pressure response at the same

location but the depth of water was changed to 32 in. Figure 5-31 is the pressure response under Parkfield earthquake. In addition to the pressures, Figs. 5-27 through 5-31 also show the water displacements at water gage location 3 which are quite small.

5.9 Comparison of Test and Analytical Results for Annular Tank

Comparison of the measured and analytical results in the case of water surface displacements and dynamic pressures shows a good agreement for small displacements. Comparison of surface displacements is shown in Figs. 5-32 through 5-38. Figures 5-39, 5-40, and 5-41 show a similar comparison between the pressures at pressure gage 1. A brief discussion on the comparison is given below.

5.9.1 Water displacements

Figure 5-32 shows time-history plots of water surface displacements at the inner (water gage location no. 4) and outer (water gage location no. 5) walls. The thinner line in both cases represents the measured results. Water depth in the tank was 16 inches. The same results are given for 32 in.water depth in Fig. 5-33. The intensity of ground shaking in Figs. 5-32 and 5-33 is about the same and the accelerogram is the horizontal record of the El Centro earthquake of 1940. The maximum ground acceleration is 0.24g in Fig. 5-32 which is roughly 80% of the recorded value. It can be seen that the agreement between the theory and test results is quite good. Figure 5-34 shows comparison of the same results under the full intensity of the El Centro earthquake and the

agreement between the measured and predicted results is still quite satisfactory.

Figures 5-35 and 5-36 show similar comparison at water depths of 16 in. and 32 in. The intensity of the ground shaking in both of these figures is approximately 40% higher than the actual recorded motion of the El Centro earthquake. It will be observed in Figs. 5-35 and 5-36 that there is a good agreement in the initial part of these plots, but as the amplitude of the measured response grows and clearly becomes nonlinear, the discrepancy between the test results and the linear analytical solution increases. In the nonlinear range the measured displacements are much higher than the analytical (linear) results. It can also be observed that the change in the sloshing period is quite small even with the large nonlinearities in the response motion.

Figures 5-37 and 5-38 show comparisons of the water displacements under Parkfield earthquakes. The maximum ground accelerations in Figs. 5-37 and 5-38 are 0.39 g and 0.60 g respectively. Again it can be seen that the agreement between the test and analytical results is quite good.

Based upon these comparisons it can be concluded that the linear theory gives satisfactory results as long as average surface slopes are less than 25%.

5.9.2 Pressures

Figures 5-39 and 5-40 show the time-history plots of measured and predicted pressures at the base of the outer wall (pressure gage location 1) under the El Centro earthquake for water depths of 16 in. and 32 in. Figure 5-41 shows the same comparison under the Parkfield earthquake with a depth of water equal to 16 in. It will be seen from these figures that the test and theoretical results match each other quite closely.

5.10 Comparison of Test and Analytical Results for a Simple Circular Tank

It was pointed out in Chapter 4 that the theoretical results for the annular tank can also be applied to simple-circular tanks which is a limiting case of an annular tank as the inner radius of the annular tank approaches zero.

Figure 5-42 shows a comparison between the measured and analytical results for the surface displacements at the tank walls under El Centro earthquake (1940) motion. The test results were available from another study [16] on a 12-ft-diameter flexible tank. The height of the tank was 6 ft and the water depth was 5 ft. It can be seen in Fig. 5-42 that the agreement between the test and analytical results is quite good and the response is well within the linear range. The flexibility of the tank does not seem to have any appreciable effect on the sloshing response.

5.11 Discussion and Important Observations on Test Results

The following observations can be made from the test results for the sloshing and pressure response in annular and simple-circular tanks under earthquake ground motions.

5.11.1 Effect of vertical ground motion

Vertical ground motion alone does not produce any sloshing response but it does produce dynamic pressures as may be seen in Table 5-2 (Test No. 201276.3). The addition of vertical ground acceleration to a prescribed horizontal ground accelerogram has virtually no effect on the sloshing response in the linear range and this effect remains very small even in the nonlinear range. This can be seen in Tests 201276.4 through 201276.17 in Table 5-2. It can also be seen in Table 5-2 that the vertical component of ground motion produces dynamic pressures of the same order of magnitude as those produced by the horizontal component.

5.11.2 Linearity range

Figure 5-43 shows the extreme values of water surface displacements at water gage locations 1 and 2 under varying intensity of El Centro earthquake. It can be seen that the displacements increase linearly with increasing ground motion intensity as long as the maximum displacements remain less than 2 in. in the 8 ft model which corresponds to 30 in. in the prototype [see the upper two plots in Fig. 5-43(a) and (b)]. The linear solution gives satisfactory results up to full intensity of El Centro (1940) earthquake. This applies to the annular tank considered here and the linearity range may increase or decrease depending upon the tank configuration (i.e., ratio of the outer to inner radius of the tank).

5.11.3 Nonlinearity

It is interesting to note that once the sloshing becomes nonlinear the displacements amplify quickly and the sloshing response grows even after the ground motion stops as may be seen in Figs. 5-18, 5-21 and 5-35. It can also be noticed that compared with the nonlinearity in the amplitude of the motion, the change in the sloshing period remains quite insignificant.

5.11.4 Effect of the internal damping mechanism

The internal screen increases the damping and thus reduces the sloshing response considerably as may be seen in Fig. 5-43. It can be seen that the upwards displacements are affected more and are reduced by a factor of more than two even in the linear range. For the nonlinear range the damping screen is very effective as may be seen by comparing Fig. 5-12 with Fig. 5-24 for the same ground motion. Also compare Figs. 5-10 and 5-11 with Figs. 5-22 and 5-23.

It should also be seen in Table 5-2 that the presence of the damping screen has very little effect on the dynamic pressures (compare Test Nos. 211276.17 and 291276.22) indicating that the major contribution to dynamic pressures comes from the impulsive part and not the convective part.

The damping values in the model were of the order of 4.0% and 0.3% with and without the damping mechanism (see Table 5-1).

5.11.5 Dominant mode of sloshing

Second antisymmetric mode was the dominant mode of sloshing response in all these tests and the maximum displacement always occurred at the inner boundary under both the El Centro and Parkfield earthquakes (scaled down by a factor of $\sqrt{15}$ on the time scale). In the linear range the prototype displacements can be obtained from the model data by multiplying with the scaling factor of 15. However, it should be pointed out that at present, sufficient information is not available regarding ground motions at the very low frequencies associated with the first sloshing mode of these tanks. The fact that the dominant response in these tests is in mode 2 is of course related to the given input motion and any significant input energy at 0.08 Hz would cause a response in mode 1.

5.11.6 Tank flexibility

The flexibility of the tank does not seem to have any appreciable effect on the sloshing response as may be seen in Fig. 5-42 where the test results of a flexible tank (first frequency is approximately equal to 10 Hz) show a good agreement with the analytical results based upon the rigid tank assumption. The dominant mode of vibration in this 12-ft - diameter tank is the first antisymmetric mode (with a natural frequency of 0.48 Hz). The agreement is good because the sloshing frequencies and the tank frequencies are well separated.

5.11.7 Pressures

The dynamic pressures are approximately linear with the ground accelerations as may be seen in Fig. 5-44 which shows the extreme values of the pressures with varying ground motion intensities of the El Centro earthquake. The values are plotted for pressure gages 1 and 2.

5.12 Conclusions

A good correlation between the test and computer results shows that the linearized small displacement theory can accurately predict the sloshing displacements and dynamic pressures in annular-circular tanks as well as in simple-circular tanks under actual earthquake ground motions. The range of linearity is quite large even in annular tanks of the type considered here and satisfactory results can be obtained from the computer model as long as the displacements remain less than 30 in. in the prototype tank being studied. The linearity range for the simple-circular tanks of the same size are much larger. Second mode is the dominant sloshing mode of vibration under the scaled accelerogram records used in all of the tests on the typical annular tank considered here having first and second sloshing periods of 12.6 and 2.8 seconds respectively.

CBB 760-9582A

FIG. 5-1 8 FOOT DIAMETER STEEL TANK

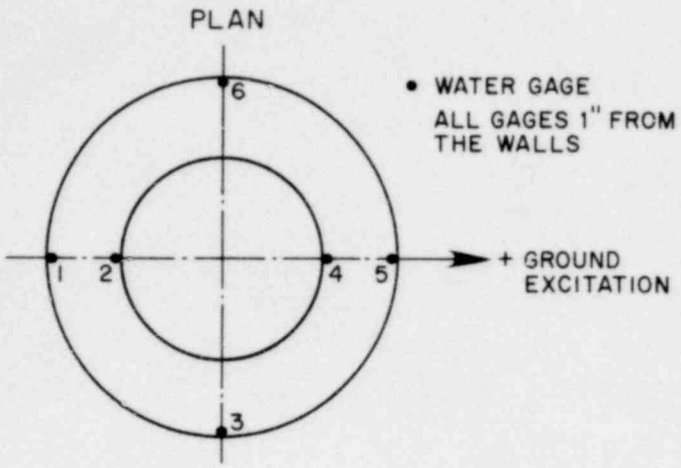

FIG. 5-2 LOCATION OF WATER DISPLACEMENT GAGES

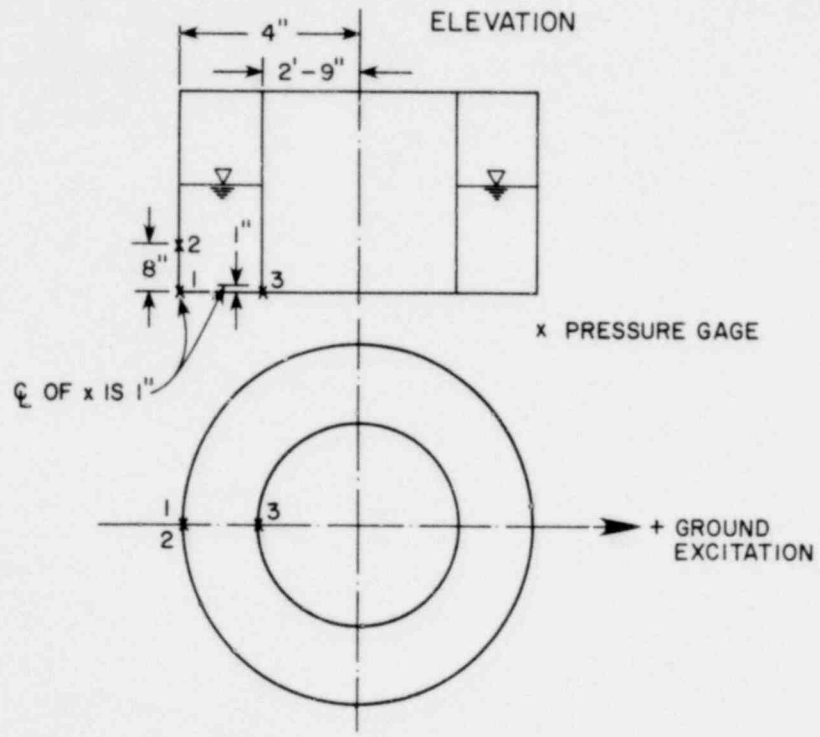

FIG. 5-3 LOCATION OF PRESSURE GAGES

XBL 782-7215

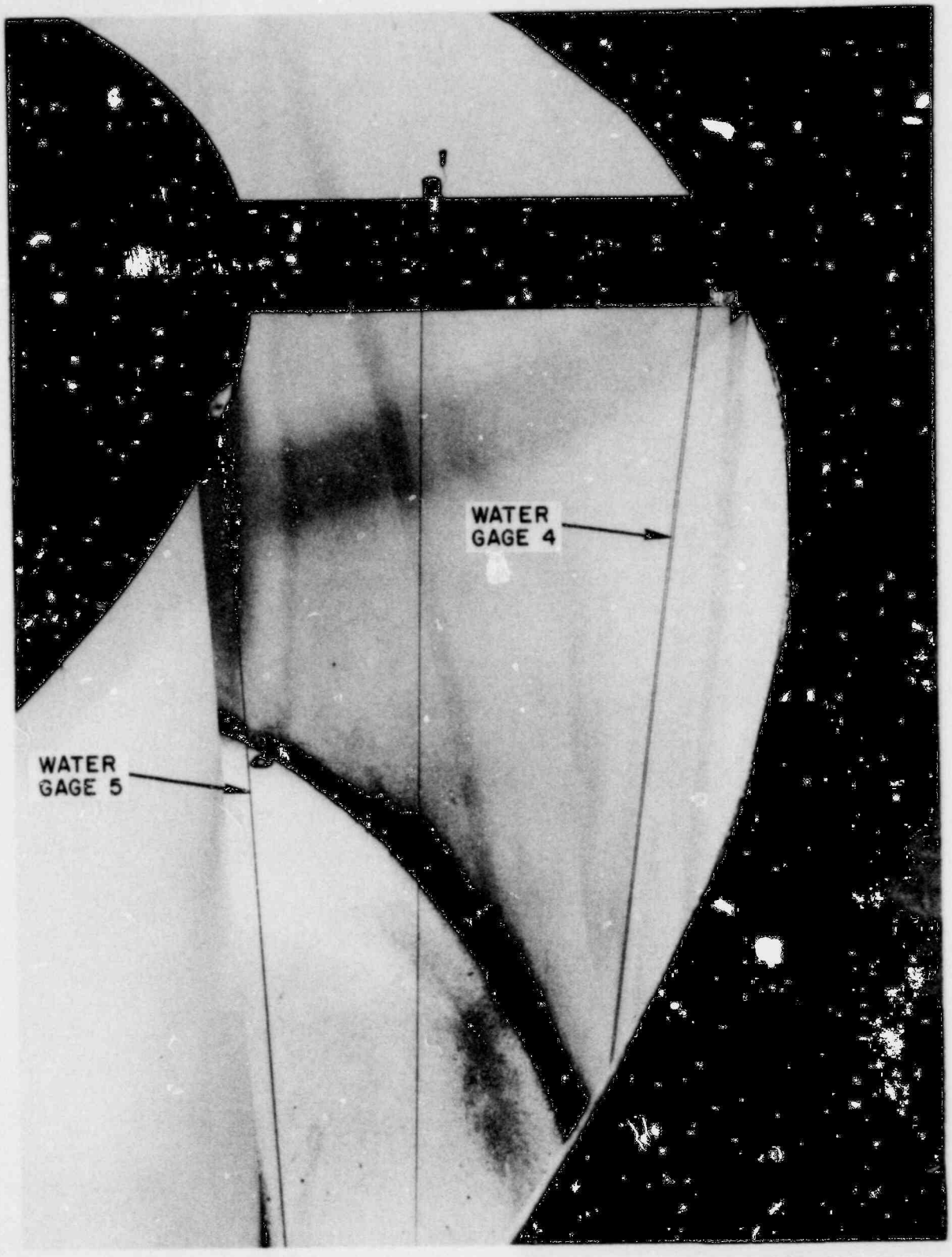

CBB 768-7280A

FIG. 5-4 CLOSE-UP VIEW OF WATER DISPLACEMENT GAGES

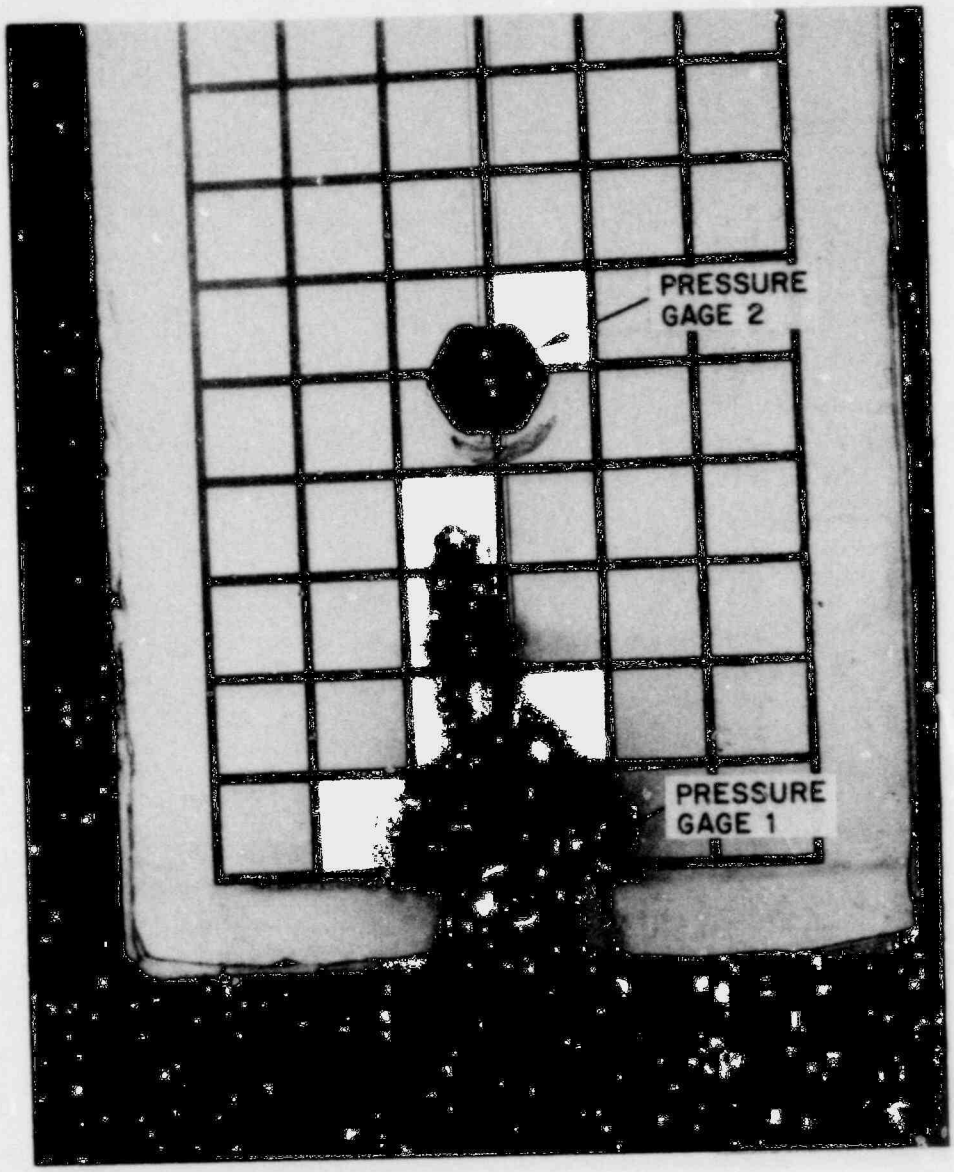

XBB 779-8773

FIG. 5-5 CLOSE-UP OF PRESSURE GAGES 1 AND 2

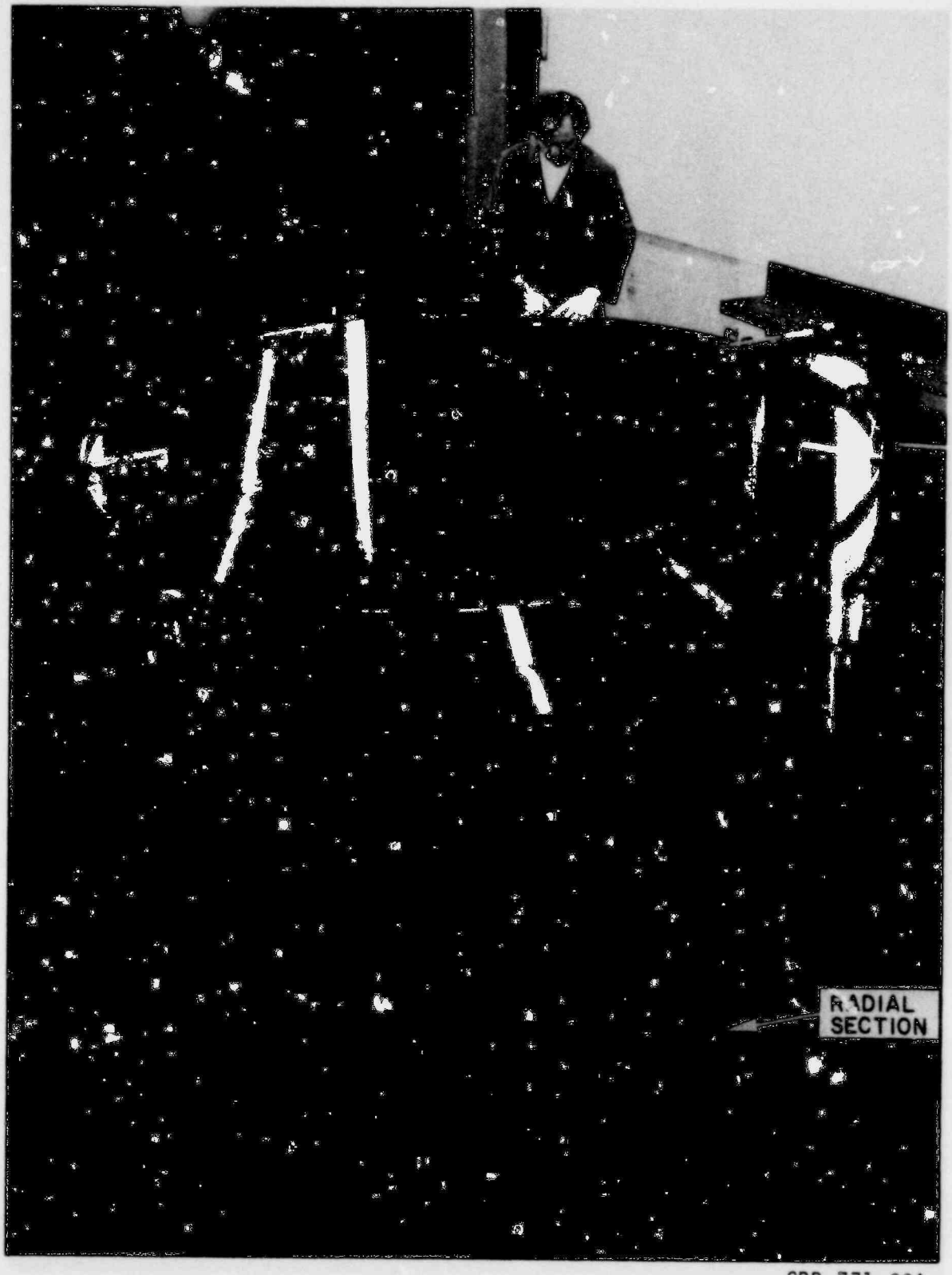

CBB 771-88A

FIG. 5-6 INTERNAL DAMPING MECHANISM CONSISTING OF ALUMINUM SCREENS

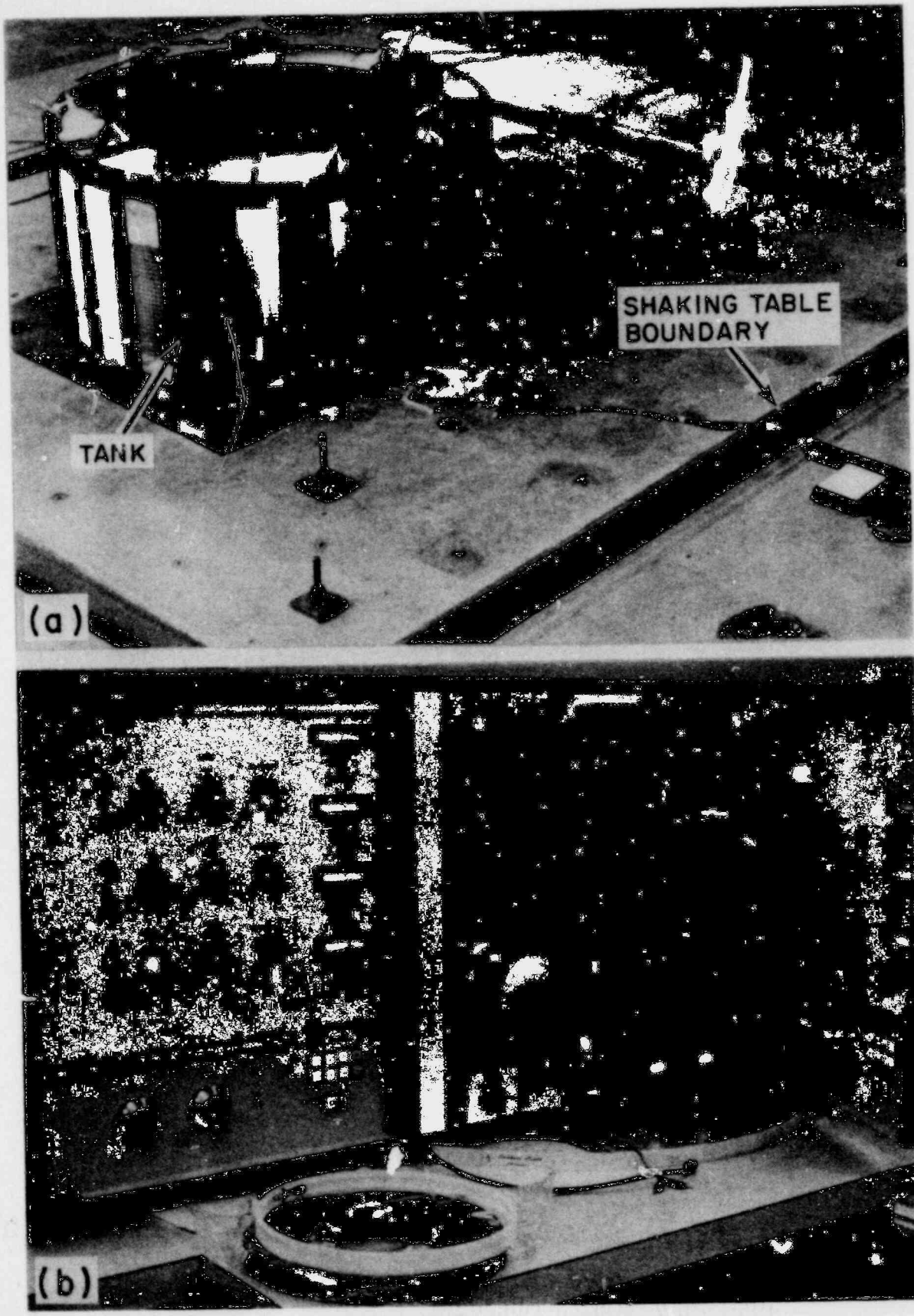

FIG. 5-7 SHAKING TABLE (a) AND CONTROL SYSTEM (b)

XBB 779-8772

FIG. 5-8 DATA ACQUISITION AND PROCESSING SYSTEM OF THE SHAKING TABLE

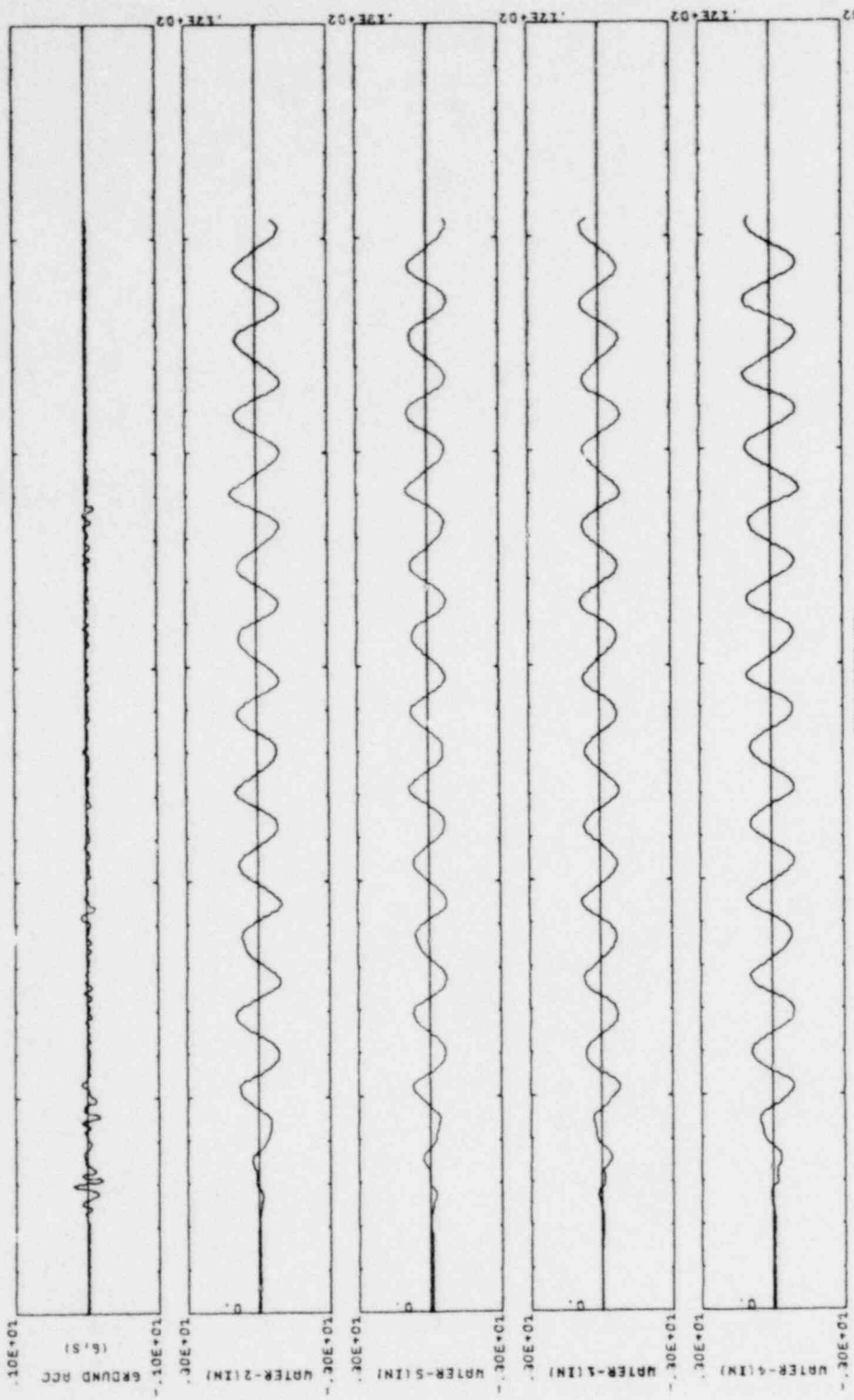

FIG. 5-9 SLOSHING RESPONSE IN 8FT ANNULAR TANK UNDER ELCENTRO EQ (1940), H=16 IN, MAX. HORIZONTAL/VERT. ACC=.24/.06, 211276.1

XBL 7812-13918

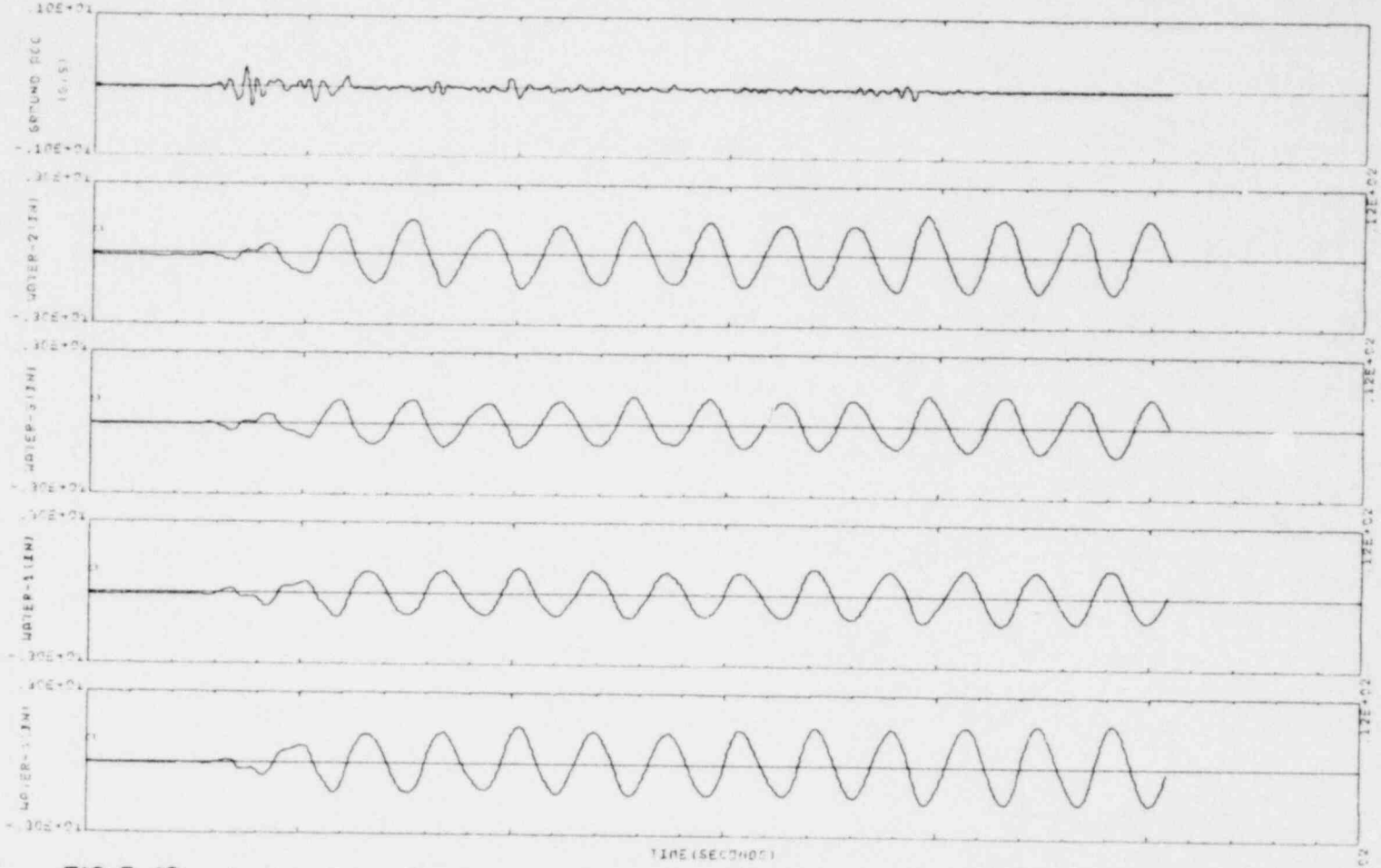

FIG. 5-10 SLOSHING RESPONSE IN 8FT ANNULAR TANK UNDER ELCENTRO EQ (1940), H=16 IN, TIME SCALE=3.87, MAX AC=.316, TEST201276.21

XBL 7812-13919

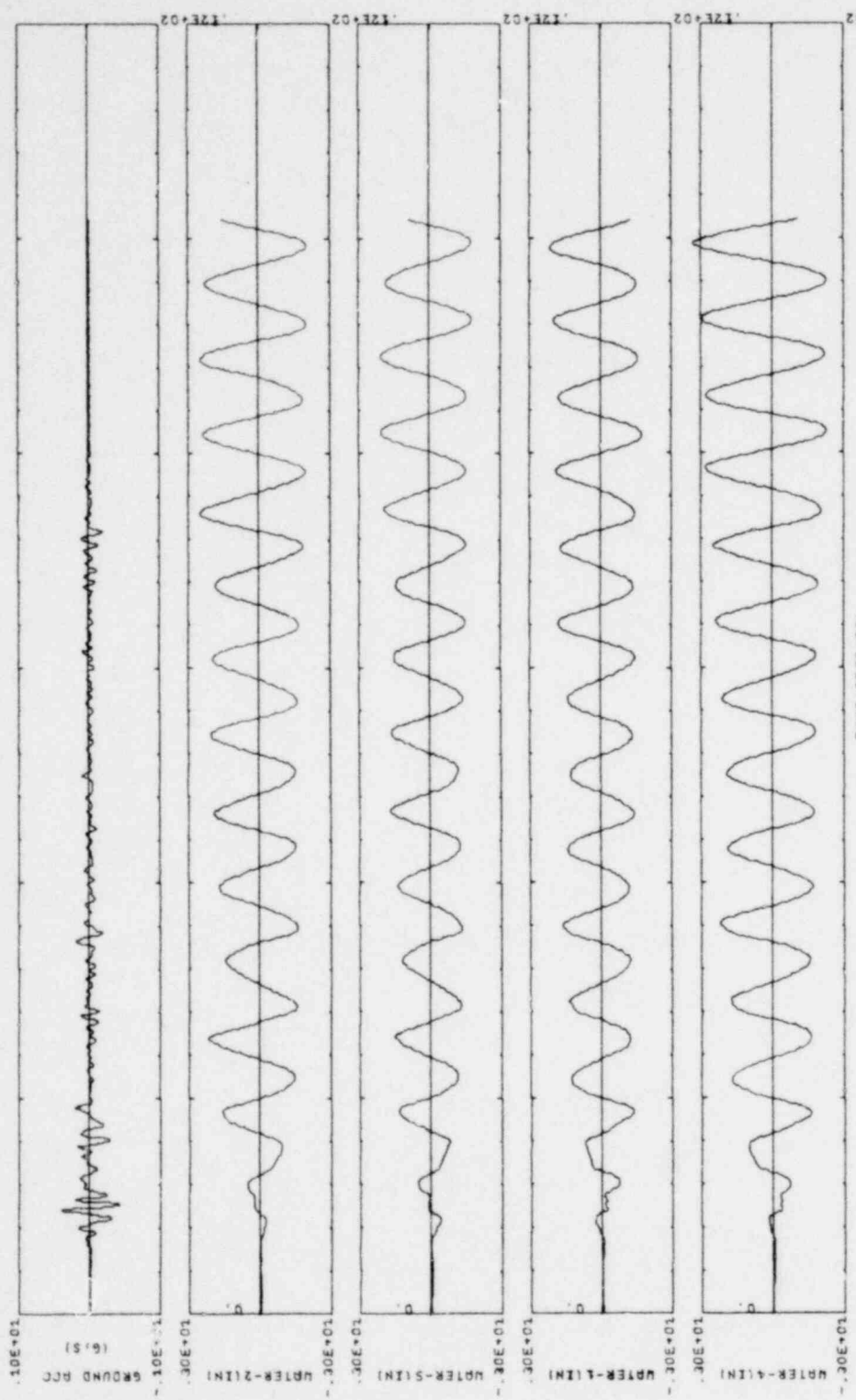

FIG. 5-11 SLOSHING RESPONSE IN BFT ANNULAR TANK UNDER ELCENTRO EQ (1940), H=16 IN, MAX. HORIZONTAL/VERT. ACC=.44/.06, 211276.2

XBL 7812-13920

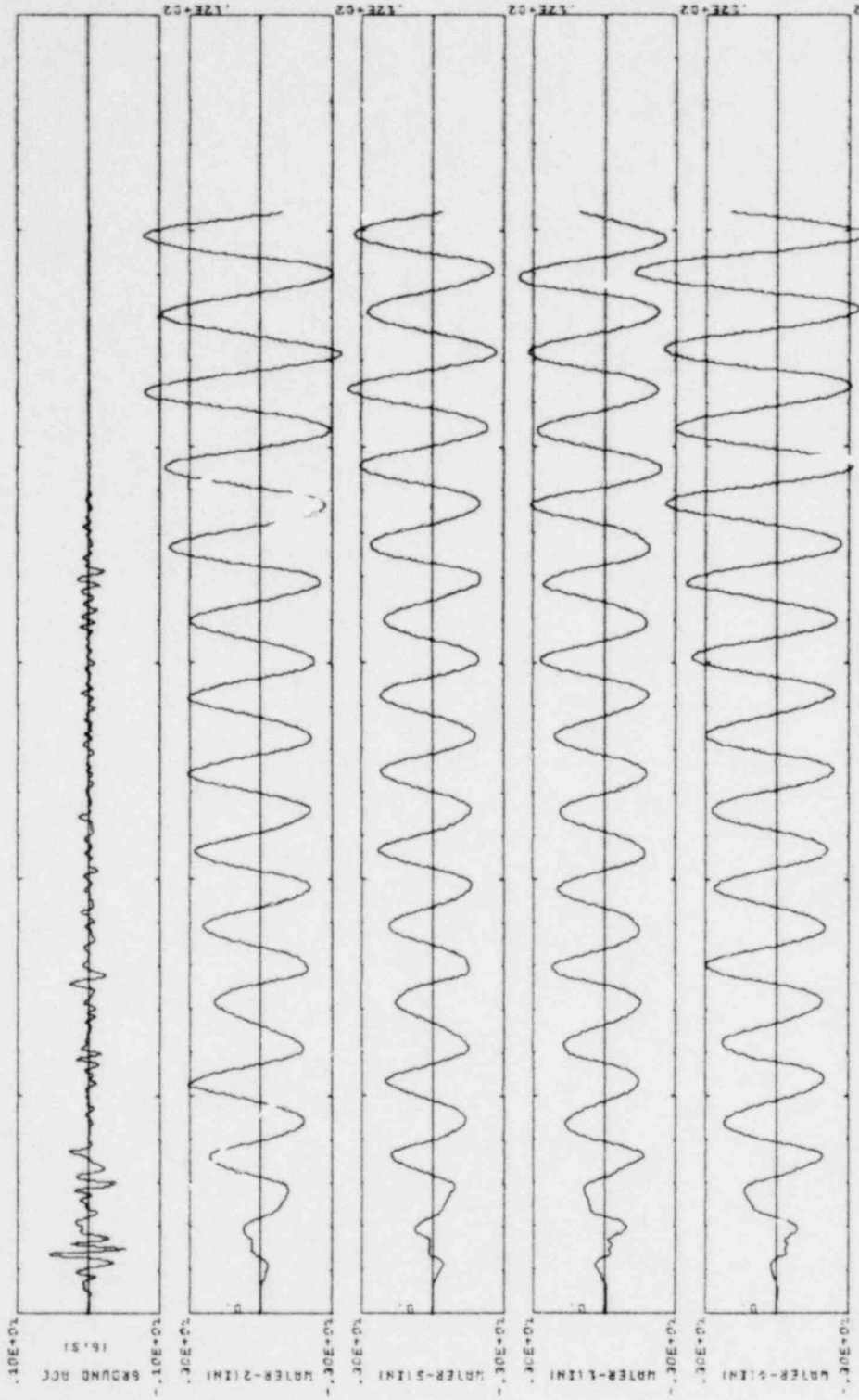

FIG. 5-12 SLOSHING RESPONSE IN 8FT ANNULAR TANK UNDER ELCENTRO EQ (1940), H=16 IN, MAX. HORIZONTAL/VERT. ACC=.56/.06, 211276.3

XBL 7812-13921

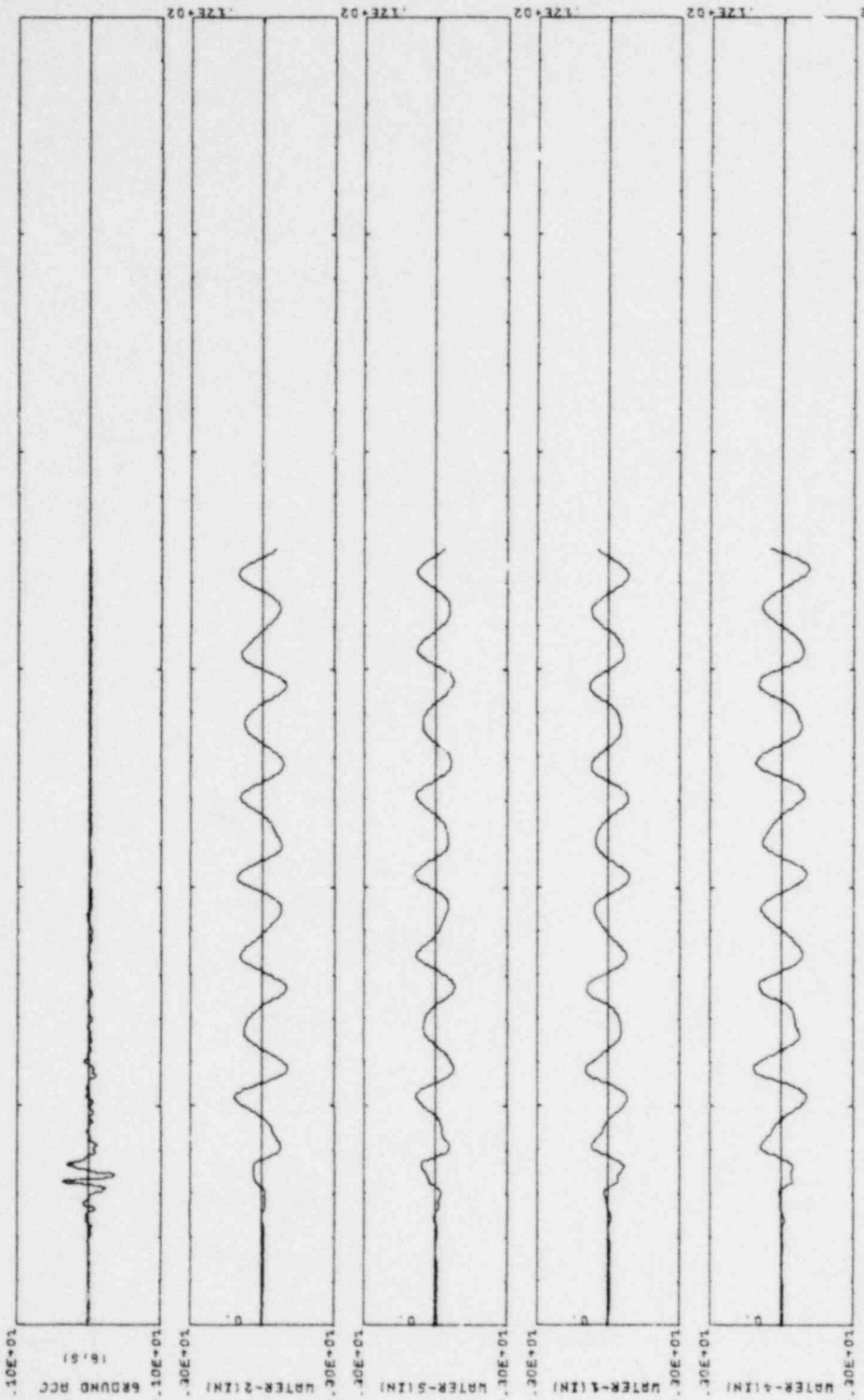

FIG. 5-13 SLOSHING RESPONSE IN 8FT ANNULAR TANK UNDER PARKFIELD EQ H=16 IN, MAX. HORIZONTAL ACCELERATION=.396, T.NO=211276.4

XBL 7812-13922

1361 294

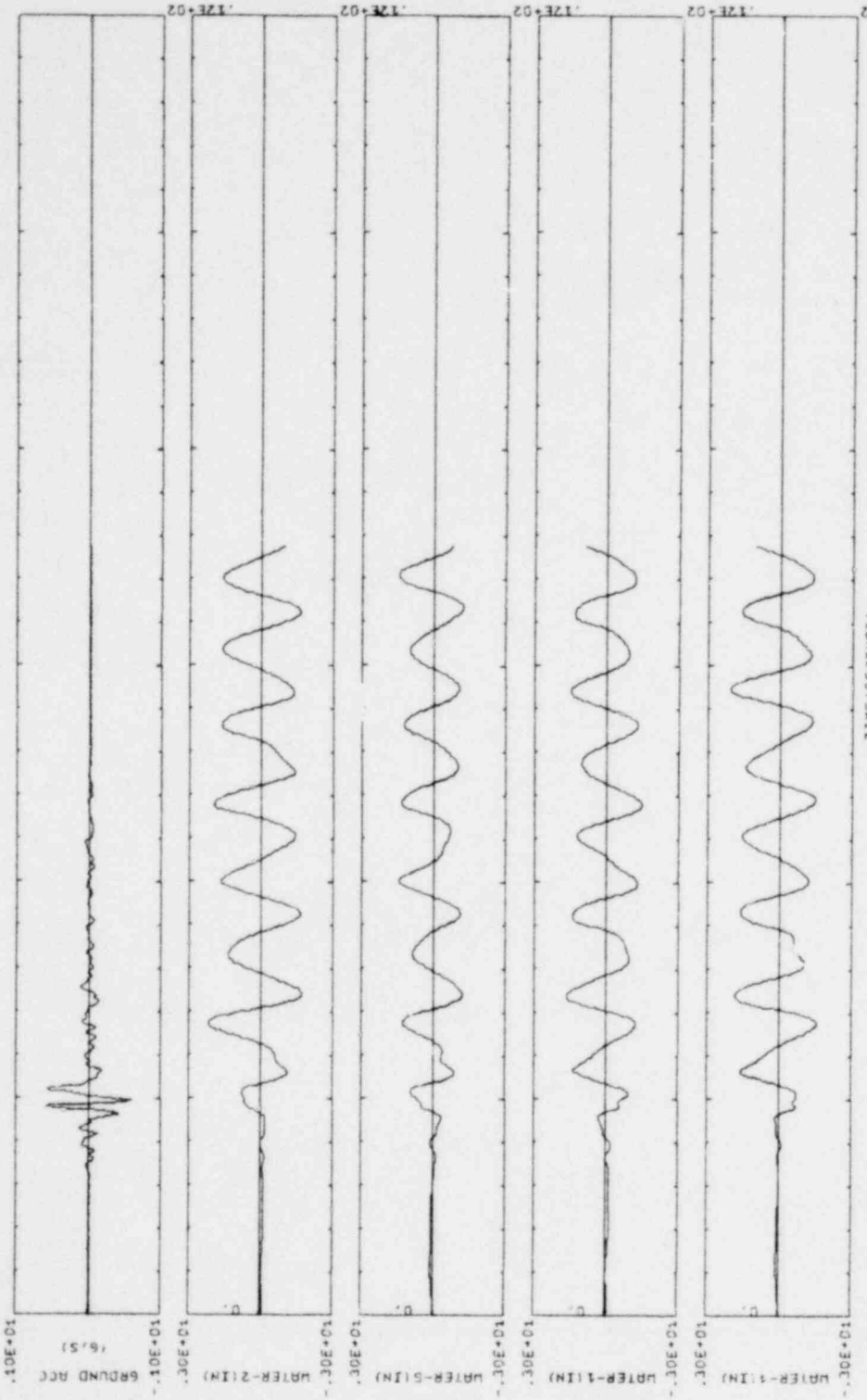

FIG. 5-14 SLOSHING RESPONSE IN 8FT ANNULAR TANK UNDER PARKFIELD EQ
H=16 IN, MAX. HORIZONTAL ACCELERATION=.606, T. NO=211276.5

XBL 7812-13923

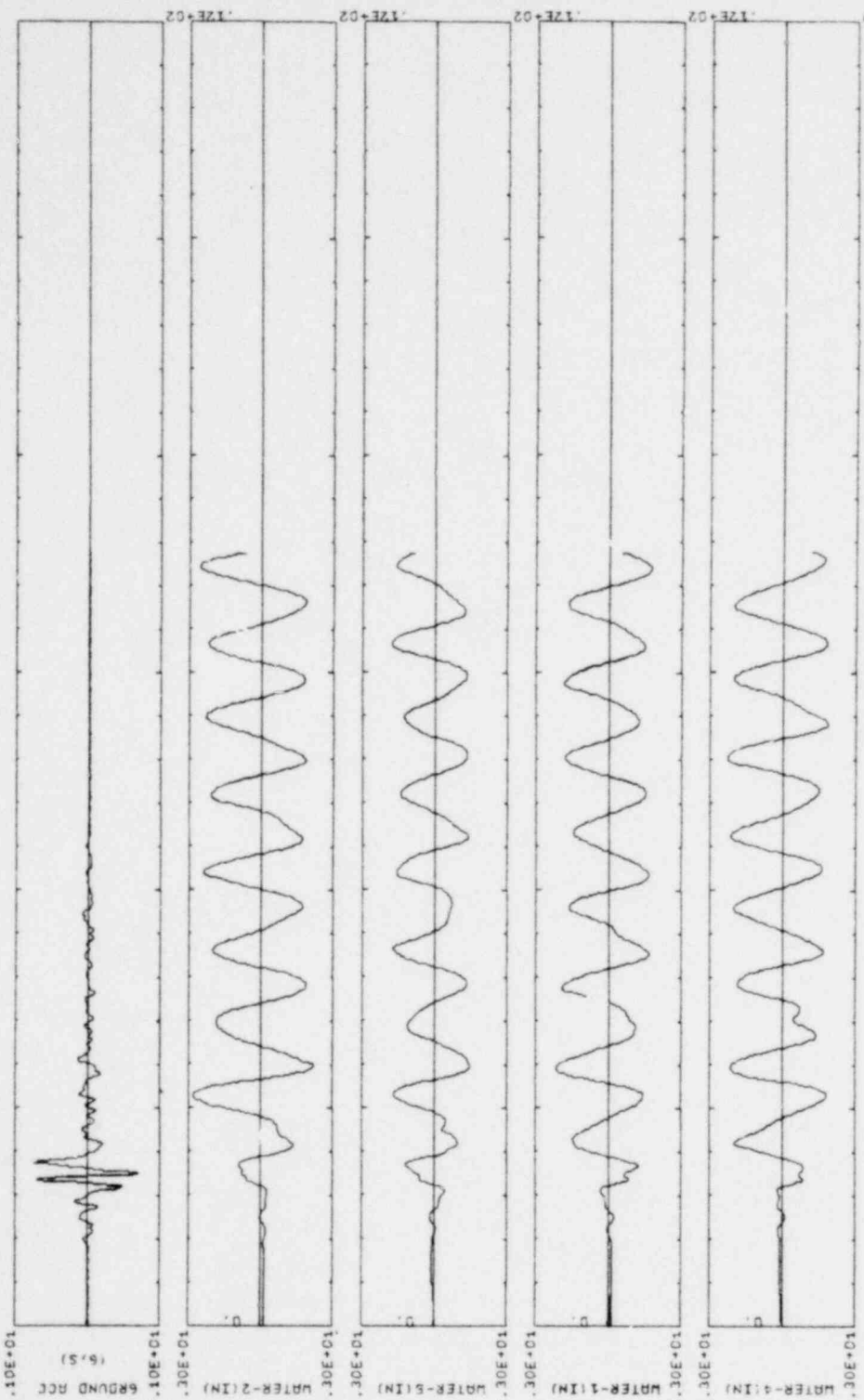

FIG. 5-15 SLOSHING RESPONSE IN 8FT ANNULAR TANK UNDER PARKFIELD EQ H=16 IN,MAX.HORIZONTAL ACCELERATION=.766,T,NO=211276.6

XBL 7812-13924

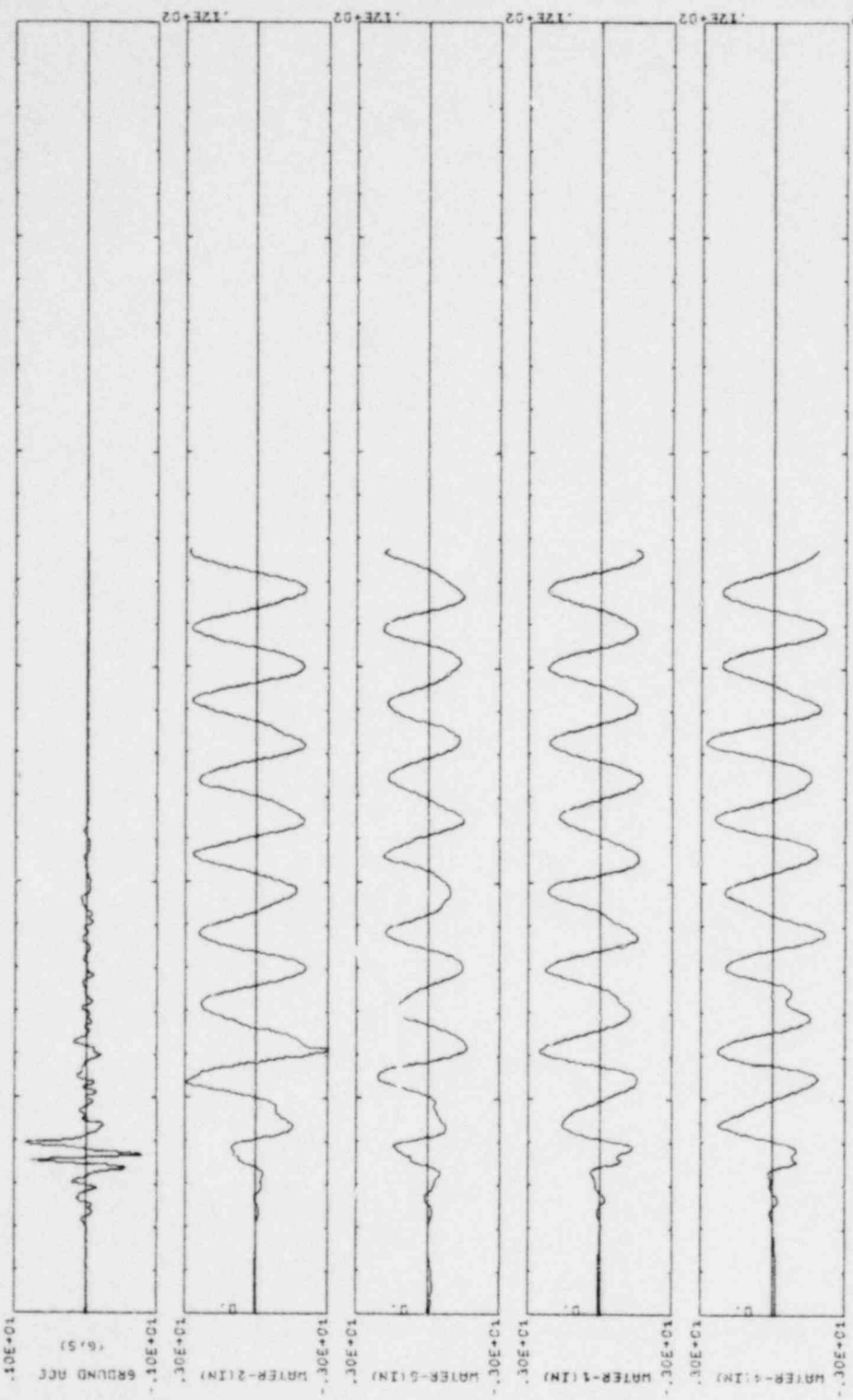

FIG. 5-16

XBL 7812-13967

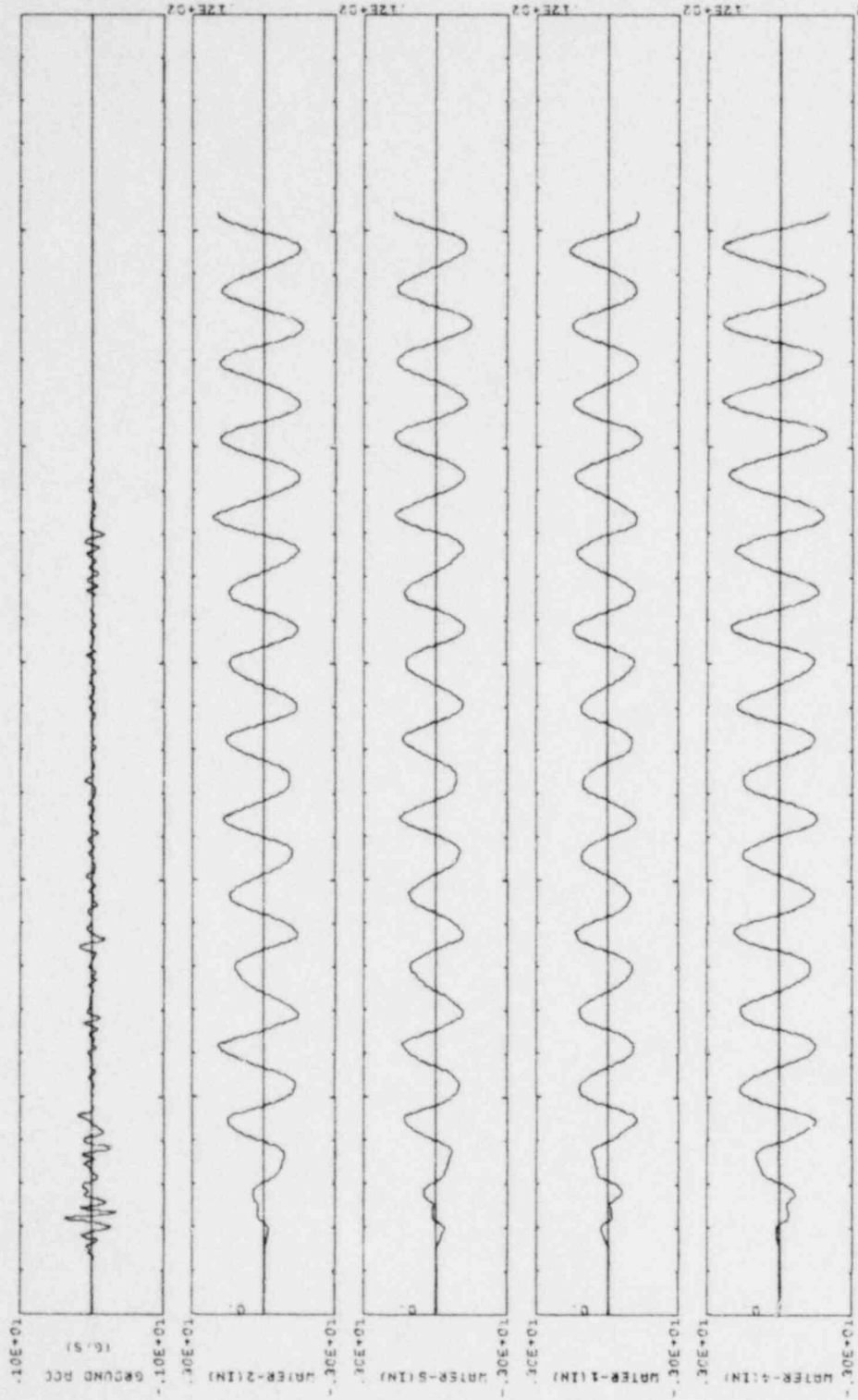

FIG. 5-17 SLOSHING RESPONSE IN 8FT ANNULAR TANK UNDER ELCENTRO EQ (1940), H=16 IN, MAX. HORIZONTAL/VERT. ACC=.33/.266, 211276.8

XBL 7812-13966

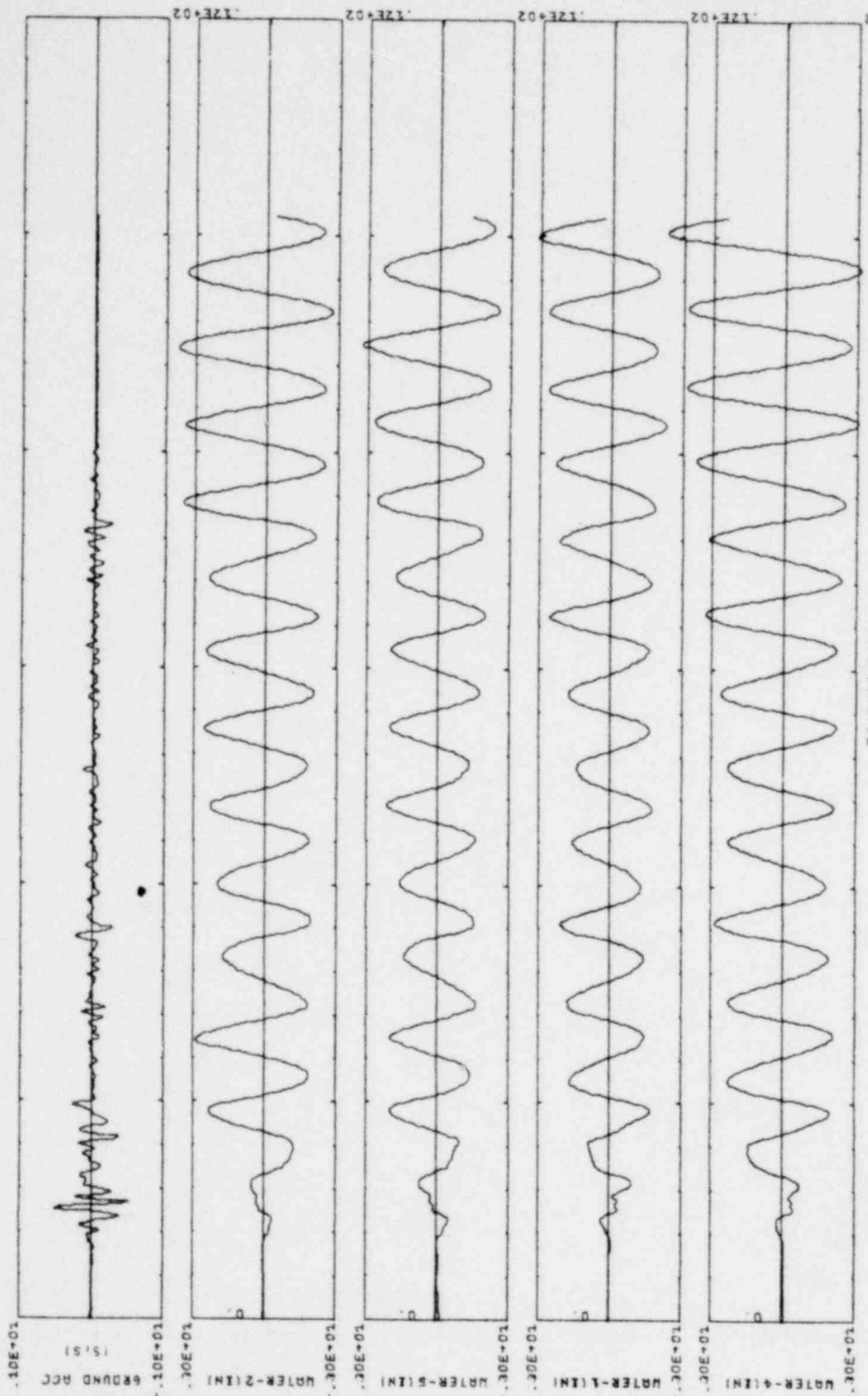

FIG. 5-18 SLOSHING RESPONSE IN 8FT ANNULAR TANK UNDER ELCENTRO EQ (1940),H=16 IN,MAX.HORIZONTAL/VERT.ACC=.540/.396,211276.9

XBL 7812-13965

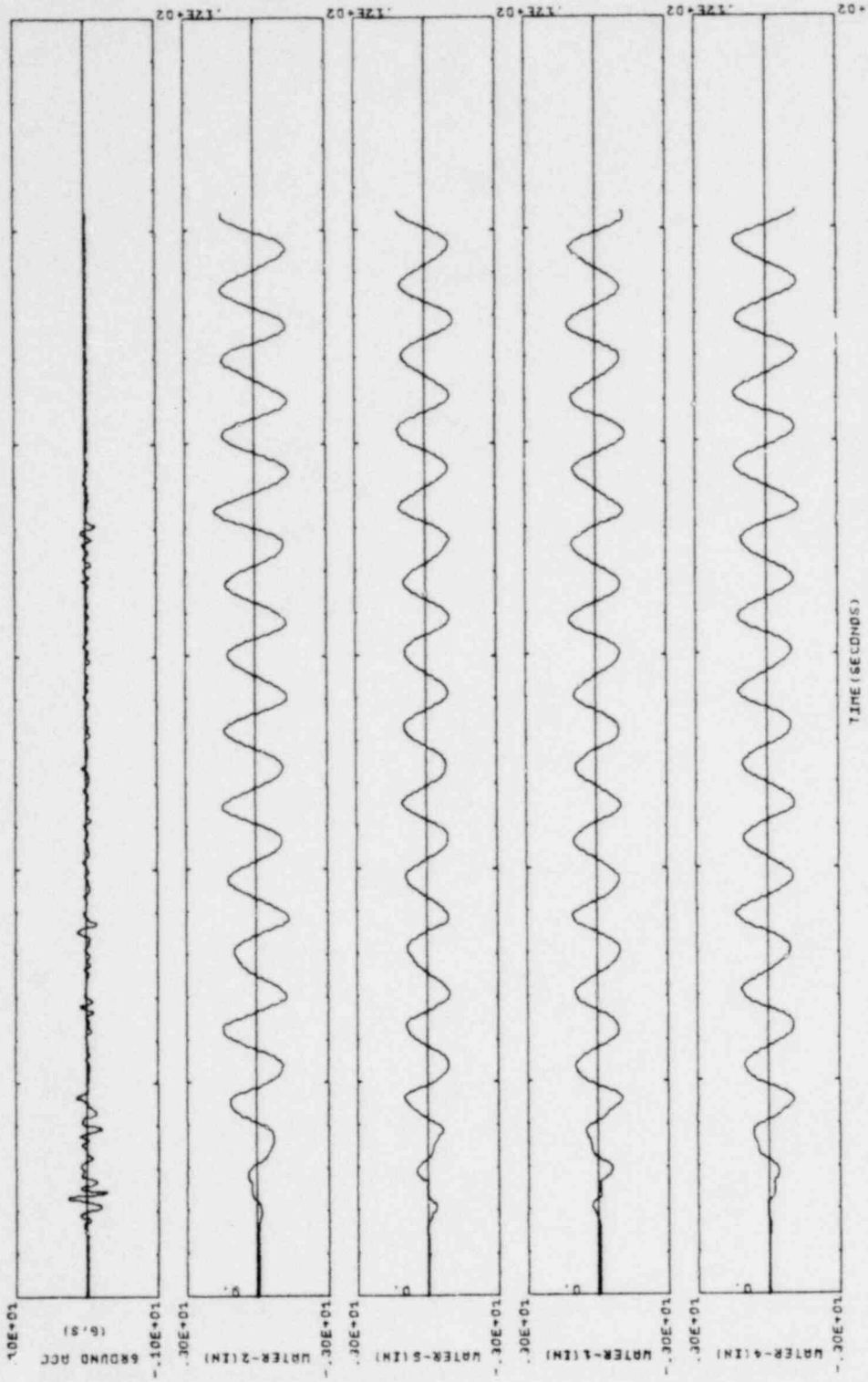

FIG. 5-19 SLOSHING RESPONSE IN 8FT ANNULAR TANK UNDER ELCENTRO EQ (1940), H=32 IN, MAX. HORIZONTAL/VERT. ACC=.29/.06, 211276.11

XBL 7812-13964

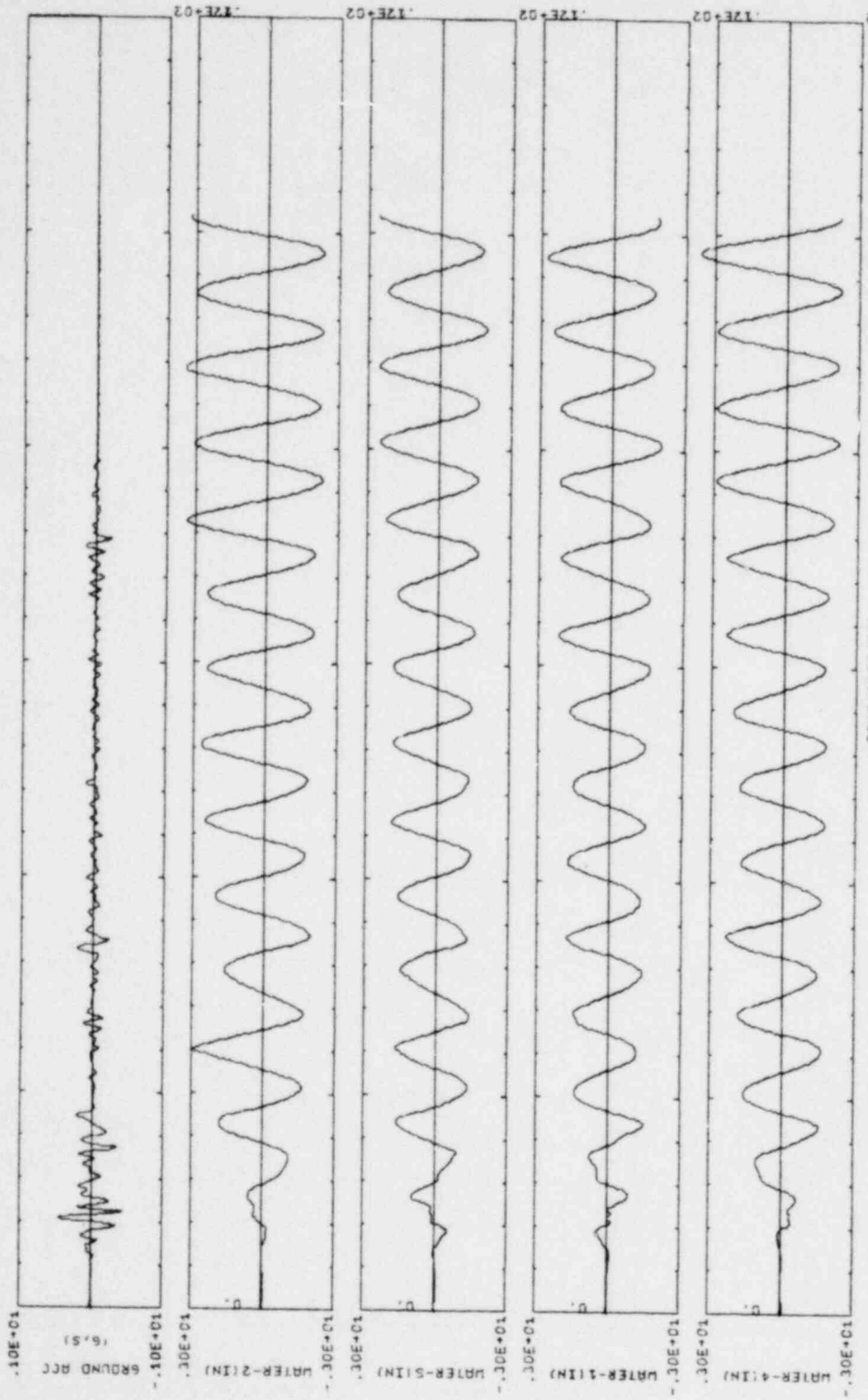

FIG. 5-20 SLOSHING RESPONSE IN 8FT ANNULAR TANK UNDER ELCENTRO EQ (1940),H=32 IN,MAX.HORIZONTAL/VERT.ACC=.47/.06,211276.13

XBL 7812-13963

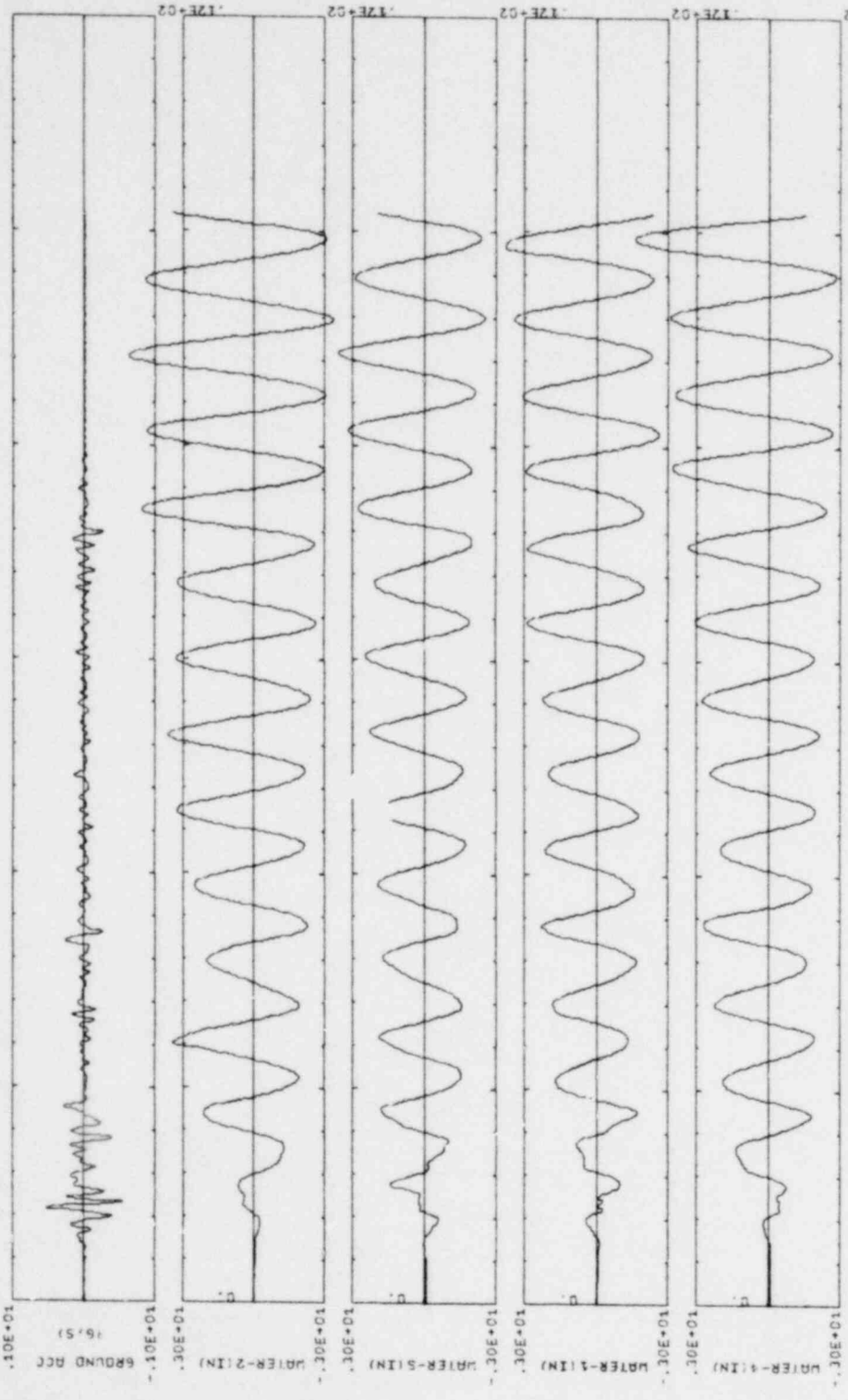

FIG. 5-21 SLOSHING RESPONSE IN 8FT ANNULAR TANK UNDER ELCENTRO EQ (1940), H=32 IN, MAX. HORIZONTAL/VERT. ACC=.54/.06, 211276.14

XBL 7812-13961

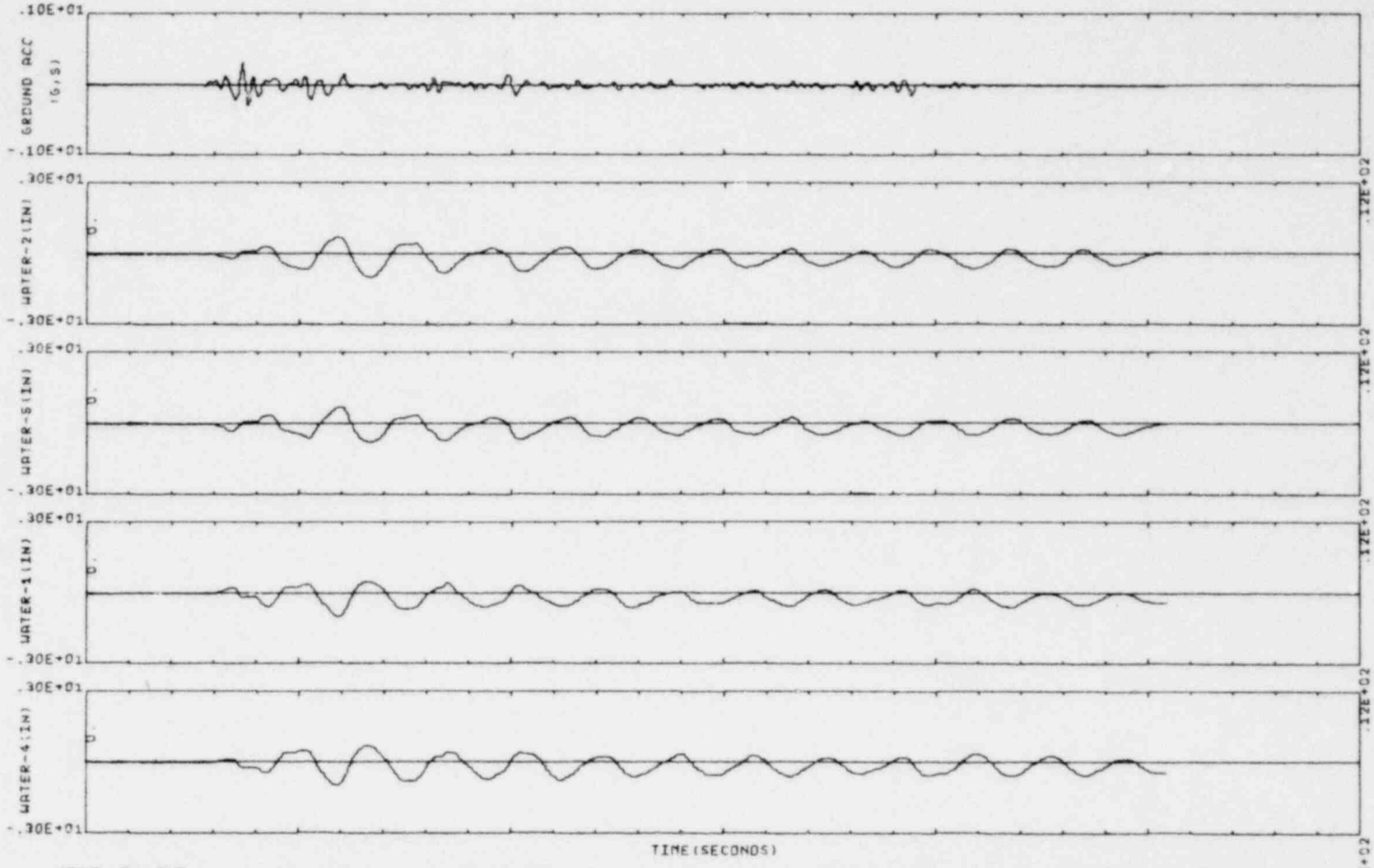

FIG. 5-22 SLOSHING RESPONSE IN 8FT ANNULAR TANK UNDER ELCENTRO EQ (1940), H=16 IN, MAX. HORIZONTAL/VERT. ACC=.32/.06, 291276.2 WITH SCREEN

XBL 7812-13960

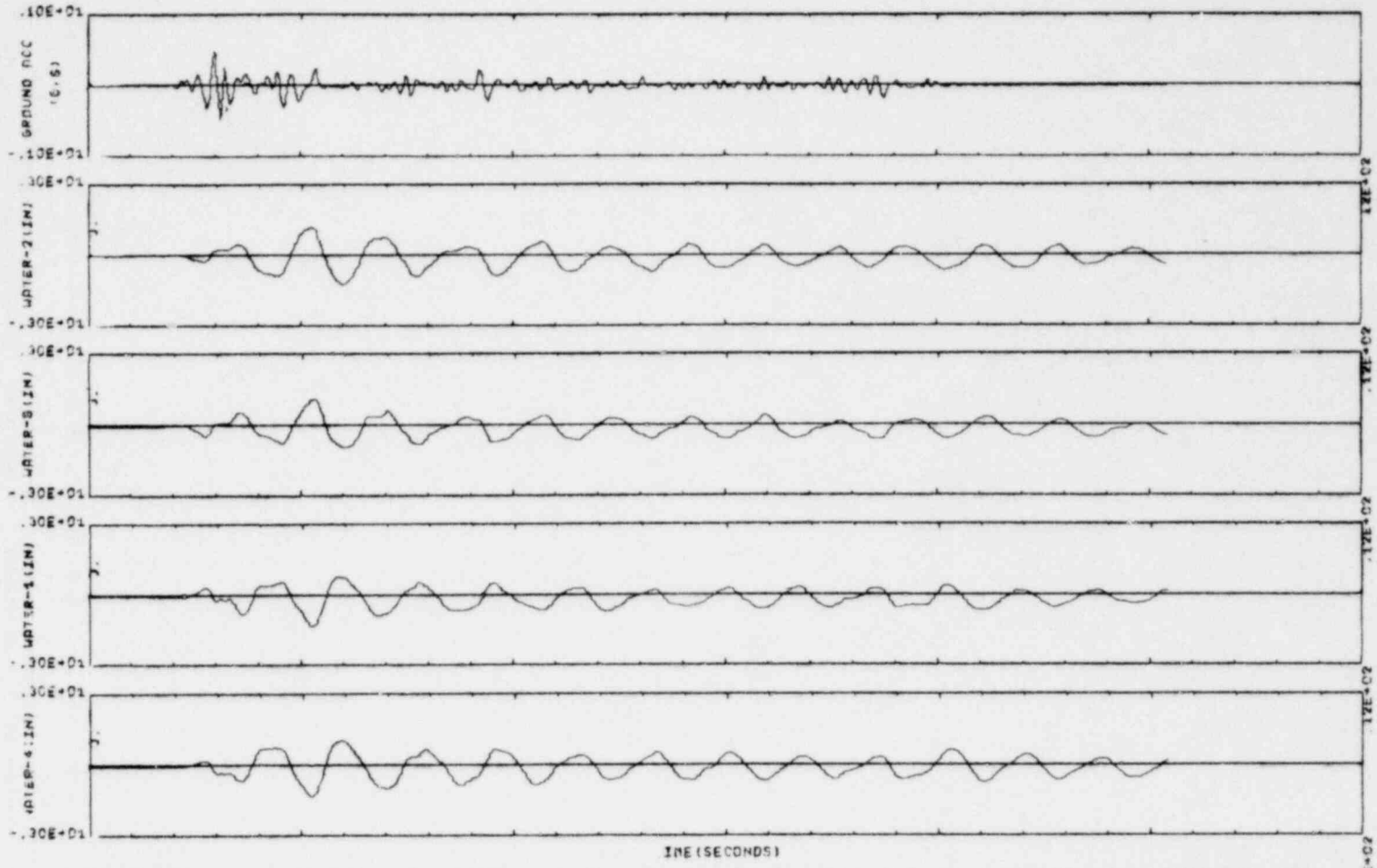

FIG. 5-23 SLOSHING RESPONSE IN 8FT ANNULAR TANK UNDER ELCENTRO EQ (1940), H=16 IN, MAX. HORIZONTAL/VERT. ACC=.48/.05, 291276.4 WITH SCREEN

XBL 7812-13959

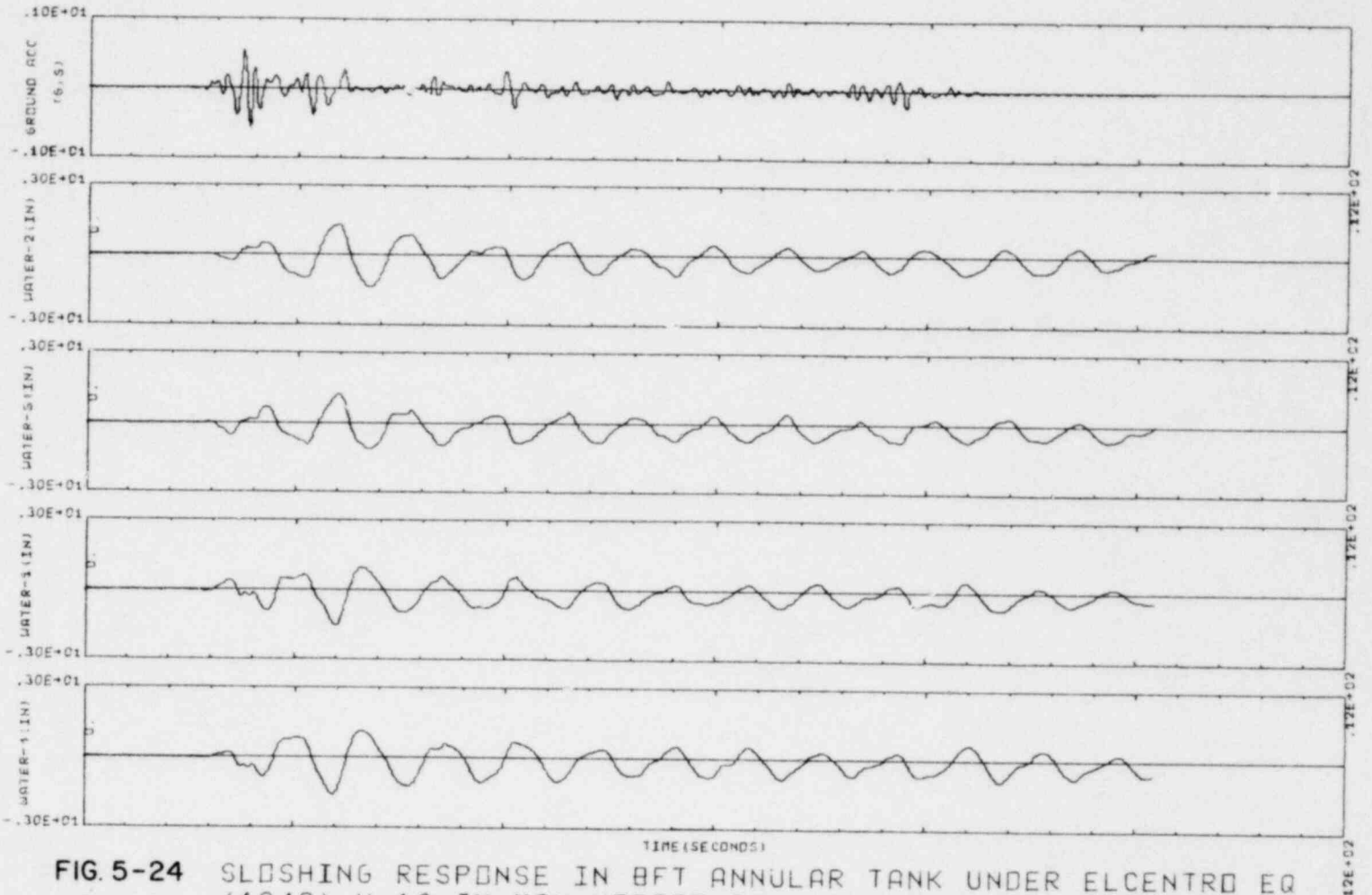

FIG. 5-24 SLOSHING RESPONSE IN 8FT ANNULAR TANK UNDER ELCENTRO EQ (1940), H=16 IN, MAX. HORIZONTAL/VERT. ACC=.57/.06, 291276.5 WITH SCREEN

XBL 7812-13958

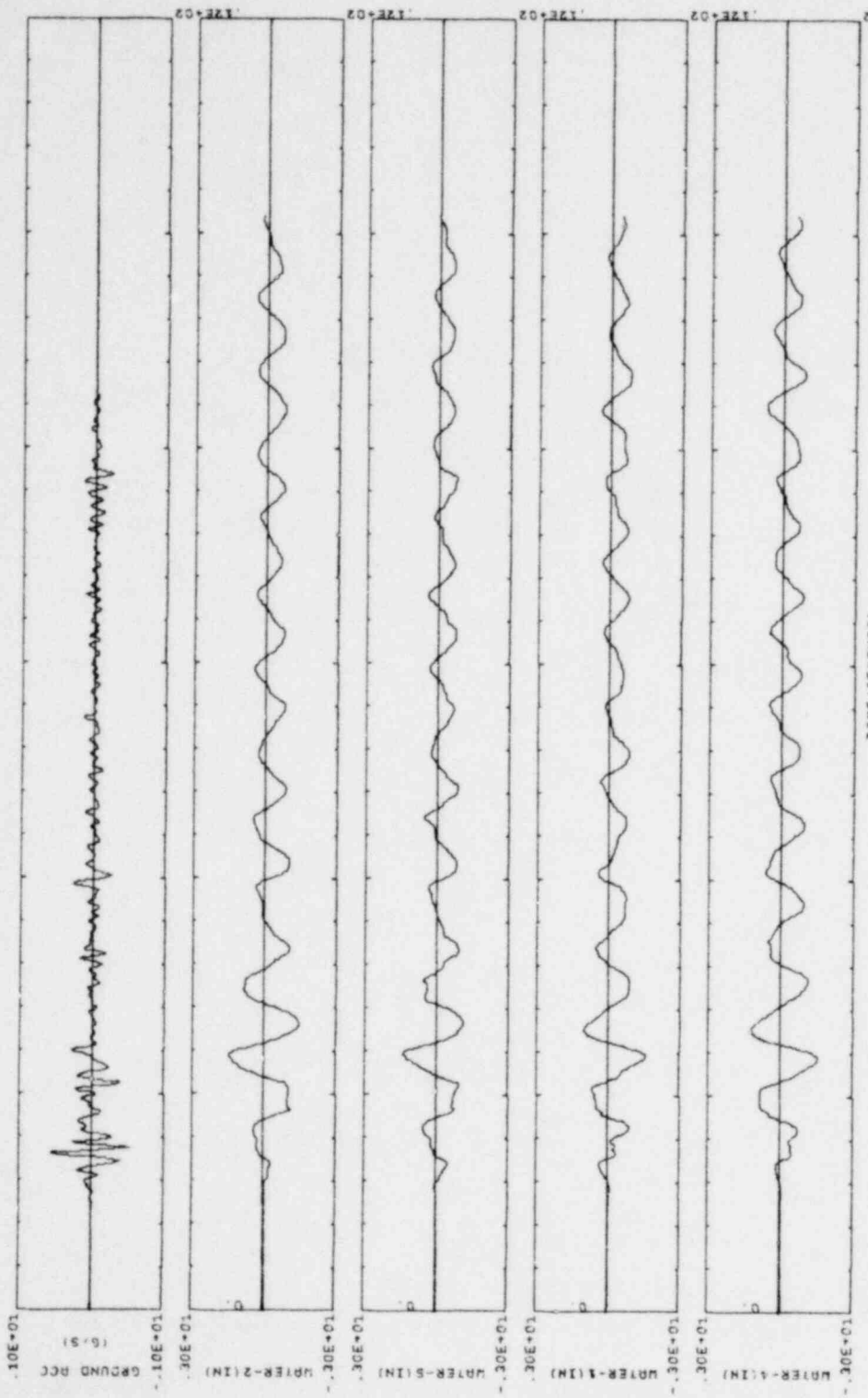

FIG. 5-25 SLOSHING RESPONSE IN BFT ANNULAR TANK UNDER ELCENTRO EQ (1940), H=16 IN, MAX. HORIZONTAL/VERT. ACC=.57/.406; 291276.8 WITH SCREEN

XBL 7812-13957

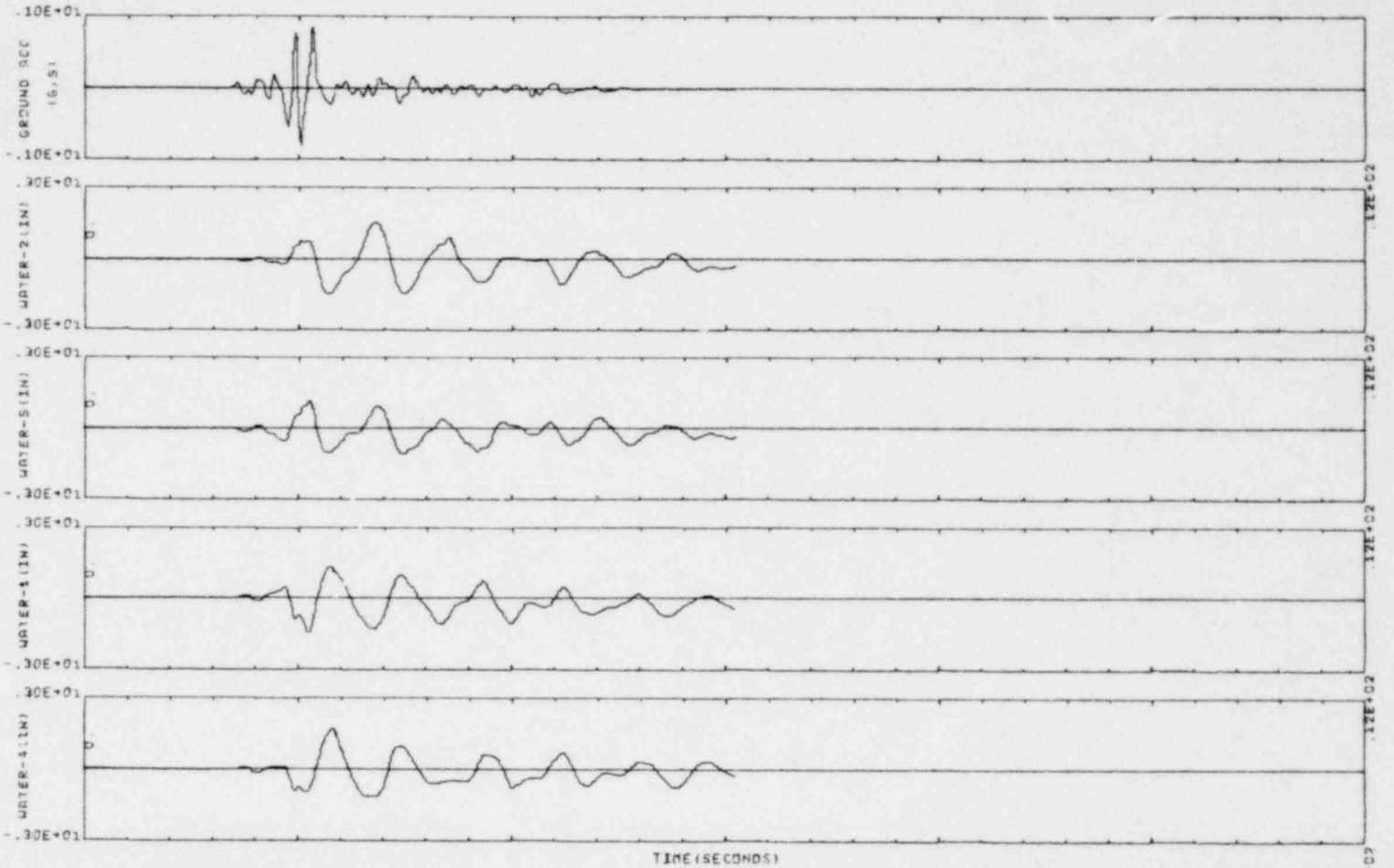

FIG. 5-26 SLOSHING RESPONSE IN 8FT ANNULAR TANK UNDER PARKFIELD EQ H=16 IN, MAX. HORIZONTAL ACCELERATION=.876, T.NO=291276.13 WITH SCREEN

XBL 7812-13956

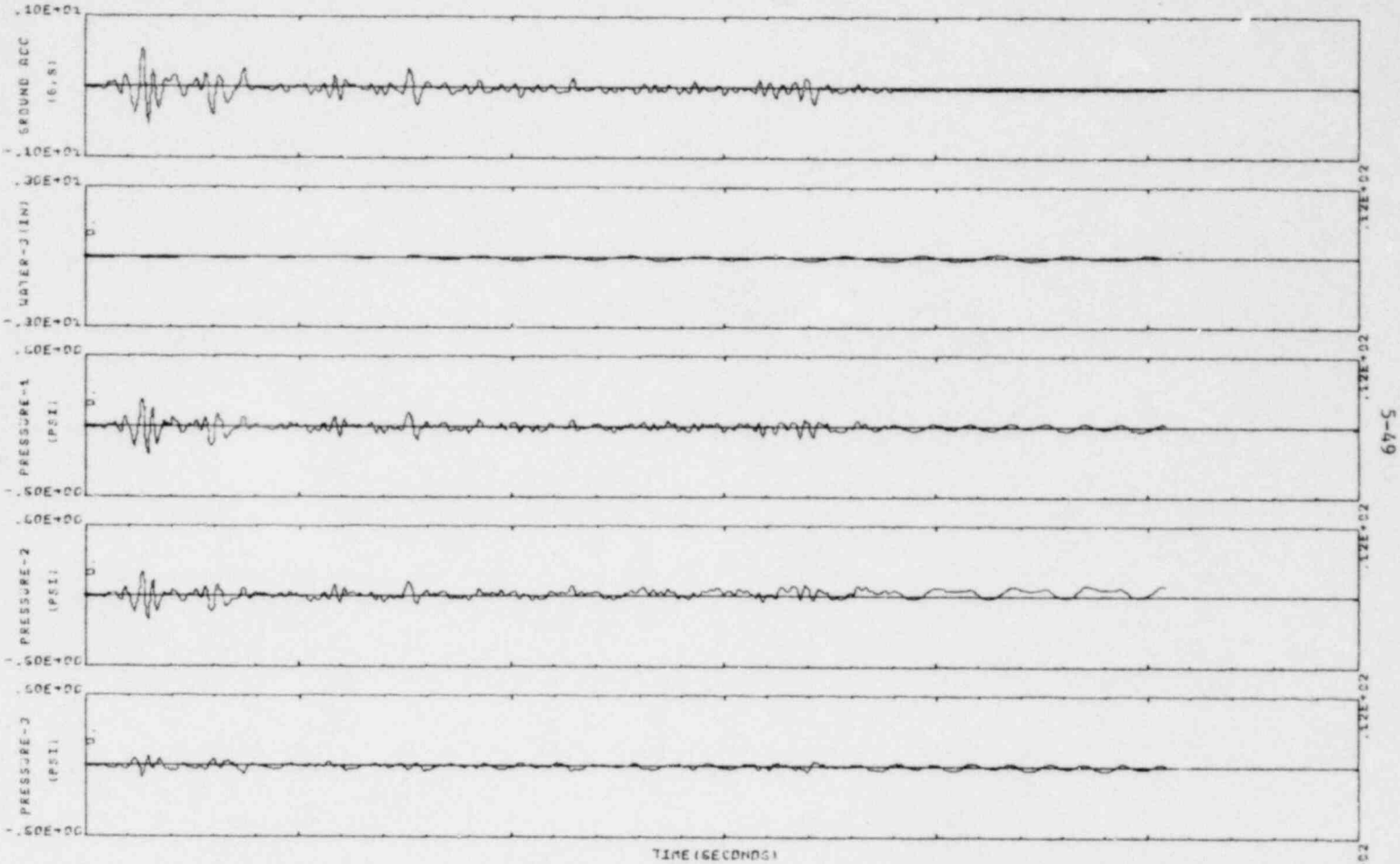

FIG. 5-27 PRESSURE RESPONSE IN 8FT ANNULAR TANK UNDER ELCENTRO EQ (1940), H=16 IN, MAX. HORIZONTAL/VERT. ACC=.56/.06, 211276.3

XBL 7812-13955

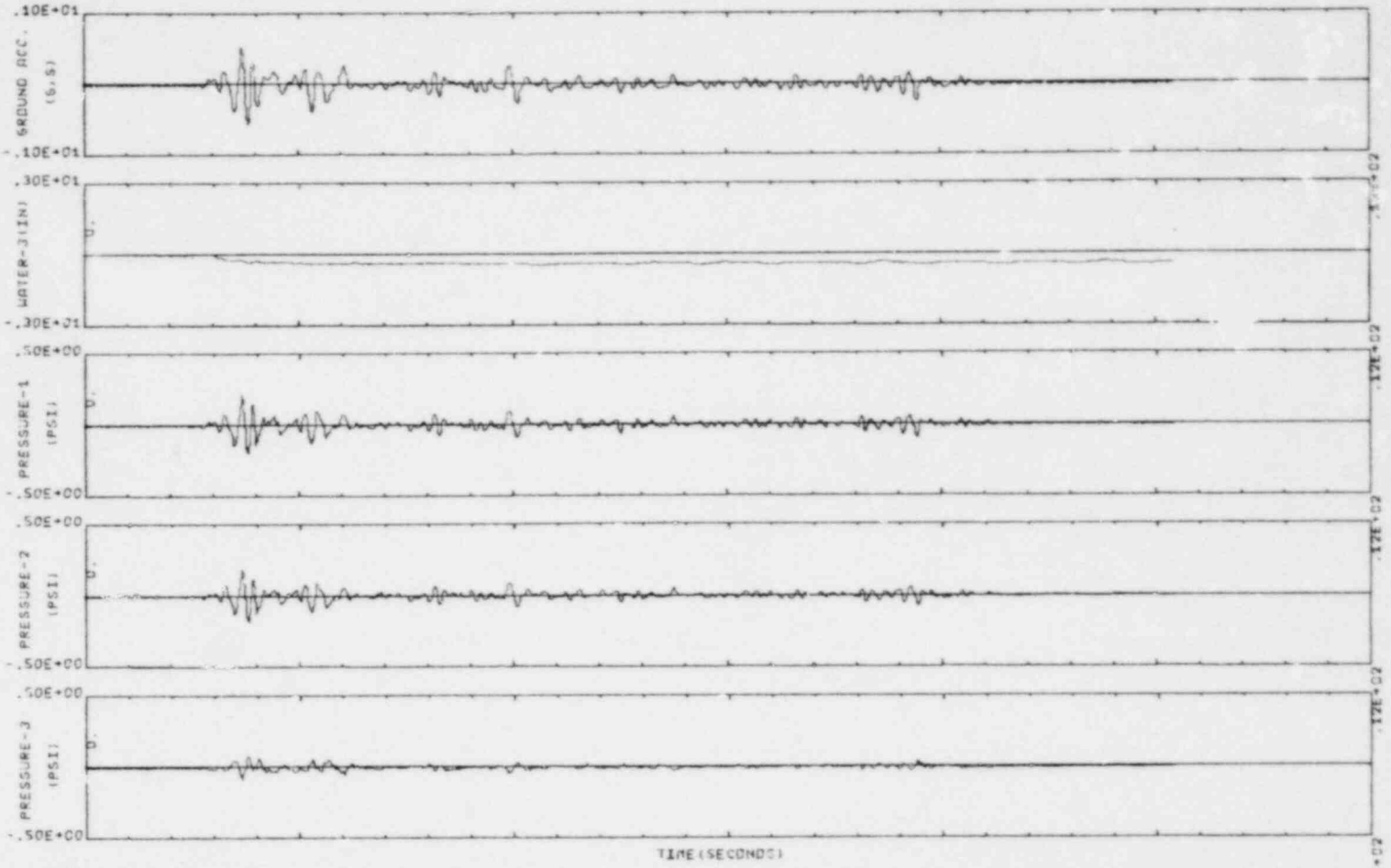

FIG. 5-28 PRESSURE RESPONSE IN 8FT ANNULAR TANK UNDER ELCENTRO EQ (1940), H=16 IN, MAX. HORIZONTAL/VERT. ACC=.57/.06, 291276.5 WITH SCREEN

XBL 7812-13954

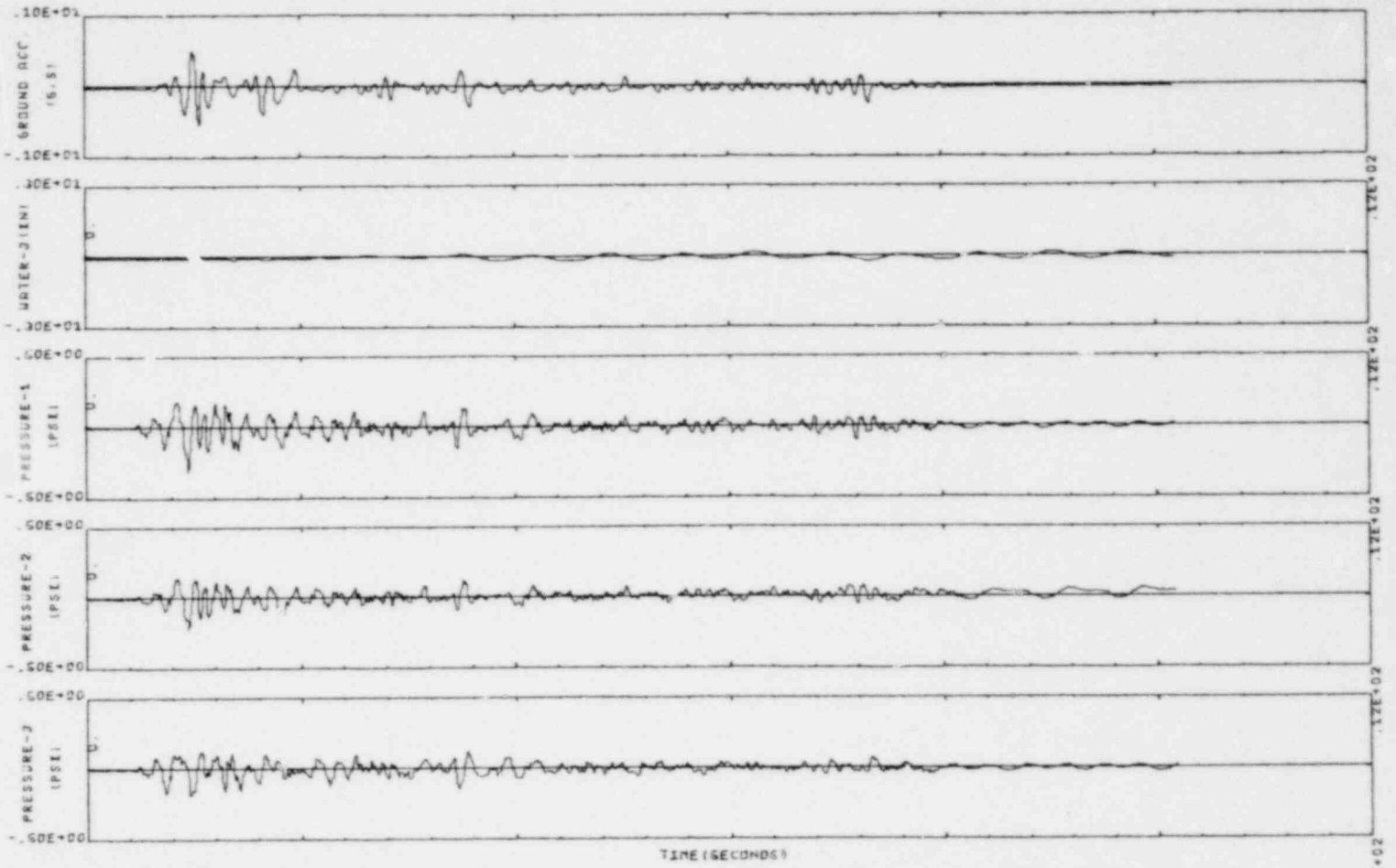

FIG. 5-29 PRESSURE RESPONSE IN 8FT ANNULAR TANK UNDER ELCENTRO EQ (1940), H=16 IN, MAX. HORIZONTAL/VERT. ACC=.540/.396, 211276.9

XBL 7812-13953

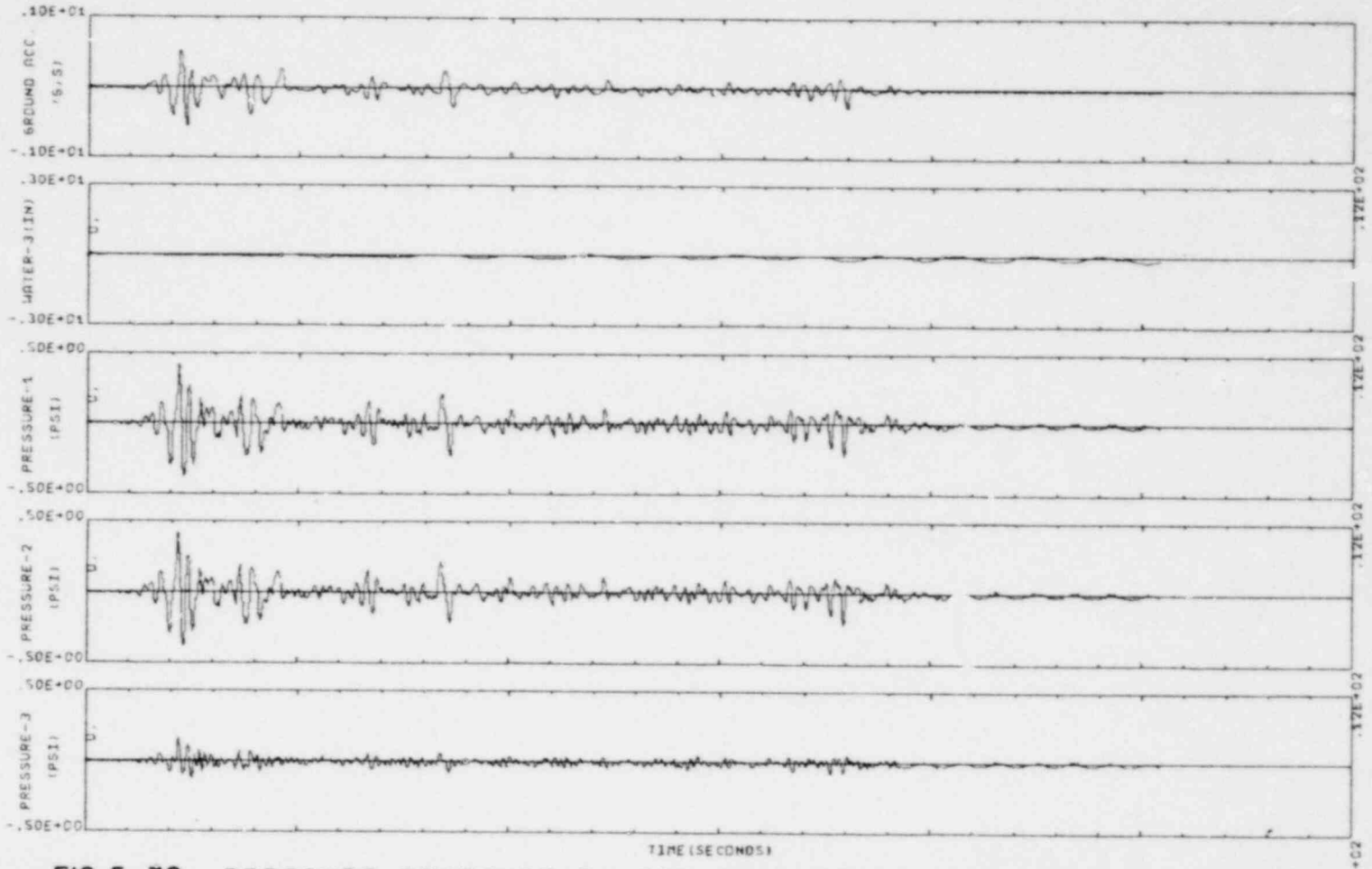

FIG. 5-30 PRESSURE RESPONSE IN 8FT ANNULAR TANK UNDER ELCENTRO EQ (1940); H=32 IN; MAX. HORIZONTAL/VERT. ACC=.54/.06, 211276.14

XBL 7812-13952

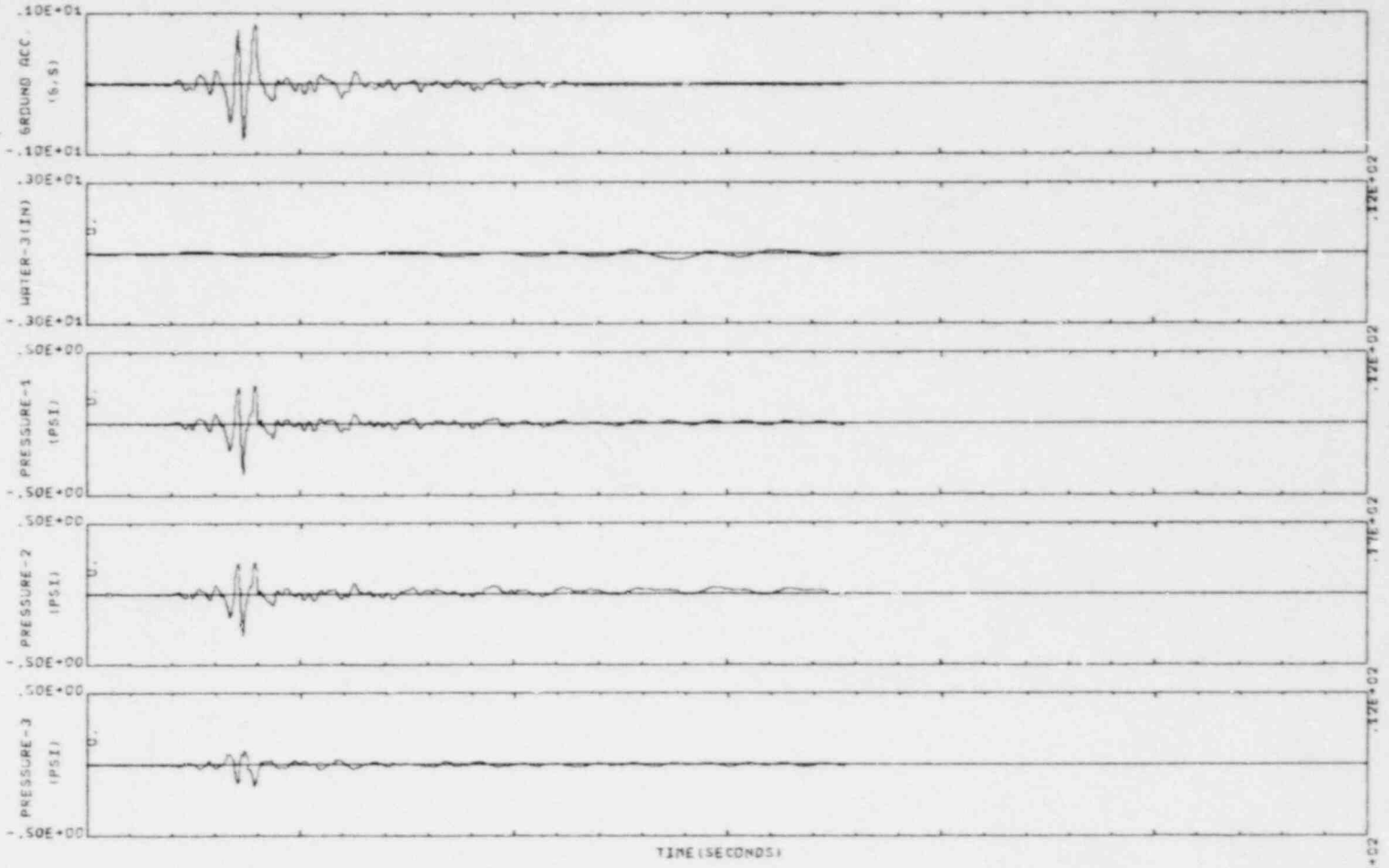

FIG. 5-31 PRESSURE RESPONSE IN 8FT ANNULAR TANK UNDER PARKFIELD EC
H=16 IN,MAX.HORIZONTAL ACCELERATION=.876,T.NO=211276.7

XBL 7812-13951

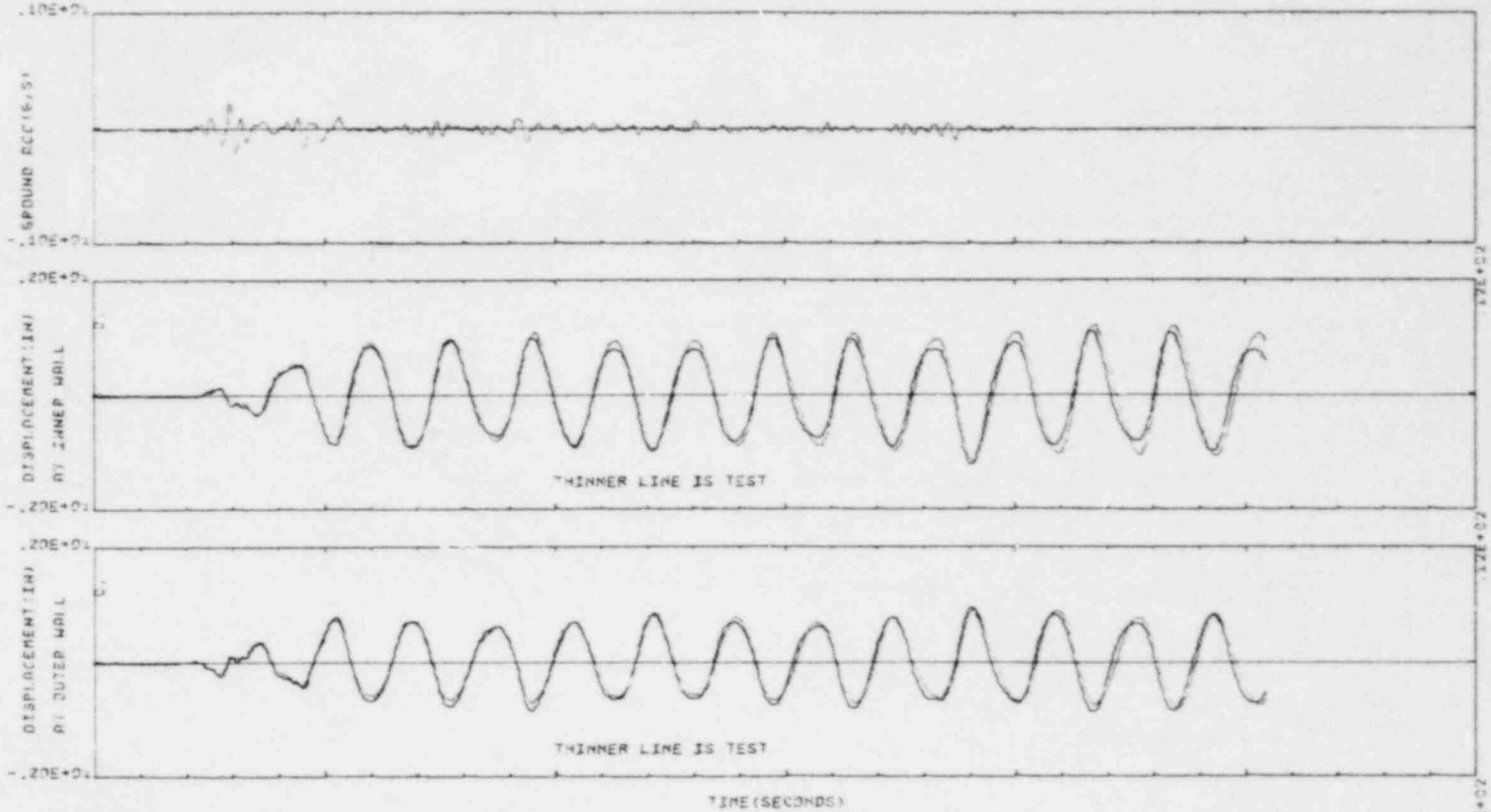

FIG. 5-32 SLOSHING RESPONSE OF WATER IN ANNULAR TANK(INNER RADIUS =33.2IN, OUTER RAD=48.0IN, DEPTH OF WATER=16.0IN) UNDER ELCENTRO EQ.1940(COMPARISON OF THEORY AND TEST 211276.1)

XBL 782-7209

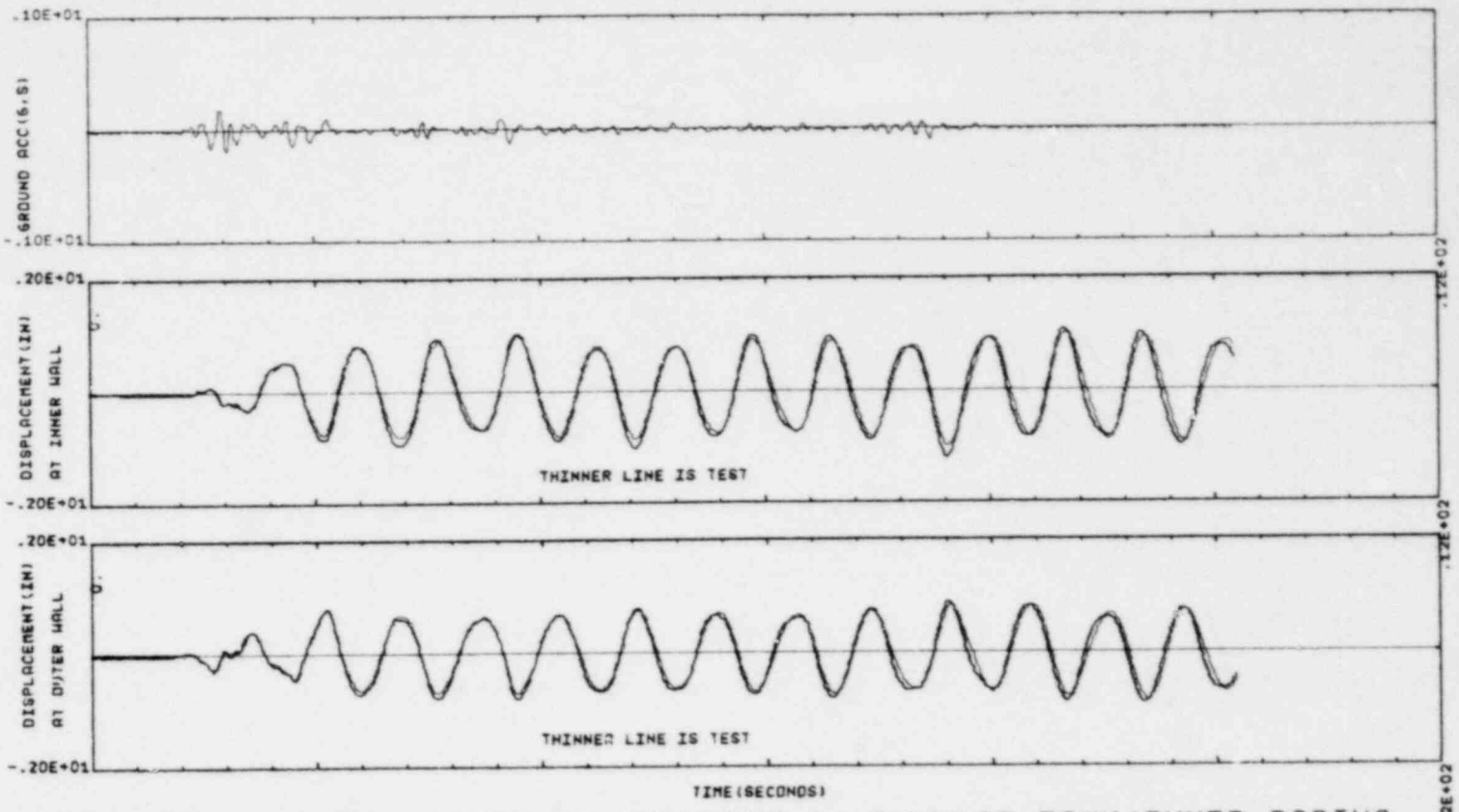

FIG. 5-33 SLOSHING RESPONSE OF WATER IN ANNULAR TANK(INNER RADIUS =33.2IN, OUTER RAD=48.0IN, DEPTH OF WATER=32.0IN UNDER ELCENTRO EQ.1940(COMPARISON OF THEORY AND TEST 211276.10)

XBL 7812-13950

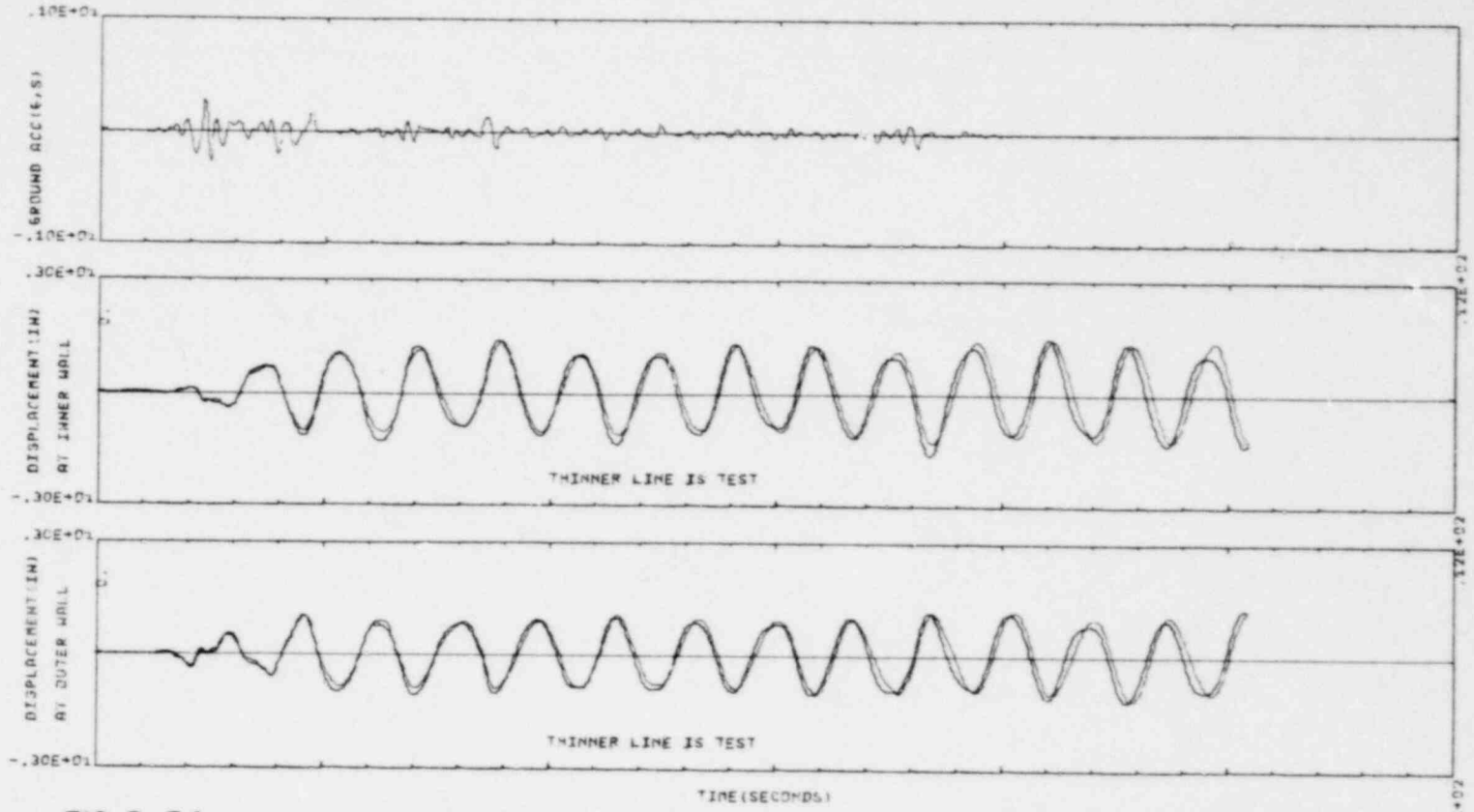

FIG. 5-34 SLOSHING RESPONSE OF WATER IN ANNULAR TANK(INNER RADIUS =33.2IN, OUTER RAD=48.0IN, DEPTH OF WATER=32.0IN UNDER ELCENTRO EQ.1940(COMPARISON OF THEORY AND TEST 211276.11)

XBL 7812-13949

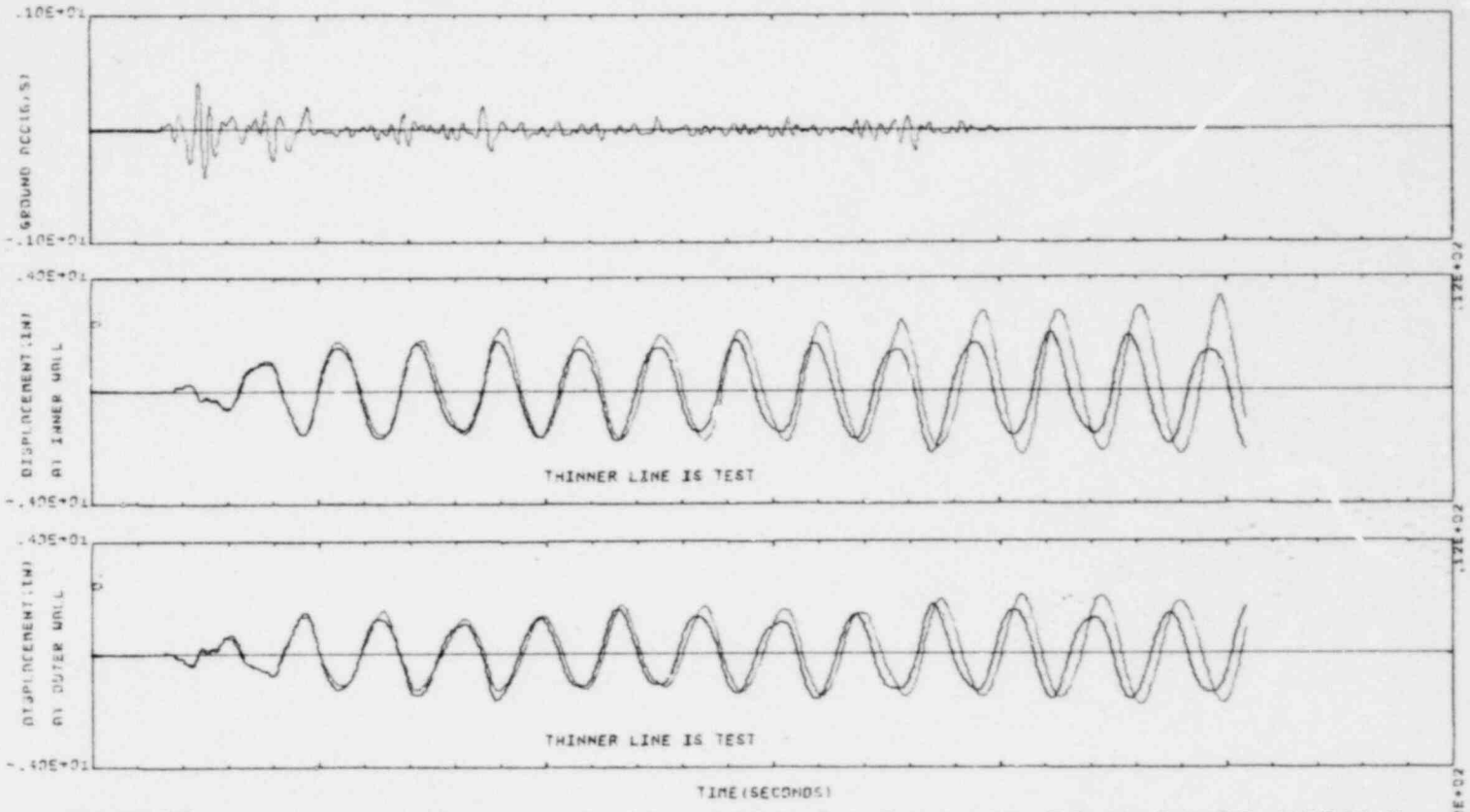

FIG. 5-35 SLOSHING RESPONSE OF WATER IN ANNULAR TANK(INNER RADIUS =33.2IN, OUTER RAD=48.0IN, DEPTH OF WATER=16.0IN) UNDER ELCENTRO EQ.1940(COMPARISON OF THEORY AND TEST 211276.2)

XBL 782-7216

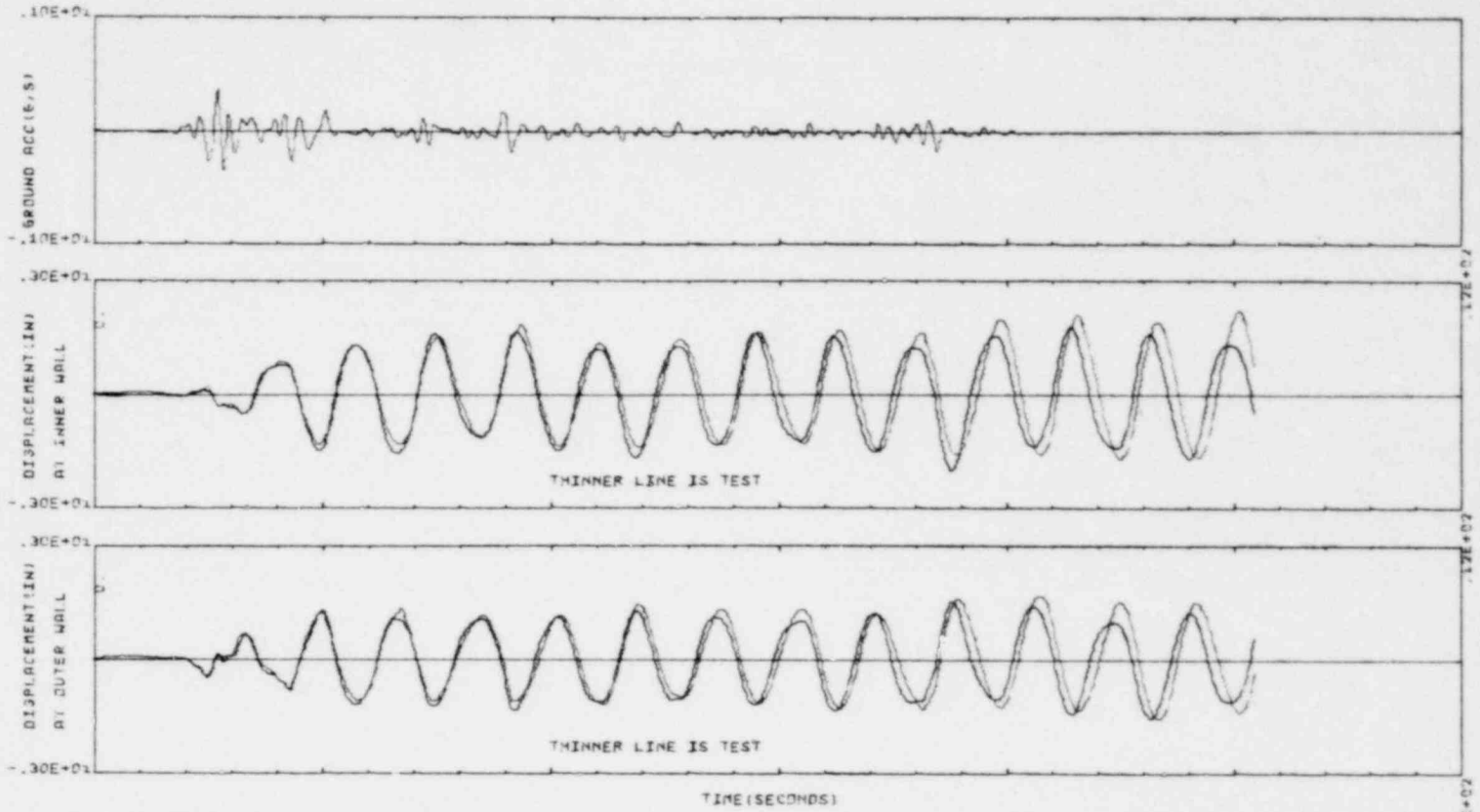

FIG. 5-36 SLOSHING RESPONSE OF WATER IN ANNULAR TANK(INNER RADIUS =33.2IN, OUTER RAD=48.0IN, DEPTH OF WATER=32.0IN UNDER ELCENTRO EQ.1940(COMPARISON OF THEORY AND TEST 211.276.12)

XBL 7812-13948

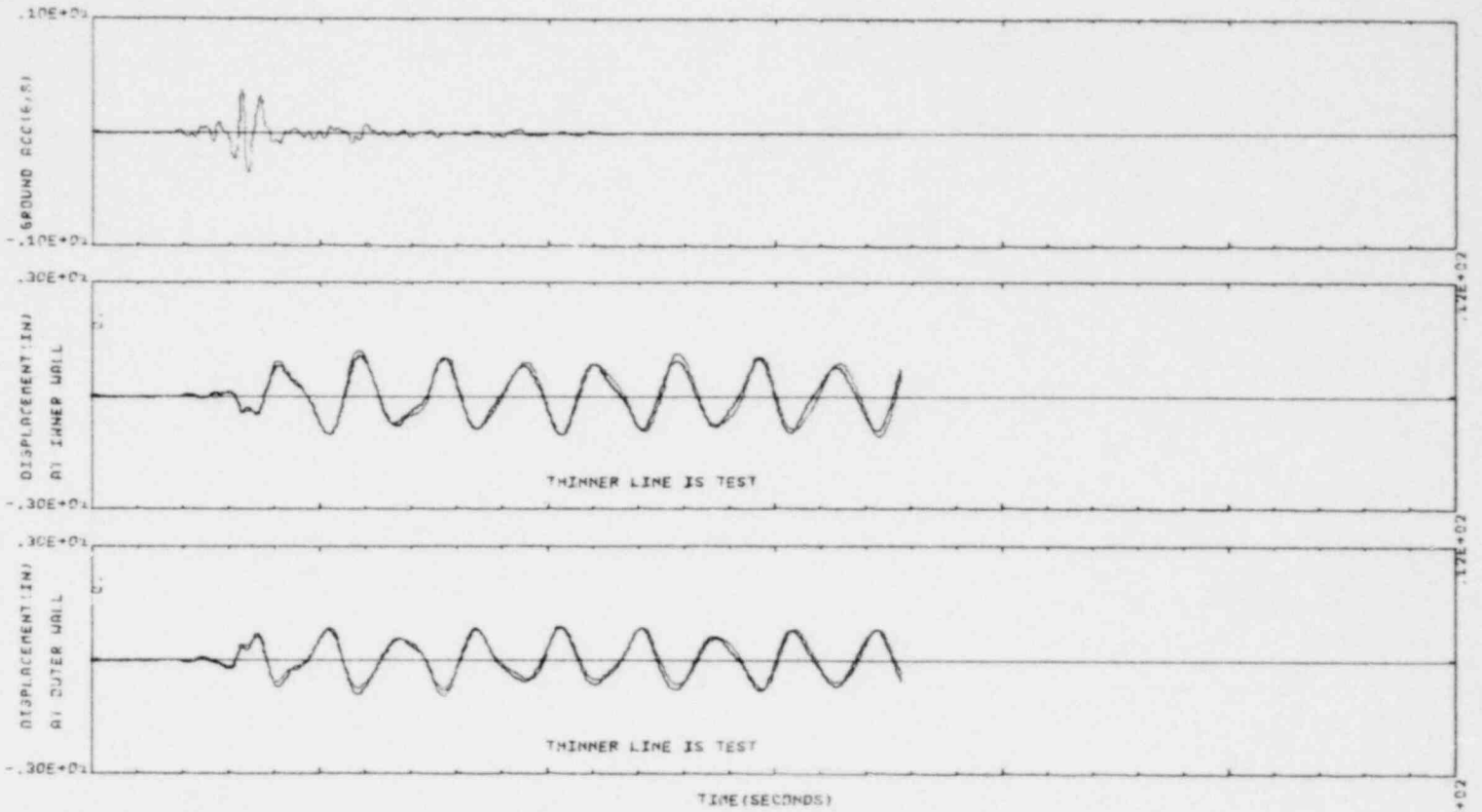

FIG. 5-37 SLOSHING RESPONSE OF WATER IN ANNULAR TANK(INNER RADIUS =33.2IN, OUTER RAD=48.0IN, DEPTH OF WATER=16.0IN) UNDER PARKFIELD EQ.(COMPARISON OF THEORY VS TEST 211276.4)

XBL 7812-13947

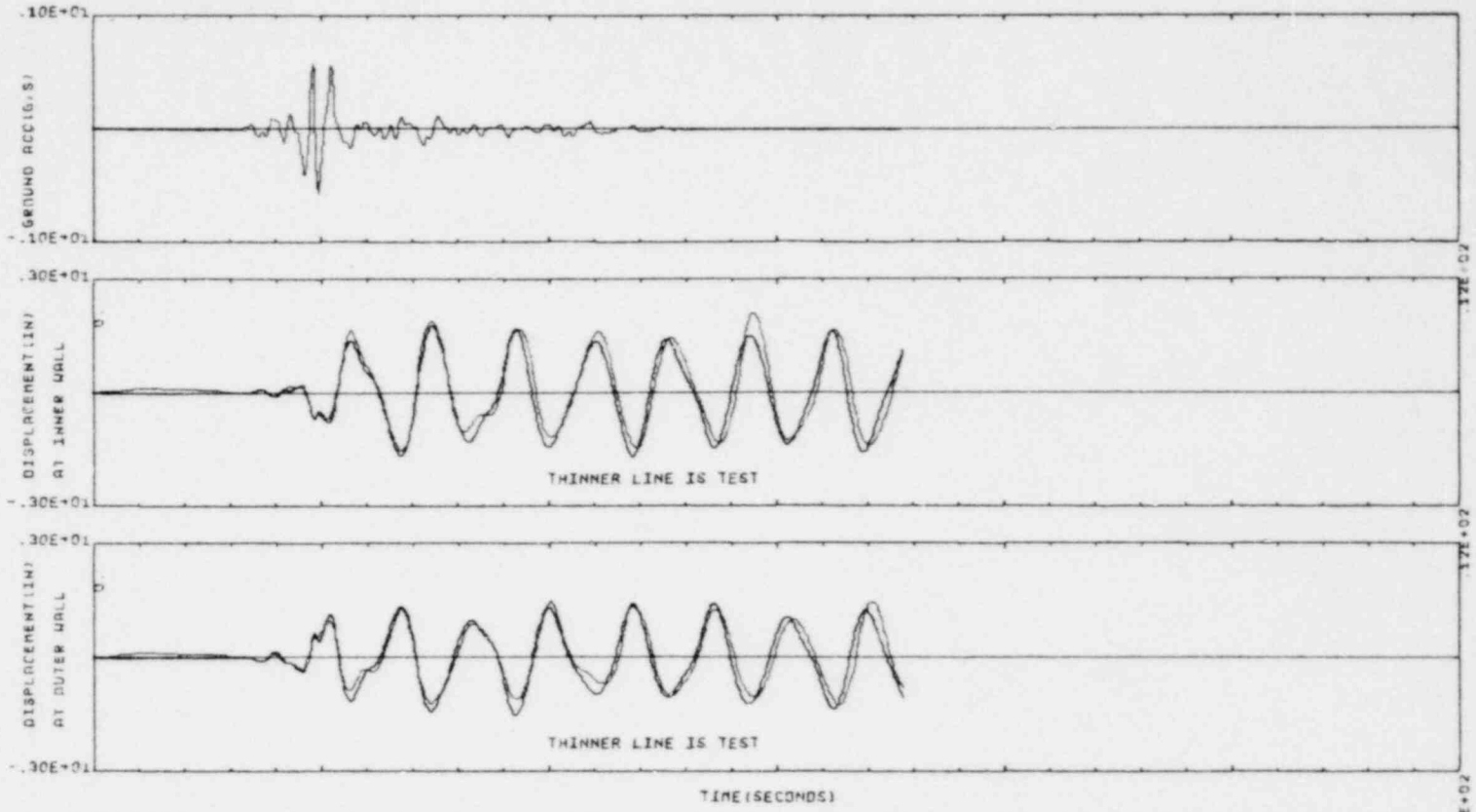

FIG. 5-38 SLOSHING RESPONSE OF WATER IN ANNULAR TANK(INNER RADIUS =33.2IN, OUTER RAD=48.0IN, DEPTH OF WATER=16.0IN) UNDER PARKFIELD EQ.(COMPARISON OF THEORY VS TEST 211276.5)

XBL 7812-13946

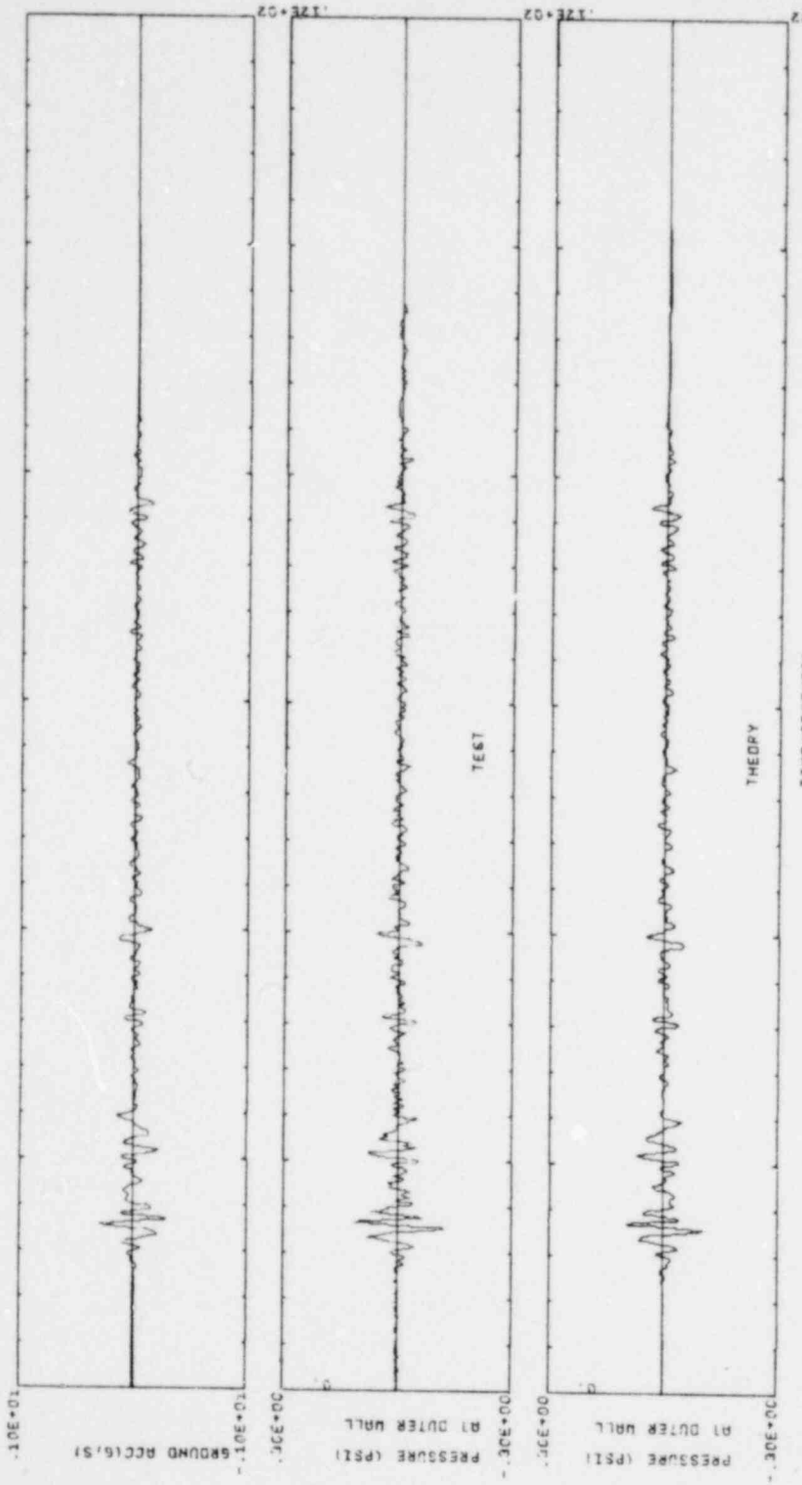

FIG. 5-39 PRESSURE RESPONSE OF WATER IN ANNULAR TANK (INNER RADIUS =33.2IN, OUTER RAD=48.0IN, DEPTH OF WATER=16.0IN) UNDER ELCENTRO EQ.1940 (COMPARISON OF THEORY AND TEST 201276.21)

XBL 7812-13945

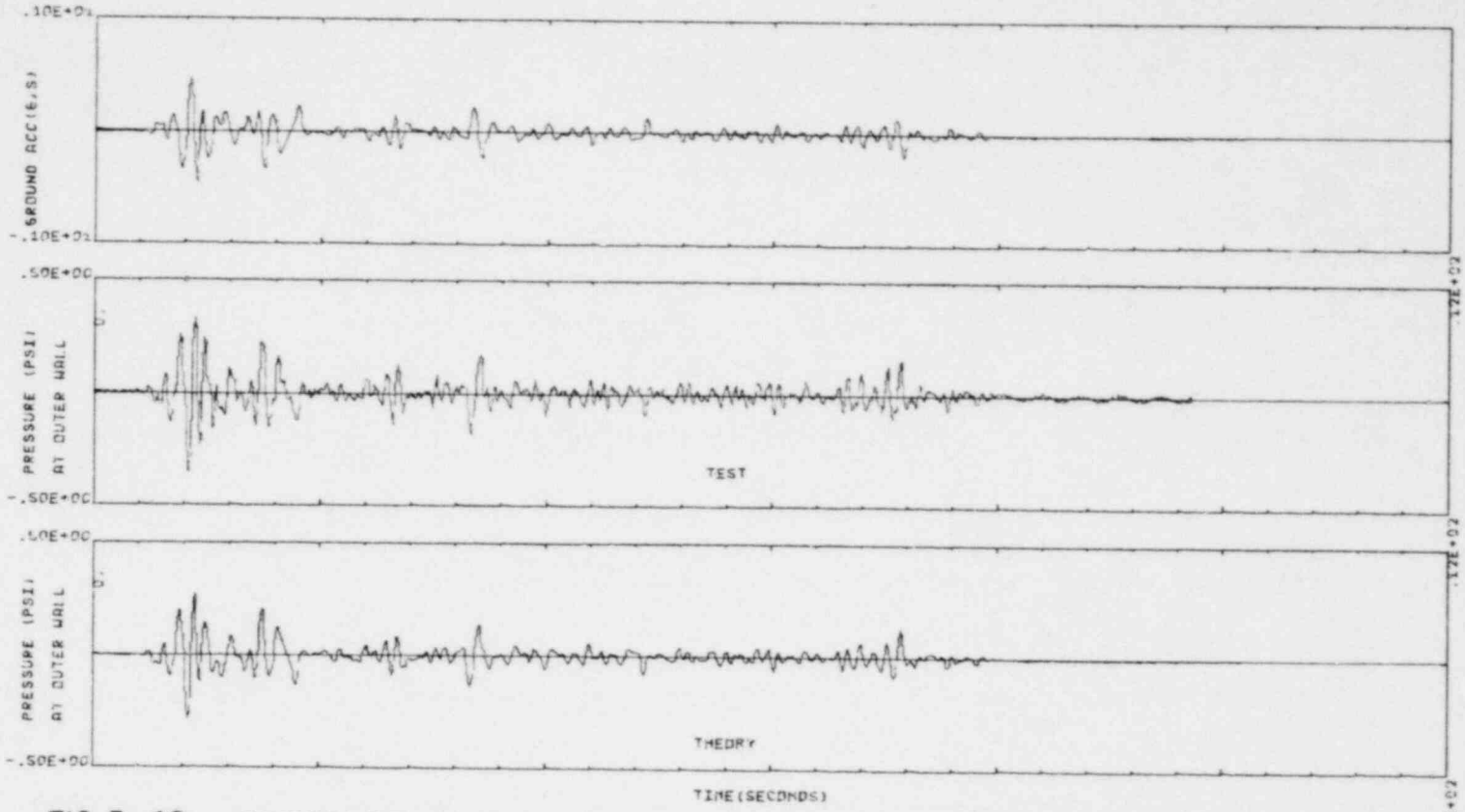

FIG. 5-40 PRESSURE RESPONSE OF WATER IN ANNULAR TANK(INNER RADIUS =33.2IN, OUTER RAD=48.0IN,DEPTH OF WATER=32.0IN UNDER ELCENTRO EQ.1940(COMPARISON OF THEORY AND TEST 211276.13)

XBL 7812-13944

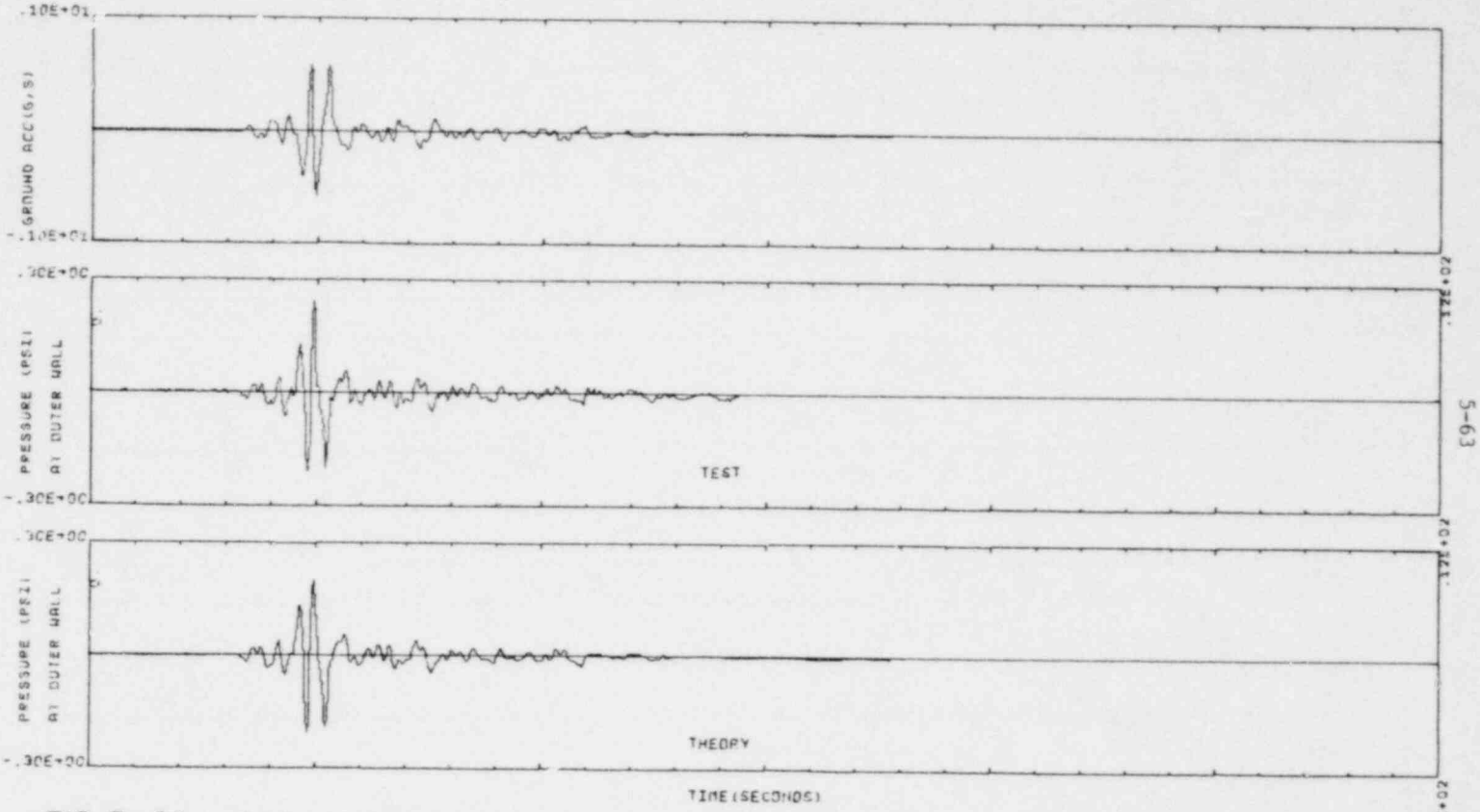

FIG. 5-41 PRESSURE RESPONSE OF WATER IN ANNULAR TANK(INNER RADIUS =33.2IN, OUTER RAD=48.0IN,DEPTH OF WATER=16.0IN) UNDER PARKFIELD EQ.(COMPARISON OF THEORY VS TEST 211276.5)

XBL 7812-13943

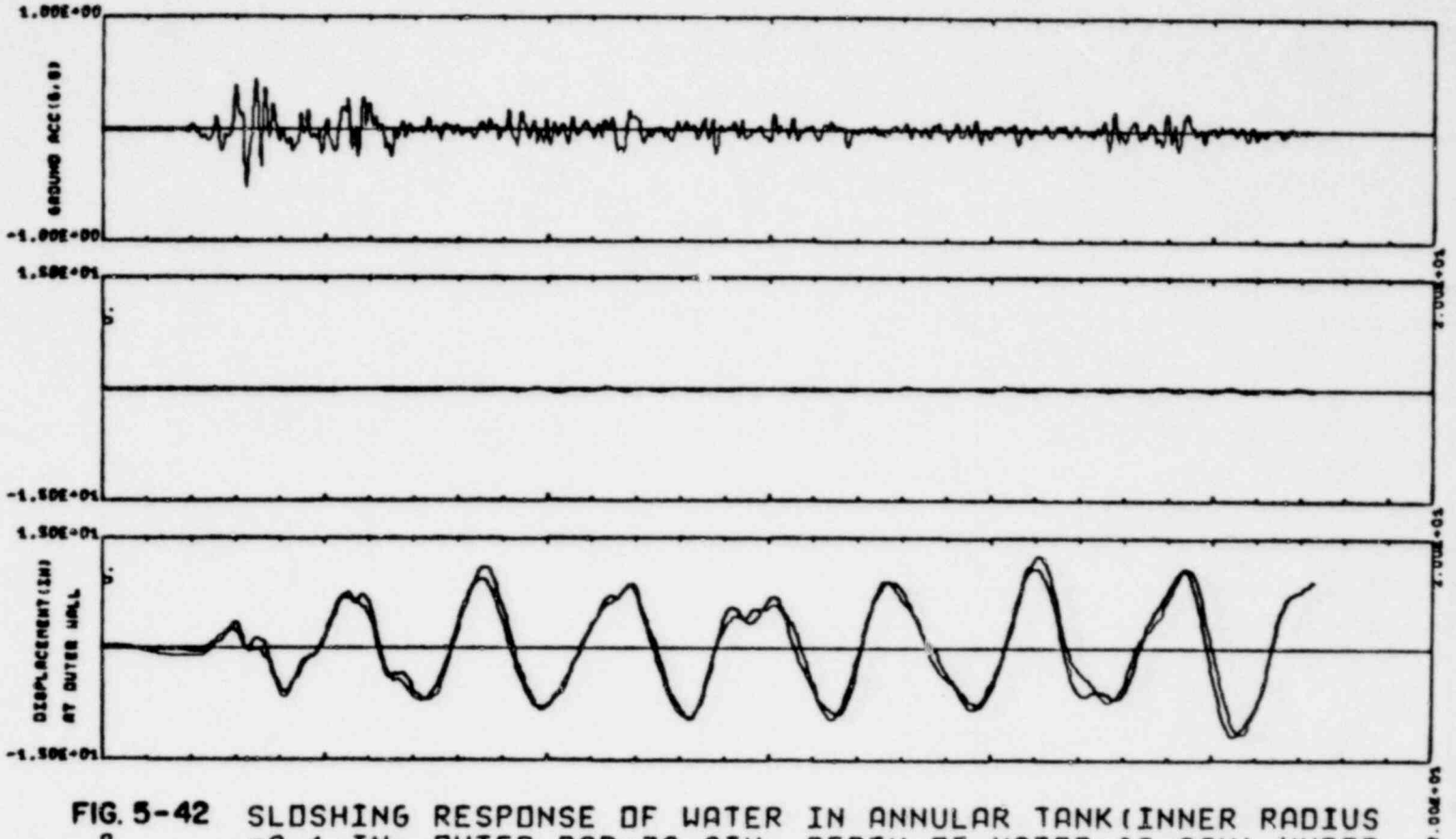

FIG. 5-42 SLOSHING RESPONSE OF WATER IN ANNULAR TANK(INNER RADIUS =0.1 IN, OUTER RAD=72.0IN, DEPTH OF WATER=60.0IN) UNDER ELCENTRO EARTHQUAKE(1940)TIME SCALE=1.73

XBL 7812-13942

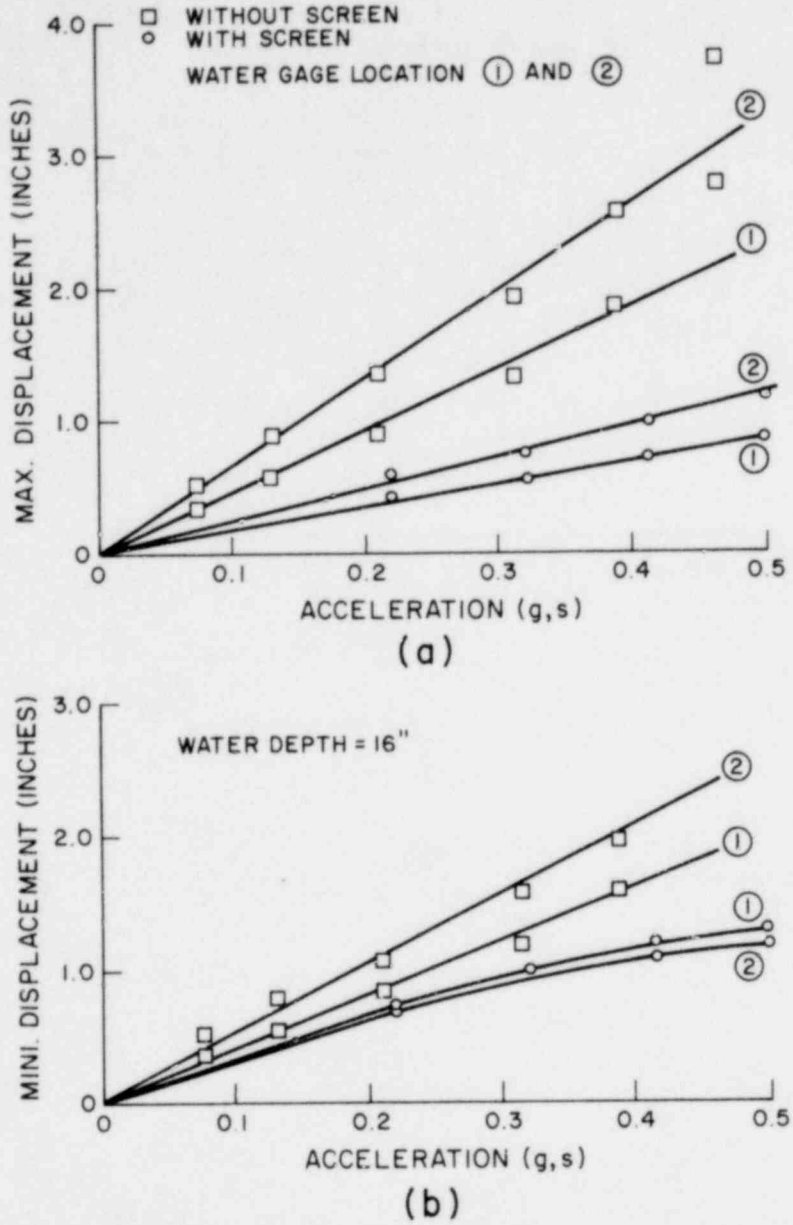

FIG. 5-43 EXTREME VALUES OF DISPLACEMENTS UNDER ELCENTRO EARTHQUAKE (WITH AND WITHOUT DAMPING SCREEN)

XBL 7812-13941

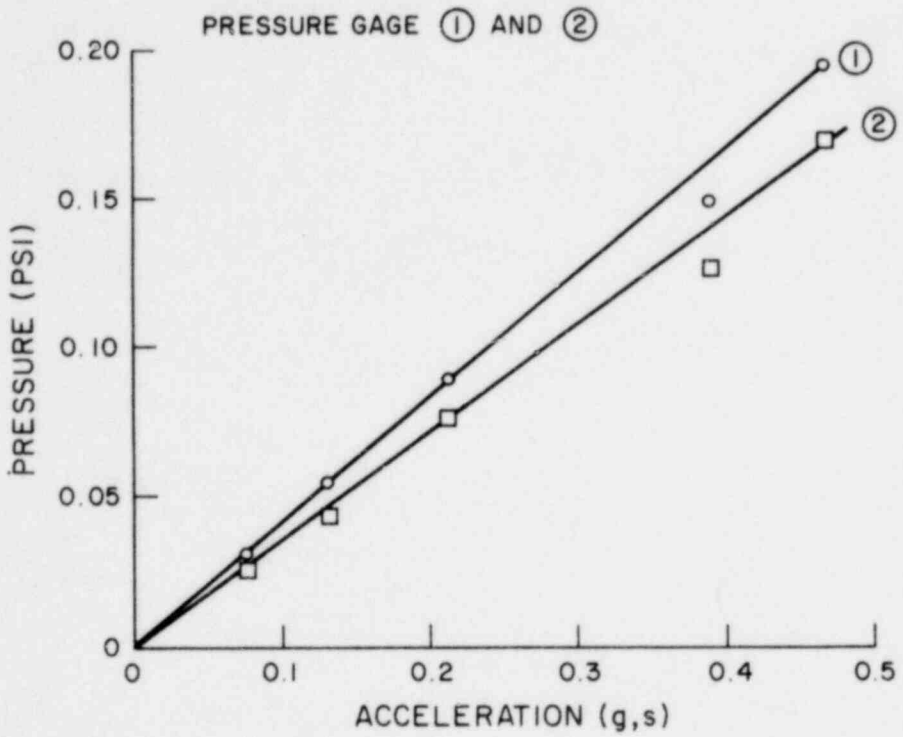

FIG. 5-44 EXTREME VALUES OF DYNAMIC PRESSURE UNDER ELCENTRO EARTHQUAKE (H = 16 IN.)

XBL 7812-13940

ACKNOWLEDGMENTS

This investigation was sponsored by the United States Nuclear Regulatory Commission and was done with support from the United States Energy Research and Development Administration.

REFERENCES

1. E.W. Graham and A.M. Rodriguez, The Characteristics of Fuel Motion which Affect Airplane Dynamics, Journal of Applied Mechanics, Vol. 19, No. 3, Sept. 1952.

2. L.S. Jacobson and R.S. Ayre, Hydrodynamic Experiments with Rigid Cylindrical Tanks Subjected to Transient Motions. Bulletin of Seismological Society of America, Vol. 41, Oct. 1951.

3. J. Miles, On the Sloshing of Liquid in a Flexible Tank, ASME, Paper No. 57-A-12, 1957.

4. J. Miles, On the Sloshing of a Liquid in a Cylindrical Tank, Ramo-Wooldridge AM-6-5, CM-TR-18, 1956.

5. B. Budiansky, Sloshing of Liquids in Circular Canals and Spherical Tanks, Lockheed Aircraft Corp. LMSD-5151, Dec. 1958.

6. H.F. Bauer, Fluidoscillations in a Circular Cylindrical Tank, American Boilers Manufacturers Association (ABMA) Report DA-TR-1-58.

7. H.F. Bauer, Fluidoscillations in a Cylindrical Tank with Damping, ABMA Report DA-TR-4-58.

8. H.F. Bauer, Fluidoscillations in a Circular Cylindrical Tank Due to Bending of Tank Walls, ABMA Report DA-3-58.

9. H.F. Bauer, Damped Fluidoscillations in a Circular Cylindrical Tank Due to Bending Walls, ABMA Report DA-9-58.

10. K. Kachigan, Forced Oscillations of a Fluid in a Cylindrical Tank, Convair Report ZU-7-046, Oct. 1956.

11. A.F. Schmitt, Forced Oscillations of a Fluid in a Cylindrical Tank Undergoing Both Translation and Rotation, Convair Report ZU-7-069, Oct. 1956.

12. H.F. Bauer, The Dynamic Behavior of Liquids in Moving Containers, National Aeronautics and Space Administration, Washington, D.C., 1966, edited by H. Norman Abramson.

13. J.J. Stoker, Water Waves, Interscience Publishers, Inc., New York, 1957.

14. L.S. Jacobson and R.S. Ayre, Hydrodynamic Experiments with Rigid Cylindrical Tanks Subjected to Transient Motions, Bull. Seism. Soc. Am., Vol. 41, 1952.

15. P.C. Jennings, G.W. Housner, and N.C. Tsai, Simulated Earthquake Motion, California Institute of Technology, Pasadena, California, April, 1968.

16. D.P. Clough, Experimental Evaluation of Seismic Design Methods for Broad Cylindrical Tanks, Ph.D. Dissertation, University of California, Berkeley, 1976.

NRC FORM 335 (7-77)

U.S. NUCLEAR REGULATORY COMMISSION

BIBLIOGRAPHIC DATA SHEET

1. REPORT NUMBER (Assigned by DDC): NUREG/CR-1083

4. TITLE AND SUBTITLE (Add Volume No., if appropriate): "Sloshing of Water in Annular Pressure - Suppression Pool of Boiling Water Reactors Under Earthquake Ground Motions"

2. (Leave blank)

3. RECIPIENT'S ACCESSION NO.

7. AUTHOR(S): M. Alsan, W. G. Godden, and D. T. Scalise

5. DATE REPORT COMPLETED: MONTH March, YEAR 1978

9. PERFORMING ORGANIZATION NAME AND MAILING ADDRESS (Include Zip Code)
Lawrence Berkeley Laboratory
University of California
Berkeley, CA 94720

DATE REPORT ISSUED: MONTH October, YEAR 1979

6. (Leave blank)

8. (Leave blank)

12. SPONSORING ORGANIZATION NAME AND MAILING ADDRESS (Include Zip Code)
U.S. Nuclear Regulatory Commission
Washington, D.C. 20555

10. PROJECT/TASK/WORK UNIT NO.

11. CONTRACT NO.

13. TYPE OF REPORT: Technical Report

PERIOD COVERED (Inclusive dates)

15. SUPPLEMENTARY NOTES

14. (Leave blank)

16. ABSTRACT (200 words or less)

This report presents an analytical investigation of the sloshing response of water in annular-circular as well as simple-circular tanks under horizontal earthquake ground motions, and the results are verified with tests. This study was motivated because of the use of annular tanks for pressure-suppression pools in Boiling Water Reactors. Such a pressure-suppression pool would typically have 80 ft and 120 ft inside and outside diameters and a water depth of 20 ft.

The analysis was based upon potential flow theory and a computer program was written to obtain time-history plots of sloshing displacements of water and the dynamic pressures. Tests were carried out on 1/80th and 1/15th scale models under sinusoidal as well as simulated earthquake ground motions. Tests and analytical results regarding the natural frequencies, surface water displacements, and dynamic pressures were compared and a good agreement was found for relatively small displacements. The computer program gave satisfactory results as long as the maximum water surface displacements were less than 30 in., which is roughly the value obtained under full intensity of El Centro earthquake (N-S component 1940).

17. KEY WORDS AND DOCUMENT ANALYSIS

17a. DESCRIPTORS

Sloshing response, Pressure-suppression pool, Annular tanks, Circular tanks, Earthquake response, Dynamic pressures, Irrotational flow, Damping

17b. IDENTIFIERS/OPEN-ENDED TERMS

1364 329

18. AVAILABILITY STATEMENT: Unlimited

19. SECURITY CLASS (This report): Unclassified

21. NO. OF PAGES

20. SECURITY CLASS (This page)

22. PRICE $

UNITED STATES
NUCLEAR REGULATORY COMMISSION
WASHINGTON, D. C. 20555

OFFICIAL BUSINESS
PENALTY FOR PRIVATE USE, $300

POSTAGE AND FEES PAID
U.S. NUCLEAR REGULATORY
COMMISSION

acc
Unit
P-016

120555008386 2 ANRD
US NRC
SECY PUBLIC DOCUMENT ROOM
BRANCH CHIEF
WASHINGTON DC 20555

POOR ORIGINAL

1364 330